# Effect of neural ablation of sphingosine-1-phosphate lyase (SGPL1) in glial cells

**Dissertation**

zur

Erlangung des Doktorgrades (Dr. rer. nat.)

der

Mathematisch-Naturwissenschaftlichen Fakultät

der

Rheinischen Friedrich-Wilhelms-Universität Bonn

vorgelegt von

## Shah Alam

aus

Jaunpur, Indien

Bonn, 2021

Angefertigt mit Genehmigung der Mathematisch-Naturwissenschaftlichen Fakultät der Rheinischen Friedrich-Wilhelms-Universität Bonn in der Zeit von Juli 2017 bis Juli 2021 am Kekulé-Institut für Organische Chemie und Biochemie unter der Leitung von Frau PD. Dr. Gerhild van Echten-Deckert.

1. Referent:  PD. Dr. Gerhild van Echten-Deckert
2. Referent:  Prof. Dr. Jörg Höhfeld

Tag der Promotion:  8. November 2021
Erscheinungsjahr: 2021

# Summary

Sphingosine-1-phosphate (S1P) is an evolutionarily conserved catabolic intermediate of sphingolipid metabolism that regulates diverse biological processes in the brain, including neural development, differentiation, and survival. S1P-lyase (SGPL1) irreversibly cleaves S1P in the final step of sphingolipid catabolism. Interestingly, patients harboring mutations in the gene encoding this enzyme (*SGPL1*) often present with neurological pathologies (Choi and Saba 2019). In this study a mouse model (SGPL1[fl/fl/Nes], neural-specific SGPL1-deleted mice) in which SGPL1 was explicitly inactivated in neural cells was used to investigate the impact of SGPL1-deficiency in the brain. Previous studies in this mouse model have confirmed the importance of S1P metabolism for the presynaptic architecture and neuronal autophagy (Mitroi, Deutschmann et al. 2016, Mitroi, Karunakaran et al. 2017).

In the current study, further investigations have been done on this mouse model. The results show that SGPL1 ablation causes astrogliosis in SGPL1-deficient murine brain, a condition characterized by increased expression of GFAP and inflammatory cytokines such as IL-6 and TNFα. Expression of P2Y1R (another protein found in reactive astrocytes) was also found to be increased in SGPL1-deficient murine brain. Increased P2Y1R expression was also an indication of increased nucleotides (ATP or ADP) in the extracellular milieu. Intriguingly, the expressions of glycolytic enzymes were found to be increased, which lead to more ATP production in SGPL1-deficient astrocytes. In addition, mTOR-dependent impaired autophagy was observed in SGPL1-deficient astrocytes. However, upon pharmacological inhibition of S1P receptors (S1PR2/4), both glycolytic enzymes and P2Y1R expression were reversed. Besides, inhibition of P2Y1R reversed the GFAP expression and rescued IL-6 but not TNFα expression in the SGPL1-deficient astrocytes.

Furthermore, microglial activation was evidenced as microglial activation marker protein (Iba1) was found to be increased in SGPL1-deficient murine brains. In addition, autophagy, one of the major mechanisms in the brain that keeps inflammation in check, was also impaired in microglia. Indeed, microglial inflammation was accompanied by defective microglial autophagy in SGPL1-deficient mice. Next, S1PR2 was identified as the mediator of both impaired autophagy and proinflammatory effects (Karunakaran, Alam et al. 2019).

Moreover, two other factors involved in neurodegenerative processes, namely tau phosphorylation and histone acetylation, were also investigated in SGPL1-deficient murine brains. In hippocampal and cortical slices, S1P accumulation was accompanied by hyperphosphorylation of tau and an elevated acetylation of histone3 and histone4. Calcium chelation with BAPTA-AM rescued both tau hyperphosphorylation and histone acetylation, designating calcium as an essential mediator of these (patho)physiological functions of S1P in the brain. Afterward, it was revealed that hyperphosphorylated tau was found only in SGPL1-deficient neurons and increased histone acetylation was present only in SGPL1-deficient astrocytes (Alam, Piazzesi et al. 2020)

# TABLE OF CONTENTS

# 1 INTRODUCTION

## 1.1 LIPIDS IN BRAIN

The composition of lipids in the brain is distinctive compared to other parts of the body. More than half of the solid matter in the brain is composed of membrane lipids which in turn are mainly composed of phospholipids (Crawford and Sinclair 1971). Phospholipids are essential components of all mammalian cells and are involved in a variety of biological functions. For instance, the formation of lipid bilayers provides the structural integrity which is necessary for protein function. It serves as precursors for various second messengers such as arachidonic acid (ArAc), docosahexaenoic acid (DHA), ceramide, 1,2-diacylglycerol (DAG), phosphatidic acid, and lysophosphatidic acid. Lipids are classified into eight categories (fatty acyls, glycolipids, glycerophospholipids, sterol lipids, prenol lipids, saccharolipids, polyketides, and sphingolipids) (Fahy, Subramaniam et al. 2009). Sphingolipids were discovered in brain extracts and were named after the mythological sphinx because of their enigmatic nature (Thudichum 1884). Since the discovery of sphingolipids, their role and function have been greatly appreciated (Wollny, Watek et al. 2017). Initially, sphingolipids were thought of as a cellular building material or used in metabolic processes (Divecha and Irvine 1995). However, their role as a signaling molecule has continuously been explored (Spiegel and Milstien 2000, Karunakaran and van Echten-Deckert 2017, van Echten-Deckert and Alam 2018). Sphingolipids are highly enriched in the brain, where they play an essential role in its proper development and functions and are also vital constituents of the plasma membranes (Olsen and Faergeman 2017).

## 1.2 SPHINGOLIPID METABOLISM

Sphingolipid biosynthesis starts with the condensation reaction between serine and fatty acyl-CoA. Enzymes, namely: serine palmitoyl transferase (SPT), 3-ketodihydrosphingosine reductase, dihydroceramide synthases, and dihydroceramide desaturase, consecutively yield ceramide (Fig.1). Ceramidases convert ceramide into sphingosine, and sphingosine kinases (SKs) further phosphorylate sphingosine to form S1P (Fig.1) (van Echten-Deckert and Herget 2006, Hannun and Obeid 2008). SKs exist in two isoforms: SK1 and SK2, which differ in their cellular location and function (Kohama, Olivera et al. 1998, Maceyka, Harikumar et al. 2012). The degradation of S1P follows an irreversible cleavage, catalyzed

11

by SGPL1 to yield ethanolamine phosphate (EAP) and hexadecenal, marking the exit point of the sphingolipid degradation pathway. Thus, S1P sits at the junction between sphingolipid and phospholipid metabolism (Fig.1) (Van Veldhoven 2000, Aguilar and Saba 2012). S1P is dephosphorylated by S1P phosphatases (SPP) and can be further traced back via the salvage pathway to ceramide by ceramide synthases (Fig.1).
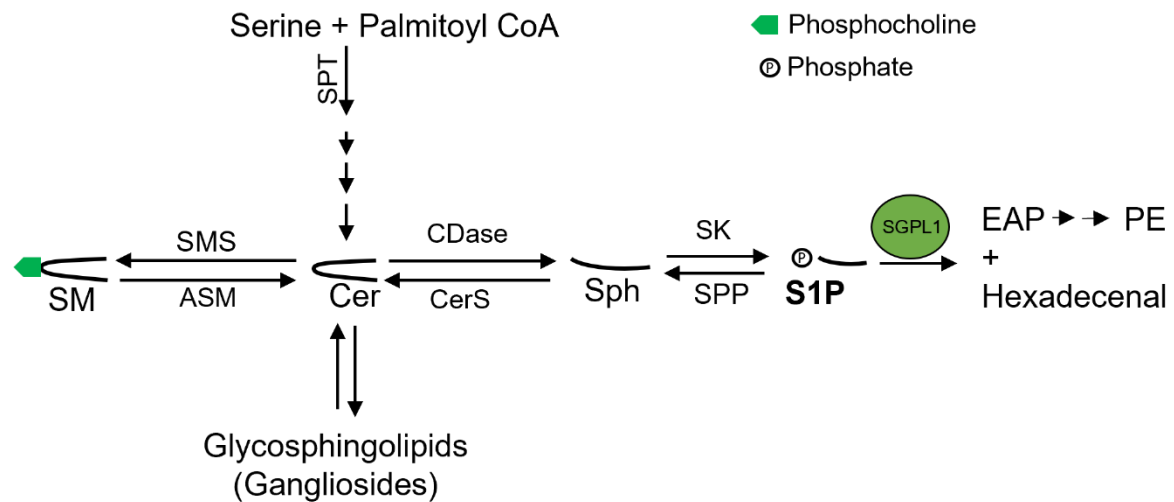


**Figure 1. Schematic representation of S1P metabolism.** De-novo synthesis of ceramide (Cer) starts through the condensation of serine and palmitoyl-CoA by serine palmitoyl transferase (SPT). After that, through several reversible metabolic reactions, sphingomyelin (SM), sphingosine, sphingosine-1-phosphate (S1P) and complex glycosphingolipids are formed. The formation of S1P is tightly regulated by sphingosine kinases (SKs), S1P Phosphatase (SPP), and S1P Lyase (SGPL1). SGPL1 irreversibly breaks down S1P into hexadecenal and ethanolamine phosphate (EAP). SM, sphingomyelin; CerS, ceramide synthases; CDase, ceramidase; SMS, sphingomyelin synthase; ASM, acid sphingomyelinase; PE, Phosphatidylethanolamine (modified image from (van Echten-Deckert and Alam 2018).

## 1.3 SPHINGOSINE 1- PHOSPHATE (S1P)

S1P is an evolutionarily conserved catabolic intermediate of sphingolipid metabolism that regulates diverse biological processes in the brain, including neural development, proliferation, differentiation, and survival (Karunakaran and van Echten-Deckert 2017, van Echten-Deckert and Alam 2018). Moreover, S1P is also known to exert its effect extracellularly through a family of five specific G protein-coupled receptors, S1PR1-5 (Blaho and Hla 2014). S1P, through its receptors, plays significant regulatory phenomenon including immune cell trafficking, migration (Spiegel and Milstien 2011, Thuy, Reimann et

al. 2014), monitoring autophagy (Karunakaran, Alam et al. 2019), regulating cell growth (Olivera and Spiegel 1993), and apoptosis (Cuvillier, Pirianov et al. 1996). Knowledge on the intracellular effects of S1P is limited; however, recent experimental pieces of evidence suggest receptor-independent actions of S1P in maintaining $Ca^{++}$ level and histone modification (Itagaki and Hauser 2003, Hait, Allegood et al. 2009, Alam, Piazzesi et al. 2020).

## 1.4   S1P IN NEURODEGENERATION

The word neurodegeneration is composed of the prefix "neuro," which indicates nerve cells (i.e., neurons), and "degeneration," which means losing the structure or function of tissues or organs. Thus, neurodegenerative disorders correspond to changes in the neurons that cause them to function abnormally and eventually results in death. Neurodegeneration's most common symptoms have been seen in people as they reach life's later stages. Most famously, neurodegeneration can lead to memory loss, depriving people of performing the most basic tasks in their life. Among hundreds of different neurodegenerative disorders so far, Alzheimer's disease (AD), Parkinson's disease (PD), Huntington disease (HD), and amyotrophic lateral sclerosis (ALS) have been given more attention. However, many of the less common or publicized neurodegenerative disorders have remained essentially ignored though no less devastating (e.g., ataxia, motor neuron disease, multiple system atrophy, progressive supranuclear palsy).

The physiological functions and pathological role of sphingolipids in various neurodegenerative diseases are increasingly elucidated (Karunakaran and van Echten-Deckert 2017, van Echten-Deckert and Alam 2018, Wang and Bieberich 2018). In recent years, a growing body of literature has implicated S1P in the pathogenesis of various brain cells (Mitroi, Karunakaran et al. 2017, Moruno-Manchon, Uzor et al. 2018). The ongoing research suggests that S1P metabolism and its signaling vary in different cell types: neurons, astrocytes, and microglia (Wang and Bieberich 2018). The role of S1P has been ambiguously and divisively discussed in neurodegenerative conditions. Some reports show the protective role of S1P-signaling (He, Huang et al. 2010, Ceccom, Loukh et al. 2014, Couttas, Kain et al. 2014). In contrast to this, some other groups, including the van Echten-Deckert group, report the morbific role of accumulated S1P in the brain (Hagen, Hans et al. 2011, Takasugi, Sasaki et al. 2011, Mitroi, Deutschmann et al. 2016, Lei, Shafique et al.

2017, Mitroi, Karunakaran et al. 2017, Karunakaran, Alam et al. 2019, Alam, Piazzesi et al. 2020).

The findings of the van Echten-Deckert group report that autophagic pathways altered by accumulated S1P vary among brain cell types, including microglia and neurons (Mitroi, Karunakaran et al. 2017, Karunakaran, Alam et al. 2019). Mitroi et al. (2017) have demonstrated that SGPL1 inhibited neuronal autophagy via reduced PE production in SGPL1-deficient neurons (PE is synthesized from ethanolamine phosphate, see Fig.1) (Mitroi, Karunakaran et al. 2017). Treatment of neurons with PE restored autophagy defects. Note that autophagy in the brain is assumed to be among the major causes of neurodegeneration (molecular mechanism of autophagy has been described in section 1.5). In contrast to that, Moruno-Manchon et al. (2015) observed that upregulated SK1, which catalyzes the phosphorylation of sphingosine forming S1P, stimulates autophagy in neurons while SPP and SGPL1, enzymes that degrade S1P, reduce autophagic flux (Moruno Manchon, Uzor et al. 2015). Another group has shown that SK2 has a primary role in preconditioning-induced autophagy. They used isoflurane and hypoxic preconditioning, which lead to the up-regulation of SK2 and induced autophagy by disrupting Bcl-2/beclin1 complexes in primary cortical neurons (Sheng, Zhang et al. 2014).

In the brain, apart from neurons, about 70% of cells are glial cells, constituting astrocytes, oligodendrocytes, and microglia (Jha, Jeon et al. 2012). S1P exerts specific action via the S1P receptors (S1PRs) on each of these cell types. In recent years, molecular mechanisms underlying S1P signaling have been extensively studied and well documented, with its functions linking inflammation (Snider, Orr Gandy et al. 2010, Aoki, Aoki et al. 2016). These aspects are briefly discussed in the following paragraph, given the specific action of S1P on various glial cell types.

Owing to a focus shift from neurons to the neuroglia (Seifert, Schilling et al. 2006), (Hanisch and Kettenmann 2007), microglia, the resident immune cells of the brain that represent about 10 % of the CNS cells, are increasingly recognized for their physiological role in the development, homeostasis and plasticity of the CNS (Salter and Stevens 2017). Microglia are the pivotal executors of immune functions (Hanisch and Kettenmann 2007), mediators of neurogenesis and other functions (De Lucia, Rinchon et al. 2016) that critically dictate the fate of neural cells. Uncontrolled inflammation from microglia has been

recognized as the common thread propelling neuronal injury in a host of neurodegenerative diseases (Cai, Hussain et al. 2014). Recent reports show that autophagy is a major mechanism that keeps microglial inflammation in check (Cho, Cho et al. 2014). Autophagy is critical for cell survival and maintenance of homeostasis (Yang and Klionsky 2010). Although the modulation of autophagy by sphingolipids has been known for quite a while (Lavieu, Scarlatti et al. 2006, Lepine, Allegood et al. 2011), the number of studies investigating this interrelationship in the brain wherein autophagy is indispensable to recycling aggregate prone proteins is relatively scant (Moruno Manchon, Uzor et al. 2015, van Echten-Deckert and Alam 2018). A recent study shows that supplementation of S1P to primary cultured microglial cells deprived of oxygen and glucose, leads to increased IL-17A expression (Lv, Zhang et al. 2016). Additionally, the van Echten-Deckert group has shown the link between autophagy and inflammation through S1P/S1PR2 in microglia cultured from neural targeted SGPL1 deficient mice (Karunakaran, Alam et al. 2019). These data suggest that the S1P metabolism is involved in the inflammatory response of activated microglia.

In astrocytes, SK1 and S1PR3 are functionally upregulated under pro-inflammatory conditions (Fischer, Alliod et al. 2011). Incubation with IL-1 induces the expression of SK1 (Paugh, Bryan et al. 2009), and exogenous S1P induces astrogliosis (Sorensen, Nicole et al. 2003). Moreover, S1PR1 modulation by FTY720, an S1P analog, in murine and human astrocytes suppressed neurodegeneration-promoting mechanisms mediated by astrocytes, microglia, and CNS-infiltrating proinflammatory monocytes (Rothhammer, Kenison et al. 2017). Dusaban et al. (2017) reported more conclusive proof of S1PR3's importance regarding an inflammatory cascade triggered in astrocytes (Dusaban, Chun et al. 2017). They found that astrocytes S1PR3 was up-regulated and involved with transforming protein RhoA. Additionally, S1P3 ligation was shown to promote IL-6, vascular endothelial growth factor A (VEGFa), and cyclooxygenase-2 (COX-2) (Dusaban, Chun et al. 2017).

## 1.5  AUTOPHAGY

Autophagy, a self-eating phenomenon, is an evolutionarily conserved process. The term autophagy was first introduced in 1966, which means "self-eating" in Greek (De Duve and Wattiaux 1966).  Autophagy is a dynamic recycling system with an essential function in maintaining cellular and tissue homeostasis securing survival during critical circumstances, including nutritional deficiency, hypoxia, and other stressful conditions (van Echten-Deckert and Alam 2018). Previously, the main role of autophagy was recognized as the degradation of dysfunctional proteins and unwanted organelles. However, in recent years, autophagy has emerged as an adaptive response to exogenous stimuli, a housekeeper mechanism for cells to maintain a steady state, and a defense mechanism to remove the damaged metabolites. (Levine and Yuan 2005, Mizushima and Komatsu 2011). Depending on the different ways cellular material is transported to lysosomes, there are three types of autophagy: microautophagy, macroautophagy, and chaperone-mediated autophagy (CMA). Macroautophagy is the most well-studied and commonly referred to as autophagy(Mizushima and Komatsu 2011). Homologous genes involved in autophagy are highly conservative during the evolution process from yeasts to humans. In 2003, Klionsky named these homologous genes as autophagy-related genes *(atg)* the corresponding proteins (ATG) to unify the standard (Klionsky, Cregg et al. 2003). Autophagy starts with sequestrating a membrane of non-lysosomal origin to form an isolation membrane (phagophore) around the cellular components targeted for degradation (Mizushima, Levine et al. 2008, Menzies, Fleming et al. 2015). The isolated membrane starts forming a double-membrane structure called an autophagosome. The targeted components are not degraded until the autophagosomes fuse with lysosomes and form autolysosomes. The acidic environment inside the lysosomes, which is required to activate lysosomal enzymes (including proteases, lipases, glycosidases, and nucleases), degrade the targeted components. The molecular mechanism of autophagy has been extensively studied and is still evolving (Ohsumi 2014). There are more than 30 highly conservative genes that have been confirmed to be related to autophagy. The autophagy molecular mechanism is very well reviewed in recent publications (Fig.2) (Ward, Martinez-Lopez et al. 2016, van Echten-Deckert and Alam 2018).

Various internal and external signaling pathways regulate autophagic machinery:  such as deprivation of growth-promoting stimuli (growth factors, amino acids, ATP) activates

autophagy via mTORC1 (mammalian or mechanistic Target of Rapamycin Complex 1) and AMPK signaling pathways (Ward, Martinez-Lopez et al. 2016). mTORC1, known as the classical regulator of autophagy, was first discovered in yeast (Williams, Sarkar et al. 2008). mTOR is inhibited when nutrients are scarce when growth factor signaling is reduced, and under ATP depletion and vice-versa. In addition to the extensively researched mTORC1-dependent regulation, autophagy can also be activated or downregulated via mTOR-independent pathways (Williams, Sarkar et al. 2008, Ward, Martinez-Lopez et al. 2016, Mitroi, Karunakaran et al. 2017).
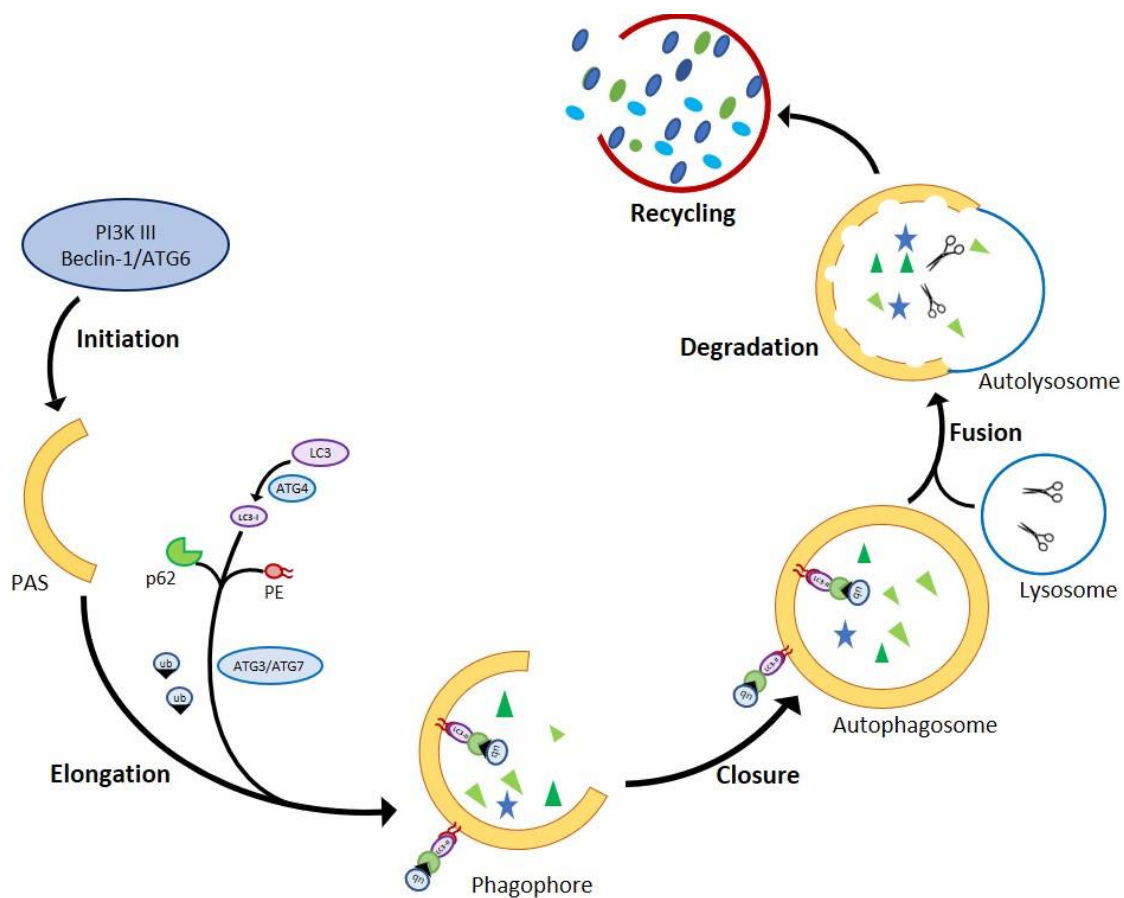


**Figure 2. A simplified model of autophagy.** Autophagy starts with the formation of a phagophore at the phagophore assembly site (PAS). The phagophore then expands by recruiting degradation-prone material, including ubiquitinated proteins via, e.g., the lipidated membrane-bound LC3-II and the adapter p62. The mature autophagosomes fuse with lysosomes generating autolysosomes in which degradation of the cargo occurs. Degraded material can be recycled after efflux into the cytoplasm. Abbreviations used are ATG, proteins encoded by autophagy-related genes; LC3, microtubule-associated protein light chain; PE, phosphatidylethanolamine; p62, also known as sequestosome 1; ub, ubiquitin (van Echten-Deckert and Alam 2018).

## 1.6 ASTROCYTES

Astrocytes are considerably abundant glial cells in the central nervous system (CNS) (Schildge, Bohrer et al. 2013). As the brain complexity increases in terms of phylogeny, the relative number of astrocytes increases (Nedergaard, Ransom et al. 2003). For example, the astrocyte to neuron ratio in the human cortex is 1:4 whereas, in *Caenorhabditis elegans*, neurons outnumber glia by 1:6 (Nedergaard, Ransom et al. 2003, Schildge, Bohrer et al. 2013). Astrocytes originate during the late prenatal to early postnatal stages from radial glial cells. After terminal differentiation, astrocytes start maturing, and in about 3-4 weeks, they achieve their typical morphology as they become mature (Bushong, Martone et al. 2002).

Astrocytes have traditionally been considered ancillary satellite cells of the nervous system (Nedergaard, Ransom et al. 2003) (astrocyte meaning "glue" in Greek (Volterra and Meldolesi 2005)). Their most crucial function is to provide structural and metabolic support to neurons, including energy delivery, production, utilization, and storage. In recent years, the research on astrocytes has been dramatically increased (Cui, Allen et al. 2001, Belanger, Allaman et al. 2011). Newly discovered roles for astrocytes cover a broad spectrum of functions, such as involvement in the formation of the blood-brain barrier (BBB) (Bozoyan, Khlghatyan et al. 2012), neural transmission, and synapse formation (Eroglu and Barres 2010, Sasaki, Matsuki et al. 2011, Min and Nevian 2012). In addition, astrocytes play an essential role in developmental synapse formation through physical support and secreted molecules such as modulating synaptic glutamate levels, purines (ATP and adenosine), and GABA (Ullian, Sapperstein et al. 2001, Neal and Richardson 2018, Karunakaran, Alam et al. 2019). The direct and interactive role of astrocytes in synaptic activity is essential for information processing by neural circuits, has given rise to the 'tripartite synapse' hypothesis (Araque, Parpura et al. 1999, Halassa, Fellin et al. 2007, Perea, Navarrete et al. 2009). A growing number of evidence suggests that astrocytes provide energy substrate to neurons (Alle, Roth et al. 2009). Astrocytes import glucose through glucose transporter 1 (GLUT1) from peripheral blood circulation, activating the glycolytic pathway and ATP generation (Staricha, Meyers et al. 2020). Additionally, astrocytes play a significant role in response to CNS injury, leading to drastic changes in themselves, and this phenomenon is known as reactive astrogliosis (Fig. 3) (Filous and Silver 2016).
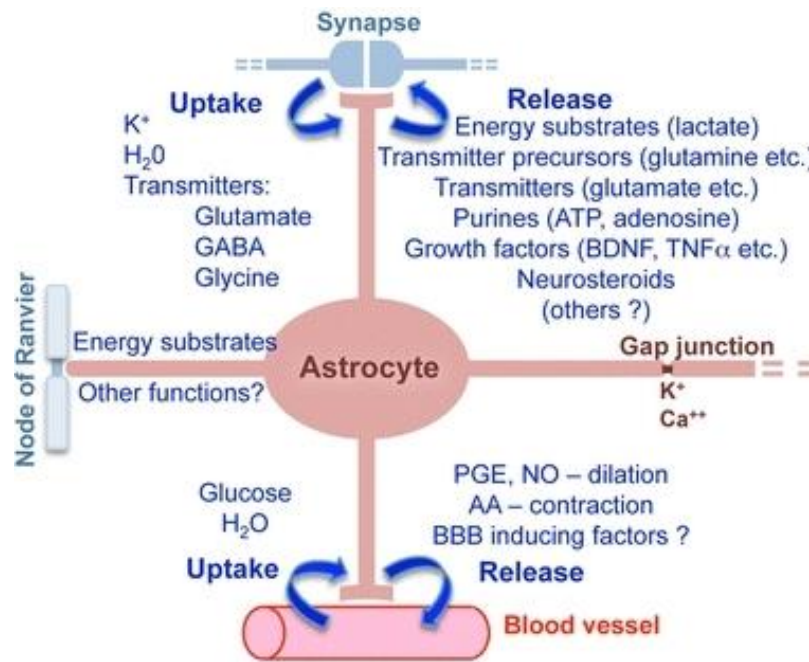
**Figure 3. Summary of functional interactions of astrocyte in healthy CNS.** Astrocytes have processes that, on the one hand, contact blood vessels and, on the other hand, contact in synapses. Astrocytes titrate blood flow in relation to levels of synaptic activity via these contacts. Astrocyte processes enclose largely all synapses and exercise essential functions in maintaining the fluid, ion, pH, and transmitter homeostasis of the synaptic interstitial fluid in a manner that is critical for healthy synaptic transmission. The transmitters are converted by enzymes such as glutamine synthetase into precursors such as glutamine and recycled back to synapses for reconversion into active transmitters. Astrocyte's processes take up glucose from blood vessels and contact neuronal perikarya, axons (at nodes of Ranvier), and synapses to provide energy metabolites to different neural elements in gray and white matter. Astrocytes can also couple to neighboring astrocytes through gap junctions formed by connexins, and that the gap junctional coupling of astrocytes into multicellular networks may play a role in both normal functions and CNS disorders. GABA, gamma-aminobutyric acid; ATP, adenosine triphosphate; BDNF, brain-derived neurotrophic factor; TNFα, tumor necrosis factor-alpha; PGE, prostaglandin E2; NO, Nitric oxide; BBB, blood-brain barrier; (Sofroniew and Vinters 2010)

## 1.7 ASTROGLIOSIS (REACTIVE ASTROCYTES)

Astrogliosis was often referred to as an increased expression of GFAP, as it was referred to as a single uniform entity (Sofroniew 2015). As of now, this is categorically not the case (Sofroniew 2015). Reactive astrogliosis is a multi-staged process (Fig. 4) (Sofroniew 2009, Neal and Richardson 2018). It is an evolutionarily conserved response characterized by both molecular and morphological changes. The morphological changes are accompanied by a reduction in the number of primary branches and hypertrophy of the cell body and

remaining processes (Neal and Richardson 2018).The molecular-level changes include widely recognized, increased expression of GFAP, vimentin, nestin, and secretion of inflammatory cytokines. Astrogliosis cover up a large spectrum of heterogeneous potential changes, and these changes are determined in a context-specific manner by diverse marking events that vary with the nature and severity of different CNS insults (Fig.4). Recent transcriptomic studies have also revealed other reactive-astrocyte genes *Tnf* (Tumor Necrosis Factor), *Il1β* (Interleukin 1 beta), that are more specific to certain types of reactive astrocytes and are highly expressed than *Gfap*. (Liddelow and Barres 2017).
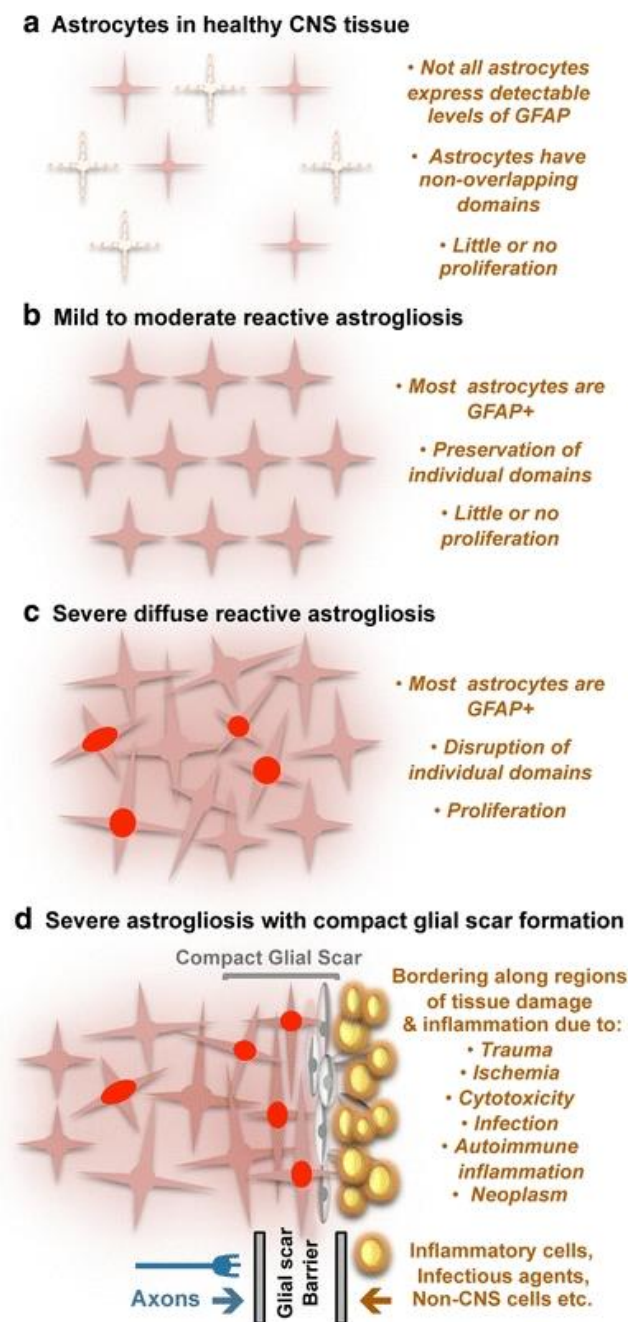


**Figure 4. Schematic representation of multi-staged reactive astrogliosis. (a)** Astrocytes in healthy CNS tissue. **(b)** Changes in molecular expression and functional activity together as astrogliosis progress. Moderate reactive astrogliosis involves variable degrees of cellular hypertrophy. **(c)** Severe diffuse reactive astrogliosis includes changes in molecular expression, functional activity, and cellular hypertrophy, as well as newly proliferated astrocytes (with red nuclei in the figure), disrupting astrocyte domains and causing a long-lasting reorganization of tissue architecture. Such changes are found in areas surrounding severe focal lesions, infections, or areas responding to chronic neurodegenerative triggers. **(d)** Severe reactive astrogliosis with compact glial scar formation occurs along borders to areas of overt tissue damage and inflammation. It includes newly proliferated astrocytes (with red nuclei in figure) and other cell types (gray in figure) such as fibromeningeal cells and other glia and dense collagenous extracellular matrix depositions. In the compact glial scar, astrocytes have densely overlapping processes. Mature glial scars tend to persist for long periods and act as barriers to axon regeneration and inflammatory cells, infectious agents, and non-CNS cells in a manner that protects healthy tissue from nearby areas of intense inflammation (Sofroniew and Vinters 2010).

## 1.8 REACTIVE ASTROCYTES AND NEUROINFLAMMATION

Many reports have already linked reactive astrocytes and inflammatory processes that can lead to neurodegeneration. Astrogliosis can be triggered by inflammation and vice-versa depending on the extent of gliosis and the specific signaling pathways activated (Fig.5) (Sofroniew 2015, Liddelow and Barres 2017).
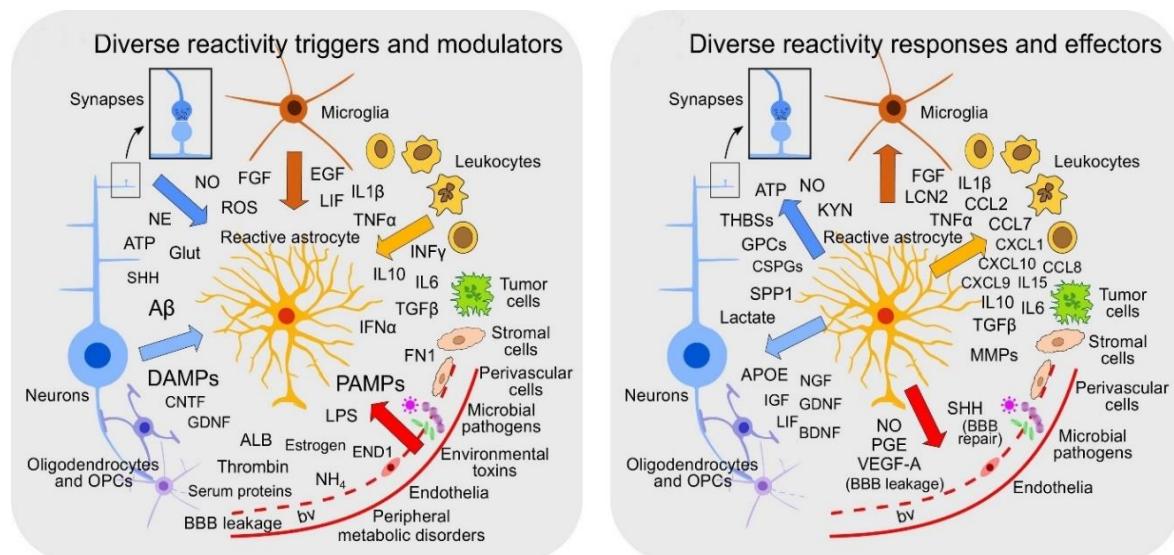


**Figure 5. Astrocytes give and take responses to CNS insults**. Astrocytes can be both targets of (left) as well as responders (right). Abbreviations: Aβ, amyloid β; ALB, albumin; APOE, apolipoprotein E; BBB, blood-brain barrier; bv, blood vessel; BDNF, brain-derived neurotrophic factor; CNS, central nervous system; CNTF, ciliary neurotrophic factor; CSPGs, chondroitin sulfate proteoglycans; DAMP, damage- or danger-associated molecular pattern; EGF, epidermal growth factor; FGF, fibroblast growth factor; GDNF, glial cell-derived neurotrophic factor; Glut, glutamate; GPCs, glypicans; KYN, kynurenine; IFN, interferon; IGF, insulin-like growth factor; Il, interleukin; LIF, leukemia inhibitory factor; LPS, lipopolysaccharide; MMP, matrix metallopeptidase; NE, norepinephrine; NGF, nerve growth factor; NO, nitric oxide; OPC, oligodendrocyte progenitor cell; PAMP, pathogen-associated molecular pattern; ROS reactive oxygen species; TGF, transforming growth factor; THBSs, thrombospondins; TNF, tumor necrosis factor (Sofroniew 2020)

Dysfunction in astrocytes leads to dysfunction in other cell types too via cell-to-cell communication. Reactive astrocytes activate microglia, which secrete inflammatory factors leading to neuronal cell dysfunction and death, culminating in producing the disease states found in neurodegenerative diseases (Fig.6) (Neal and Richardson 2018).
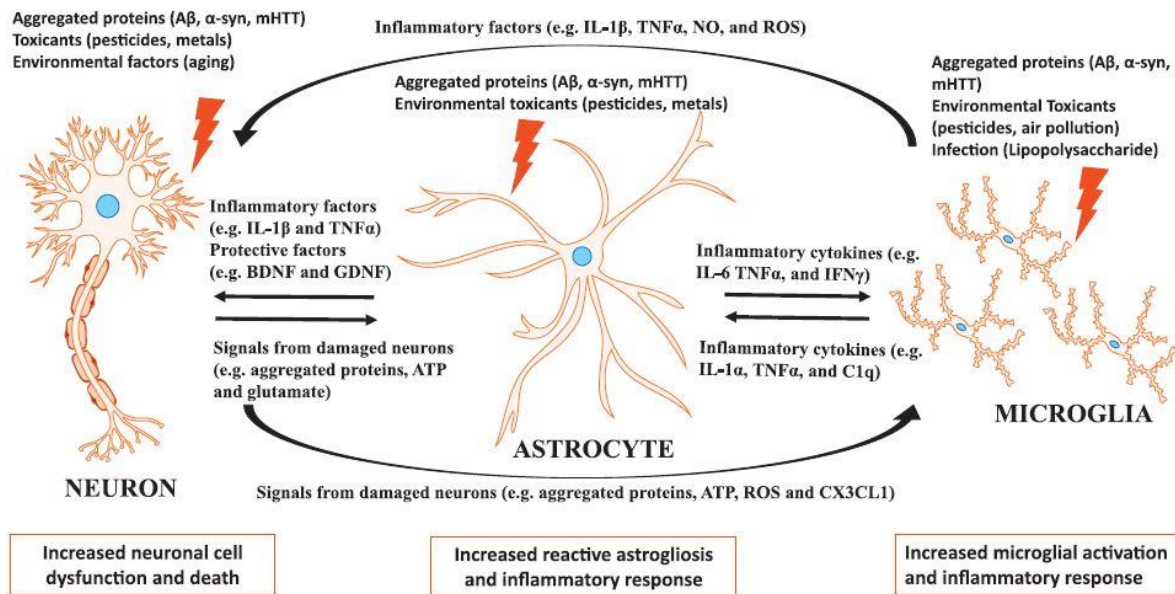
**Figure 6. Interaction between neurons, astrocytes, and microglia in response to CNS insults**. Aggregated proteins and environmental factors such as aging, and brain infections are recognized hallmarks of neurodegenerative diseases. Therefore, in response to any CNS insults, the three primary cell types: neurons, astrocytes, and microglia, communicate to each other via various factor involving aggregated proteins such as amyloid β (Aβ), α-synuclein (α-syn), toxicants, reactive oxygen species (ROS). In addition, these cells respond by releasing ATP, glutamate, Cx3cl1 or secreting inflammatory cytokines IL-1β and TNFα. (Neal and Richardson 2018).

## 1.9 PURINERGIC RECEPTOR 1 (P2Y1R) SIGNALING IN ASTROCYTES

In 1976, first-time purinergic receptors were well-defined (Burnstock 1976), and two years later, They were classified as P1 receptor for adenosine and P2 receptor for ATP and ADP (Burnstock, Fredholm et al. 2011). Further, the P2 receptor was distinguished in P2X and P2Y based on pharmacology and molecular cloning (Abbracchio and Burnstock 1994). P2X receptors are ligand-gated ion channel receptors, and P2Y receptors are G-protein-coupled receptors. P2Y receptors are further divided based on phylogenetic similarity; the presence of amino acids is important for ligand binding and selectivity of G-protein coupling (Abbracchio, Burnstock et al. 2009). Two distinct P2Y subgroups are recognized with a high level of sequence divergence. The first subgroup includes P2Y1, P2Y2, P2Y4, P2Y6, and P2Y11, and the second subgroup includes P2Y12, P2Y13, and P2Y14 (Abbracchio, Burnstock et al. 2006, Abbracchio and Verderio 2006). P2Y1R, a metabotropic receptor, has wide distribution among neurons, astrocytes, and microglia. P2Y1R plays a key role in

astrocytes in entraining the propagation of short-term calcium waves throughout the astrocyte network (Abbracchio and Burnstock 1994, Abbracchio and Verderio 2006). By any means, activated astrocytes release ATP and respond via P2Y1R with an increased propagating wave of intracellular calcium, allowing cell-to-cell communication.(Abbracchio and Verderio 2006, Burnstock, Fredholm et al. 2011, Delekate, Fuchtemeier et al. 2014).
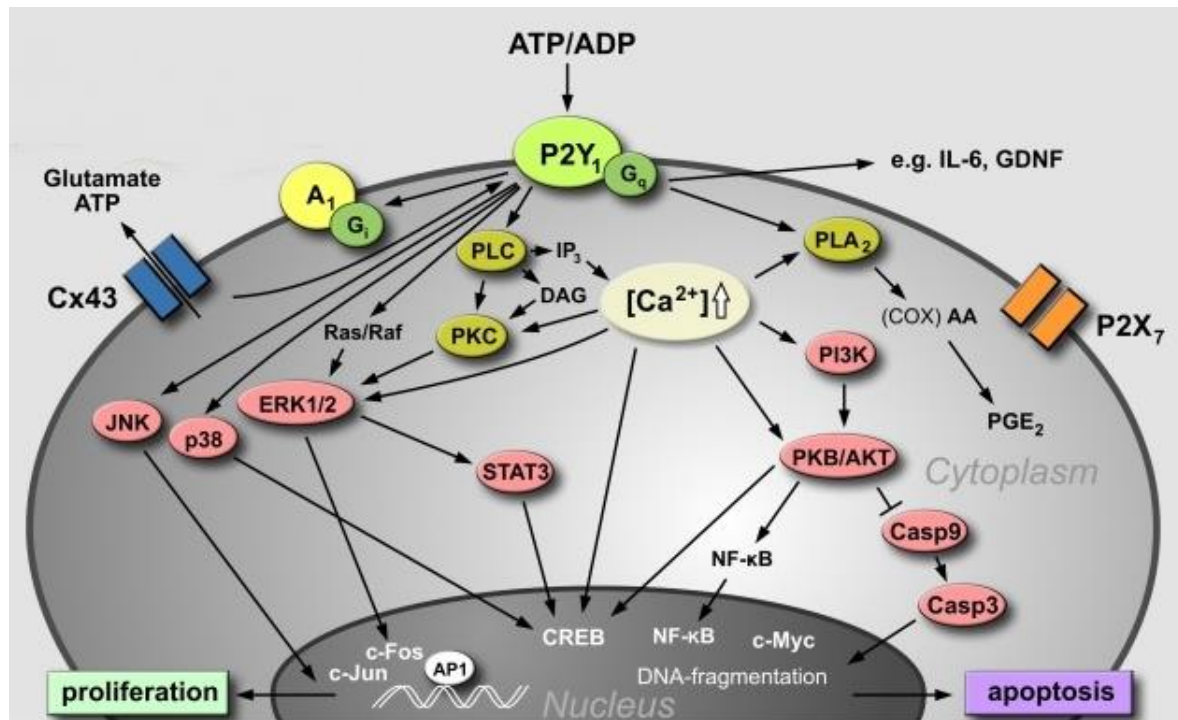


**Figure 7. Diagram summarizes the signal transduction pathway of P2Y1R-mediated effects in astrocytes.** ATP or ADP can trigger the P2Y1R signaling cascade. Upon binding of ATP/ADP, P2Y1Rs start signaling cascades, e.g., activation of the mitogen-activated protein kinase (MAPK) pathway proteins (ERK1/2), p38 MAPK, c-Jun N-terminal kinase (JNK), and PI3K/Akt activation. P2Y1R can also induce the release of a second messenger (Ca$^{++}$). P2Y1R-mediated signal transducer and activator of transcription 3 (STAT3) signaling may play a role in astrocyte proliferation and reactive astrogliosis. The present data suggest that astroglial P2Y1R stimulation is associated with neurological disorders leading to neuroinflammation and apoptosis (Franke, Verkhratsky et al. 2012).

## 1.10 GLUCOSE METABOLISM IN ASTROCYTES

Glucose is key to energy consumption. All metabolites, including carbohydrates and proteins, ultimately convert into glucose that enters the tissue cells and further converts to ATP. Glucose also serves as the primary precursor for synthesizing different carbohydrates, including glycogen, ribose, deoxyribose, galactose and all other epimers that are part of glycolipids, glycoproteins, and proteoglycans.

An adult human brain uses about 25% of glucose consumed by the body, while it constitutes only 2% of body mass (Oyarzabal and Marin-Valencia 2019). Most of the energy produced in the brain is dedicated to supporting synaptic transmission. Major brain cells, astrocytes, and neurons utilize glucose quite differently. Astrocytes are mostly glycolytic, whereas neurons are predominantly oxidative (Magistretti and Allaman 2015). By position, astrocytes are well established around neuronal synapses. So, there is no doubt glucose oxidation exceeds in astrocytes as more ATP is consumed for the synthesis of glutamine, packaging of neuronal glutamate into synaptic vesicle for the glutamate-glutamine neurotransmitter cycling process (Volterra and Meldolesi 2005).

Astrocytes are mostly glycolytic, which means the end product of glycolysis, pyruvate, is not further metabolized considerably via the TCA. Three factors explain this phenomenon-first, high pyruvate dehydrogenase (PDH) phosphorylation inactivates the enzyme. Under basal conditions, astrocytes express high levels of *PDK4*, gene encoding PDH kinase 4, which facilitates the phosphorylation of PDH and keeps the complex in a less active state (Halim, McFate et al. 2010, Oyarzabal and Marin-Valencia 2019). Second, pyruvate kinase in astrocytes catalyzes transformation of phosphoenolpyruvate into pyruvate, thus upregulating glycolysis (Halim, McFate et al. 2010). Third, the highly active 6-phosphofructo-2-kinase/ fructose-2,6-biphosphatase enzyme in astrocytes is a positive regulator of glycolysis.

In contrast, this enzyme is less active in neurons because of its constant proteasomal-mediated degradation (Dienel 2019). In general, these results indicate that astrocytes favor the generation of lactate over acetyl-CoA via PDH. Later, lactate is transferred to the neuronal compartment for oxidation. This is the so-called astrocyte-neuronal lactate shuttle (ANLS) (Halim, McFate et al. 2010, Dienel 2019). ANLS proposes that neurons utilize lactate produced by neighboring astrocytes as an energy source (Dienel 2019).

## 1.11 TAU PHOSPHORYLATION

Tau protein was discovered in the mid-1970s by studying factors necessary for microtubule formation (Kolarova, Garcia-Sierra et al. 2012). Tau protein promotes tubulin assembly into microtubules, one of the major components of the neuronal cytoskeleton that defines the normal morphology and provides structural support to neurons (Kosik 1993).

Tubulin binding of tau is regulated by its phosphorylation state, which is regulated normally by the coordinated action of kinases and phosphatases on tau molecule (Mandelkow, Biernat et al. 1995, Wang and Mandelkow 2016). In pathological conditions, such as the case in AD, not only does abnormal phosphorylation of tau protein decrease its tubulin binding capacity leading to microtubule disorganization, but also this protein self-polymerizes and aggregates in the form of neurofibrillary tangles (NFTs) (Avila 2008, Kolarova, Garcia-Sierra et al. 2012, Iqbal, Liu et al. 2016). Thus, there is no doubt that tau protein is essential regarding its involvement in the etiopathogenesis of AD and a family of related neurodegenerative disorders known as tauopathies (Iqbal, Liu et al. 2016).

Tau neurotoxicity has been linked to heterochromatin relaxation and hence to aberrant gene expression in tauopathies (Frost, Hemberg et al. 2014). Recently, an epigenome-wide study in which acetylation of lysine 9 of histone3 (H3K9ac) was used as a marker for transcriptionally active open chromatin also led to the conclusion that in aging and AD brains, tau pathology drives chromatin rearrangement (Klein, McCabe et al. 2019). Furthermore, in post-mortem AD brains, increased levels of acetylated H3 and H4 were detected and correlated with a load of hyperphosphorylated tau (Narayan, Lill et al. 2015).

## 1.12 HISTONE ACETYLATION

Nucleosomes, a fundamental unit of chromatin structure in eukaryotic cells, contain two copies each of the histone proteins H2A, H2B, H3, and H4. The core histone molecules make an octameric structure and the chromosomal DNA of 146 base pairs wrapped around it. The nucleosome is a highly conserved structure (Grunstein 1997). However, the N-terminal tails of the eight-core histones are exposed on the nucleosome surface and can be modified by acetylation, phosphorylation, methylation, ubiquitination ADP-ribosylation of specific amino acids (Turner 2000).

Histone acetylation and deacetylation are important gene regulation mechanisms. These reactions are controlled by the enzyme histone acetyltransferase (HAT) and histone deacetylase (HDAC). Histone acetylation is a covalent and reversible post-translational modification where an acetyl chemical group (CO-CH3) is added to the lateral chain of a positively charged lysine residue (Bonnaud, Suberbielle et al. 2016). Acetylation turns positively charged histone tail to neutral, leading to loosening the nucleosome components' (Grunstein 1997). Loosened core histone molecules make DNA more accessible to transcription factors, resulting in more transcription. Thus, acetylation of histones is known to increase the expression of genes (Eberharter and Becker 2002). HDAC performs the deacetylation of histone tails and, the DNA gets wrapped around the histone cores more tightly, making it harder for transcription factors to bind to the DNA, ultimately resulting in decreased levels of gene expression (de Ruijter, van Gennip et al. 2003) (Gallinari, Di Marco et al. 2007).

Tau neurotoxicity has been linked to heterochromatin relaxation and hence to aberrant gene expression in tauopathies (Frost, Hemberg et al. 2014). Studies in primary cultured neurons revealed that nuclear tau directly regulates pericentromeric heterochromatin integrity that appears disrupted in AD neurons (Mansuroglu, Benhelli-Mokrani et al. 2016). Recently, an epigenome-wide study in which acetylation of lysine9 of histone3 (H3K9ac) was used as a marker for transcriptionally active open chromatin also led to the conclusion that aging and AD brains, tau pathology drives chromatin rearrangement (Klein, McCabe et al. 2019). Remarkably, in a tumorigenic cell line, S1P generated by SK2 was reported to specifically enhance acetylation of H3 and H4 at K9 and K5, respectively, by directly inhibiting histone deacetylases 1 and 2 (HDACs 1, 2) (Hait, Allegood et al. 2009).

## 1.13 AIM OF THE WORK

Previous studies in the mouse model (SGPL1$^{fl/fl/Nes}$) have confirmed the importance of S1P metabolism for presynaptic architecture and neuronal autophagy, known to be essential for brain health. Currently, this work aimed to investigate the effect of neural-targeted ablation of SGPL1 in astrocytes and microglia of SGPL1$^{fl/fl/Nes}$ mice. Increasing amounts of data highlight the importance and contribution of astrocytes to the inflammation occurring in neurodegenerative diseases (Sofroniew 2014) which formed the basis to investigate inflammation in astrocytes. Furthermore, histone acetylation in astrocytes were planned to be investigated as epigenetic regulation in CNS dysfunction and neurodegenerative diseases has been continuously elucidated in the current time (Neal and Richardson 2018).

Neuronal damage due to SGPL1 ablation might induce inflammation, and as microglia is a key regulator of inflammation in the brain these effects were planned to be investigated. Considering the significance of sphingolipids in autophagy and inflammation and the substantial role that microglial autophagy plays in controlling inflammation in the brain, therefore, it was planned to investigate the interaction of autophagy and inflammation in microglia of SGPL1-deficient mice.

# 2 RESULTS

## 2.1 SGPL1 EXPRESSION IN SGPL1<sup>FL/FL/NES</sup> MURINE BRAIN AND S1P LEVEL IN ASTROCYTES

S1P-lyase (SGPL1) irreversibly cleaves S1P, yielding EAP and hexadecenal, marking the exit point of the sphingolipid degradation pathway. In the current study, SGPL1 was ablated in neural cells of the murine brain. SGPL1 mRNA and protein expression were determined using qPCR and western immunoblotting, respectively. There was a considerable reduction in both mRNA and protein expression of SGPL1 in brain tissues and neural cells (Fig.8A-B). SGPL1 expression was reduced by about 75-80% in brain tissue (cortex and hippocampus) as well as in primary cultured astrocytes derived from SGPL1-deficient mice, compared to the respective controls. Moreover, expression of SGPL1 was reduced by about 95-98% in neurons cultured from SGPL1-deficient mice compared to controls (Fig.8A-B).

Mitroi et al. (2016) have already shown the accumulation of S1P and to a lesser extent sphingosine in mice brains due to SGPL1 ablation (Mitroi, Deutschmann et al. 2016). Presently, the level of lipids was assessed in primary astrocytes cultured from control and SGPL1-deficient mice (in cooperation with Prof. Markus Gräler, Jena). Similar to mice brains, S1P and sphingosine amounts were found to be increased in SGPL1-deficient astrocytes (Fig.8C-D) (In cooperation with Dr. Indulekha Karunakaran). Additionally, the level of S1P was increased in the culture media, which suggests that S1P was transported from cells into culture media (Fig.8D).
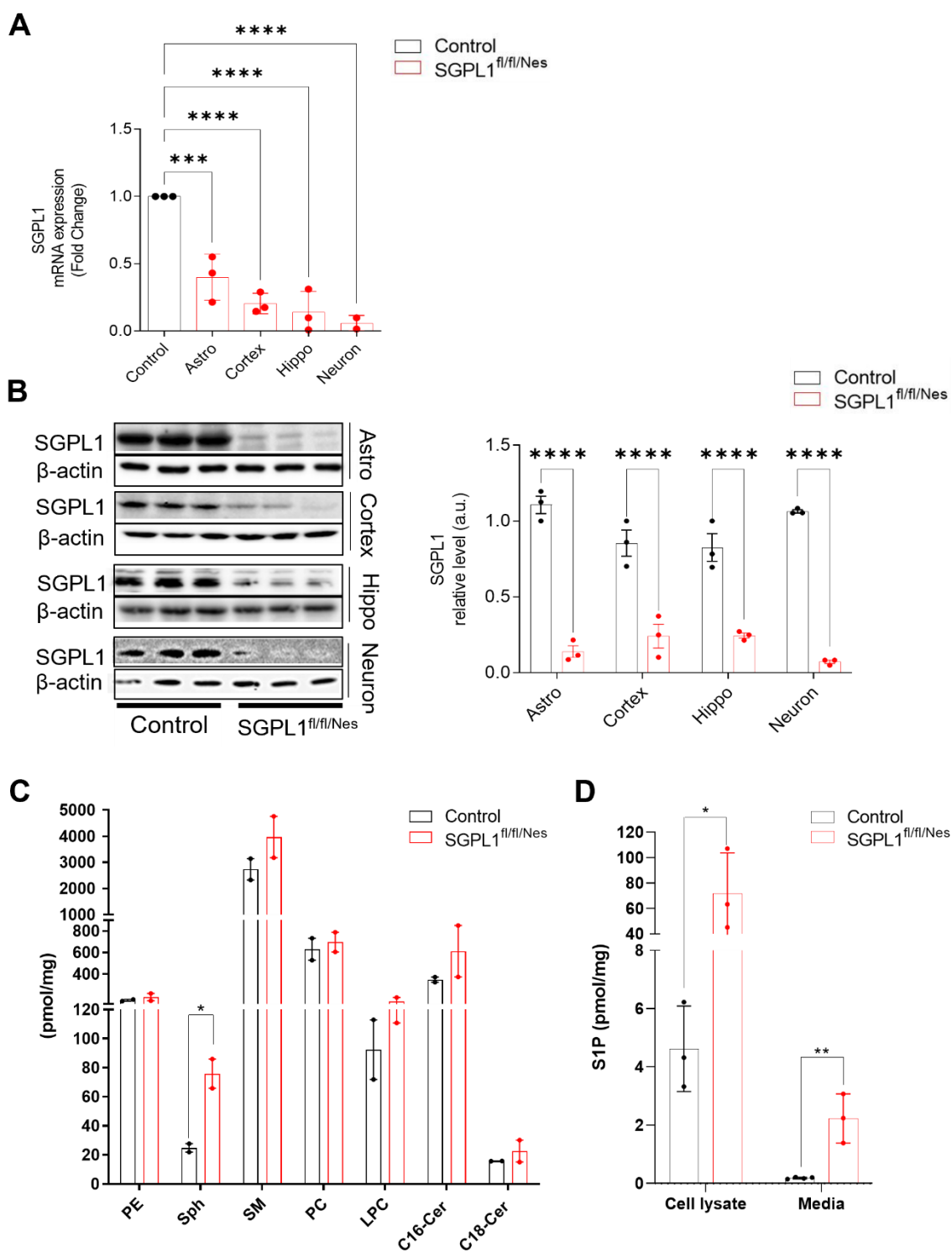
**Figure 8. SGPL1 expression in brain tissues/cells and level of lipids in SGPL1-deficient astrocytes. (A)** mRNA expression**, (B)** protein expression, and quantification of SGPL1 were assessed by qRT-PCR and western immunoblotting in astrocytes (Astro), cortex, hippocampus (Hippo), and neurons of control and SGPL1-deficient mice **(C)** The amounts of various lipids were determined by LC/MS/MS in primary astrocytes cultured from control and SGPL1-deficient mice. **(D)** The levels of S1P in cell lysates and media were measured in primary astrocyte cultures by ELISA. Cer16, C16-ceramide; Cer18, C18-ceramide; SM, sphingomyelin; Sph,

sphingosine; PE, Phosphatidylethanolamine; PC, Phosphatidylcholine; LPC, Lysophosphatidylcholine. Bars represent means ± SEM (n= 2-4, one-way ANOVA with Dunnett's multiple comparison test for qPCR and two-way ANOVA with Bonferroni's posts test for western blot, multiple unpaired t-tests for lipid content, *p<0.05, ****p<0.0005.) (see also suppl. Fig. 1 (Alam, Piazzesi et al. 2020) and Fig.1 (Karunakaran, Alam et al. 2019)).

## 2.2 NEURAL ABLATION OF SGPL1 TRIGGERS ASTROGLIOSIS IN MURINE BRAINS

Astrogliosis is a multi-staged process (Sofroniew 2009, Sofroniew 2010, Neal and Richardson 2018). Time and again, it was represented as an increased expression of GFAP. However, as of now, it is recognized as an evolutionarily conserved response characterized by both molecular and morphological changes. The molecular-level changes include increased expression of GFAP and secretion of inflammatory cytokines (Sofroniew 2015). Besides, a purinoreceptor, P2Y1R, was also shown to mediate astrocytic hyperactivity (Delekate, Fuchtemeier et al. 2014, Rodrigues, Tome et al. 2015).

An increased expression of GFAP was shown in the cortex of the SGPL1-deficient mice brain (Mitroi 2016). Presently, expression of GFAP and P2Y1R were investigated and found to be increased in SGPL1-deficient astrocytes (Fig.9A, B). Colocalization of GFAP and P2Y1R was shown by double immunofluorescence staining in the hippocampus and cortex of SGPL1-deficient murine brain (Fig.9C). Moreover, expressions of inflammatory cytokines were also investigated in SGPL1-deficient astrocytes. Expressions of IL-6, IL-11, and TNFα were found significantly increased (Fig. 9D). Furthermore, calbindin which regulates free calcium distribution (act as a buffer) in the cytoplasm, is thought to play a role in developing astrogliosis after ischemia (Toyoshima, Yamagami et al. 1996, Hong and Jeung 2013). Therefore, the expression of calbindin was investigated in primary cultured astrocytes and cortex of SGPL1-deficient mice. The expression of calbindin was found increased in primary cultured astrocyte and cortex of SGPL1-deficient mice (Fig.9E-F). These results confirmed the occurrence of astrogliosis in the SGPL1-deficient murine brain.
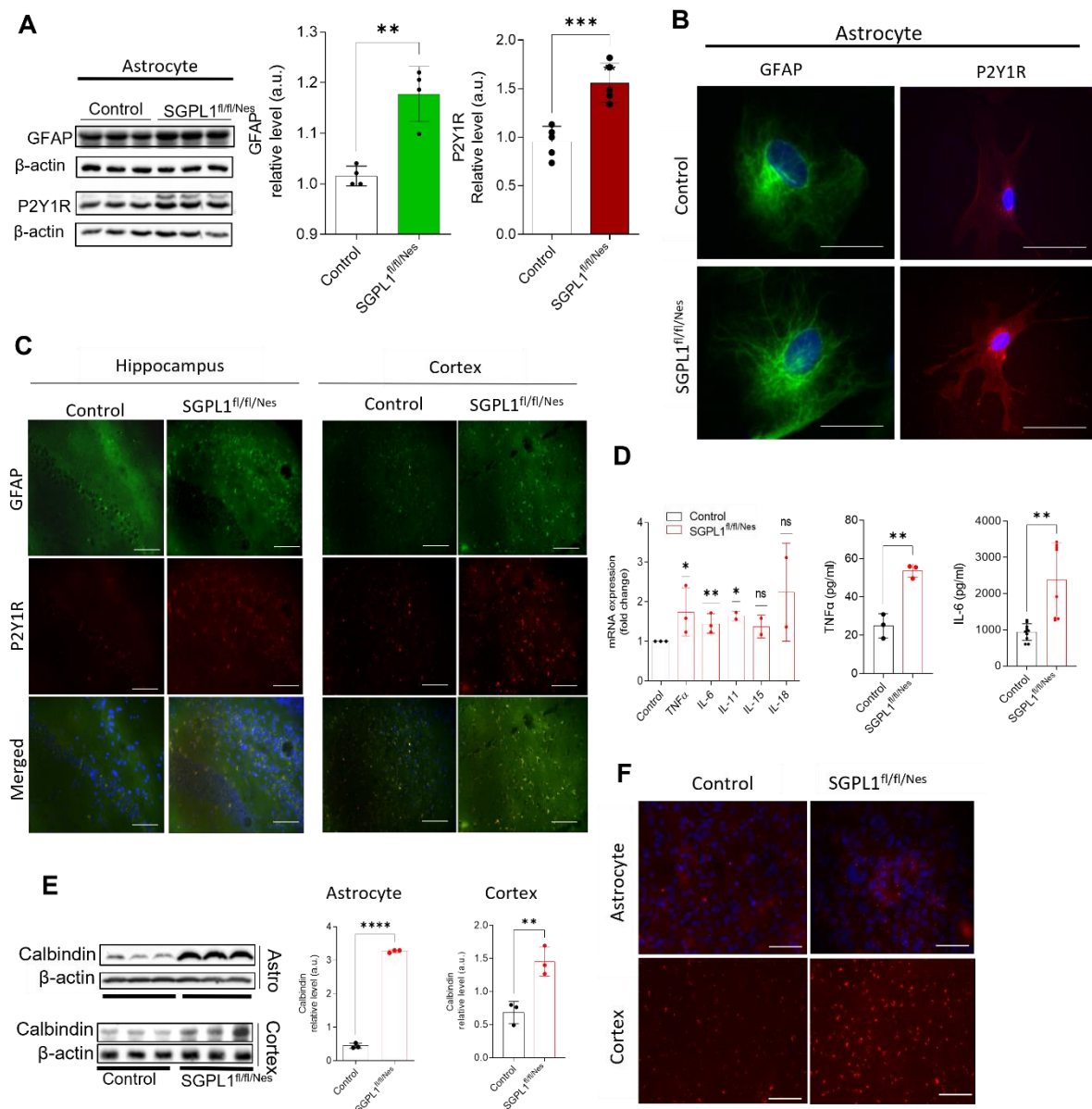
**Figure 9. SGPL1 deficiency causes astrogliosis in SGPL1^fl/fl/Nes murine brains.** (**A**) Immunoblots and quantification of GFAP and P2Y1R in SPGL1-deficient astrocytes. (**B**) Immunofluorescence image of GFAP and P2Y1R expression in single SPGL1-deficient astrocytes**.** (**C**) Confocal images of double immunofluorescence to characterize the expression of P2Y1R on activated astrocytes in the hippocampal and cortical slices of 15-months-old control and SGPL1-deficient mice. (**D**) Relative expression of the indicated cytokines in SGPL1-deficient astrocytes was assessed by qPCR, and IL-6 and TNFα were also quantified by ELISA. (**E**) western immunoblotting and quantification of calbindin in cultured astrocytes and cortex of SGPL1-deficient murine brain**.** (**F**) Representative fluorescence image of calbindin in cultured astrocytes and cortex of SGPL1-deficient murine brain. β-actin was used as a reference for western immunoblotting and qPCR. Bars represent means ± SEM (n ≥ 3; one way ANOVA with Dunnett's multiple comparison test for qPCR and student unpaired t-test for western immunoblotting; *p < 0.05; **p < 0.005; ***p < 0.0005). (Image of single astrocyte, scale bar, 50 μm, tissue section and astrocytes (calbindin) scale bar, 200 μm).

## 2.3 "INSIDE-OUT" SIGNALING OF S1P IN SGPL1-DEFICIENT ASTROCYTES

As shown above (Fig.8D), a part of the S1P accumulated in SGPL-deficient astrocytes was detected in the culture media. Other cell types have been shown to secrete or release S1P via membrane-located transporter proteins (Ihlefeld, Vienken et al. 2015). Therefore, the expressions of known S1P-transporters in SGPL-deficient astrocytes were investigated. Expression of commonly known ABC transporters (Abca1, Abcb1a, Abcb1b, Abcc1, and Abcg2) involved in S1P metabolism (Ihlefeld, Vienken et al. 2015) and a specific S1P transporter, spinster-2 (SPNS2), (Nagahashi, Kim et al. 2013, Spiegel, Maczis et al. 2019) were investigated via qPCR. Indeed, multidrug transporters Abca1, Abcb1b, and Abcc1 mRNA expression were upregulated about 2-fold, and SPNS2 was increased 2.5-fold in SGPL1-deficient astrocytes (Fig. 10A-B).

S1P is a lipid mediator that functions either as a second messenger or as a ligand for a family of 5 G-protein coupled receptors S1PR1-5. S1P released from astrocytes can bind as a ligand to S1PRs in an autocrine or paracrine manner and induces downstream signaling pathways. Therefore, the expression of S1PRs were investigated. The expression of S1PR2/4 were found to be increased in SGPL1-deficient astrocytes (Fig.10C). In section (2.6) S1PRs mediated effect have been described.
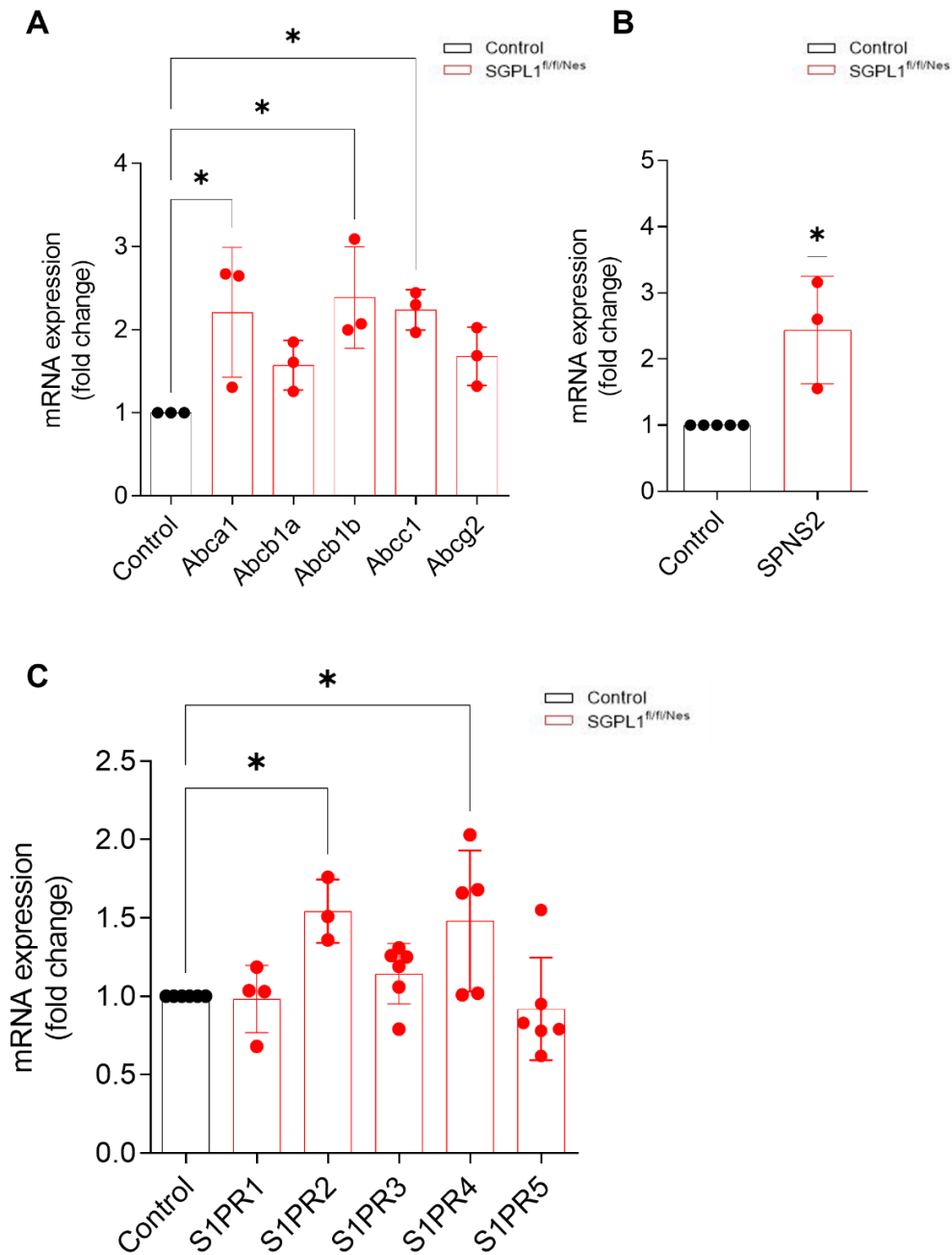
**Figure 10. Secretion and action of S1P in SGPL1-deficient astrocytes.** mRNA expression of ABC transporters (**A**), SPNS2 (**B**) and S1PRs (**C**) were determined by qPCR. ABC transporters (Abca1, Abcb1b, and Abcc1) mRNA expression was increased about 2-fold, and SPNS2 was increased 2.5-fold in SGPL1-deficient astrocytes. Among 5 S1PRs, receptors 2 and 4 were significantly increased in SGPL1-deficient astrocytes. β-actin was used as a reference. Bars represent means ± SEM (n=3-5; * P < 0.05; one-way ANOVA with Dunnett's multiple comparison test for ABC transporters and S1PRs; for SPNS2, one-sample t-test)

## 2.4 ENHANCED GLYCOLYSIS IN SGPL1-DEFICIENT ASTROCYTES

The expression of P2Y1R was increased in SGPL1-deficient astrocytes, indicating that there might be an increase of nucleotides (ATP or ADP) since nucleotides act as a ligand for P2Y1R (Gustafsson, Muraro et al. 2011). ATP released from cells into the extracellular space has a short half-life in the extracellular milieu before it is degraded to adenosine diphosphate (ADP), adenosine monophosphate (AMP), and adenosine, a process that in turn activates P2Y receptors (Ho, Yang et al. 2013). Therefore, ADP/ATP ratio was measured in astrocytes and culture medium. Interestingly, it was found that the ADP/ATP level was decreased in SGPL1-deficient astrocytes compared to control and vice-versa in cell culture media (Fig.11A). This result suggests that ATP released by cells in culture media was converted to ADP by ectonucleotidases.

Moreover, lower ADP/ATP ratio in astrocytes indicates an alteration in energy metabolism in SGPL1-deficient astrocytes. As glucose is the primary energy source in the brain hence, enzymes involved in glucose metabolism including, PFK, GAPDH, and PDH were investigated. Both mRNA and protein expressions of PFK, GAPDH, and PDH were found to be increased (Fig.11C-D). PDH is a part of the pyruvate dehydrogenase complex (PDC), which links the glycolytic pathway to the oxidative pathway of the Krebs's cycle (Patel, Nemeria et al. 2014). Therefore, the expression and activity of a rate-limiting Krebs's cycle enzyme (IDH2, found in mitochondrial matrix) was investigated. However, expression of IDH2 was not changed (Fig.11E). These results suggest that high glycolytic flux might favor the generation of lactate (over acetyl-CoA via PDH) via the so-called astrocyte-neuronal lactate shuttle (ANLS) (Oyarzabal and Marin-Valencia 2019). However, further research is needed to confirm this hypothesis. In addition, to find out how glucose was imported inside the cell, the expressions of glucose transporters (GLUTs) were investigated. Among 4 GLUTs, glucose transporter 2 (GLUT2) expression was found to be increased in SGPL1-deficient astrocytes (Fig.11B).
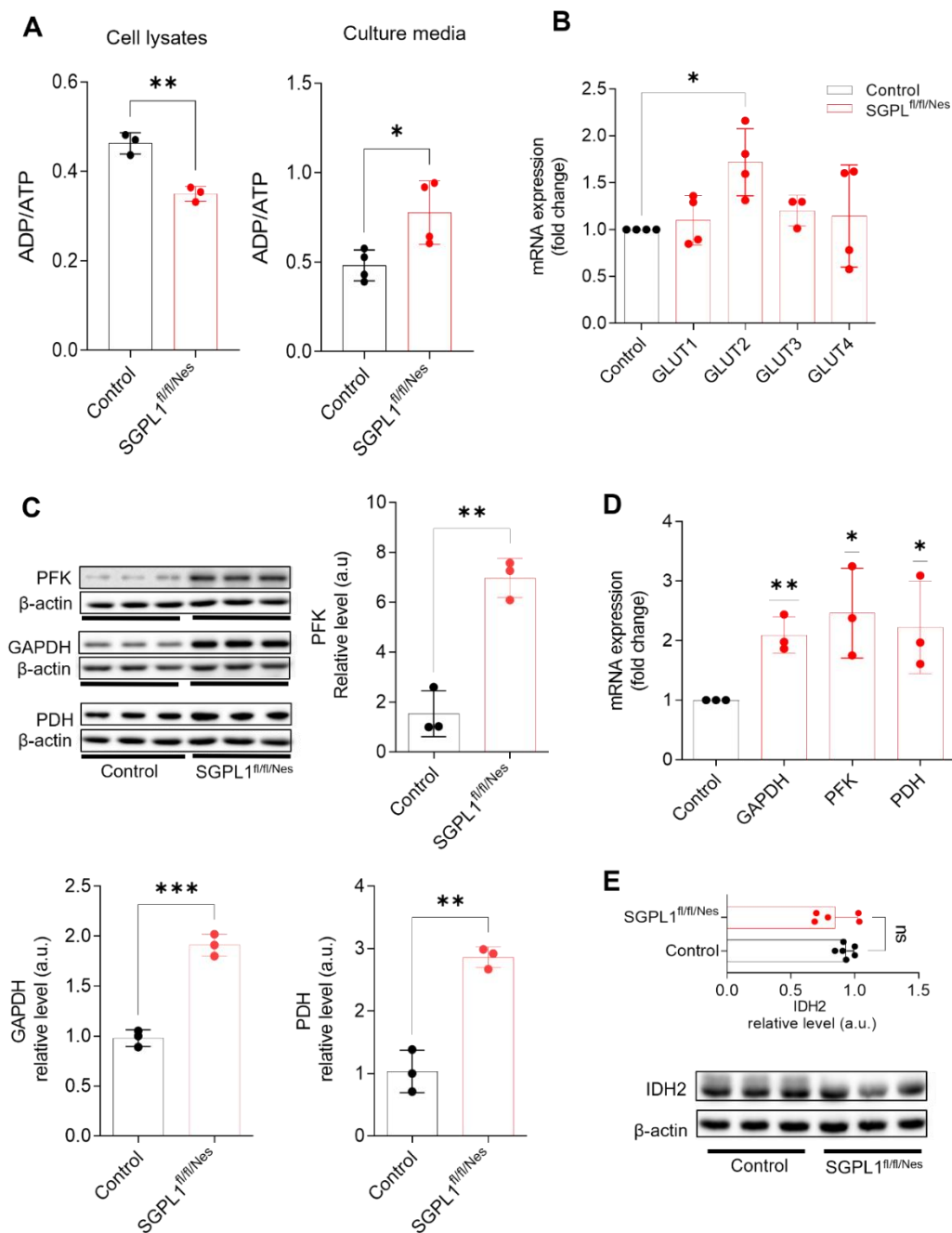
**Figure 11. Increased glycolysis in SGPL1-deficient astrocytes.** (**A**) Decreased ADP/ATP in astrocytes (left) while increased ADP/ATP ratio in the culture media (right). (**B**) mRNA expression levels of the GLUTs were assessed by qPCR. (**C**) Protein and (**D**) mRNA expression and quantification of glycolysis enzymes and PDH were assessed by western immunoblotting and qPCR. (**E**) Protein expression and quantification of IDH2 enzymes were assessed by western immunoblotting. β-actin was used as a reference for both qPCR and western immunoblotting. Bars represent means ± SEM (n ≥ 3; one-way ANOVA with Dunnett's multiple comparison test for GLUTs, one-sample t-test for glycolysis enzymes and PDH and student unpaired t-test for western immunoblotting; (Bars represent means ± SEM; n= 3-4; *p < 0.05; **p < 0.005, ***p < 0.0005).

## 2.5 mTOR DEPENDENT IMPAIRED AUTOPHAGY IN SGPL1-DEFICIENT ASTROCYTES

Mammalian target of rapamycin (mTOR) has crucial role in regulating various biological processes, including cell proliferation, energy metabolism, apoptosis and autophagy (Fan, Wu et al. 2021). Therefore, increased glycolysis prompted the investigation of autophagy in SGPL1-deficient astrocytes. Autophagy inducer protein beclin1 and a specific autophagic substrate p62, which recognizes and sequesters autophagic cargo, were assessed. Apart from these two autophagy markers, the conversion of LC3-I to its phosphatidylethanolamine-conjugated form LC3-II on the surface of elongating autophagosomal vesicles was determined. Beclin1 expression was increased, indicating a possible increase in autophagy (Fig.12A). However, increased p62 levels indicate (Fig.12A) a defective cargo processing. Further, LC3-II: LC3-I ratio was decreased (Fig.12A), showing autophagic flux blockage. To obtain further understanding on autophagy flux, the RFP–GFP tandem fluorescent-tagged LC3 (RFP–GFP–LC3) construct was expressed in astrocyte cultures from control and SGPL1[fl/fl/Nes] mice. This tandem fluorescent-tagged autophagosomal marker in which LC3 was engineered with both green-fluorescent protein (GFP) and red-fluorescent protein (RFP), allows the labelling of autophagosomes in yellow (merged green EGFP and red RFP fluorescence), whereas autolysosomes appear red only as acidification after autophagosome–lysosome fusion quenches GFP fluorescence. More autolysosomes (red puncta) were reduced in SGPL1-deficient astrocytes compared to controls (Fig. 12B).

mTOR promotes anabolic cellular processes leading to growth. This is further accelerated by the suppression of protein catabolism, particularly autophagy (Schmeisser and Parker 2019). Therefore, treatment with rapamycin (mTOR inhibitor) (500 nM, 5 h) decreased expression of p62 and beclin1 and rescued conversion of LC3-I to LC3-II, (Fig.12C-D) suggesting that S1P induced defective autophagy was mTOR dependent in SGPL1-deficient astrocytes.
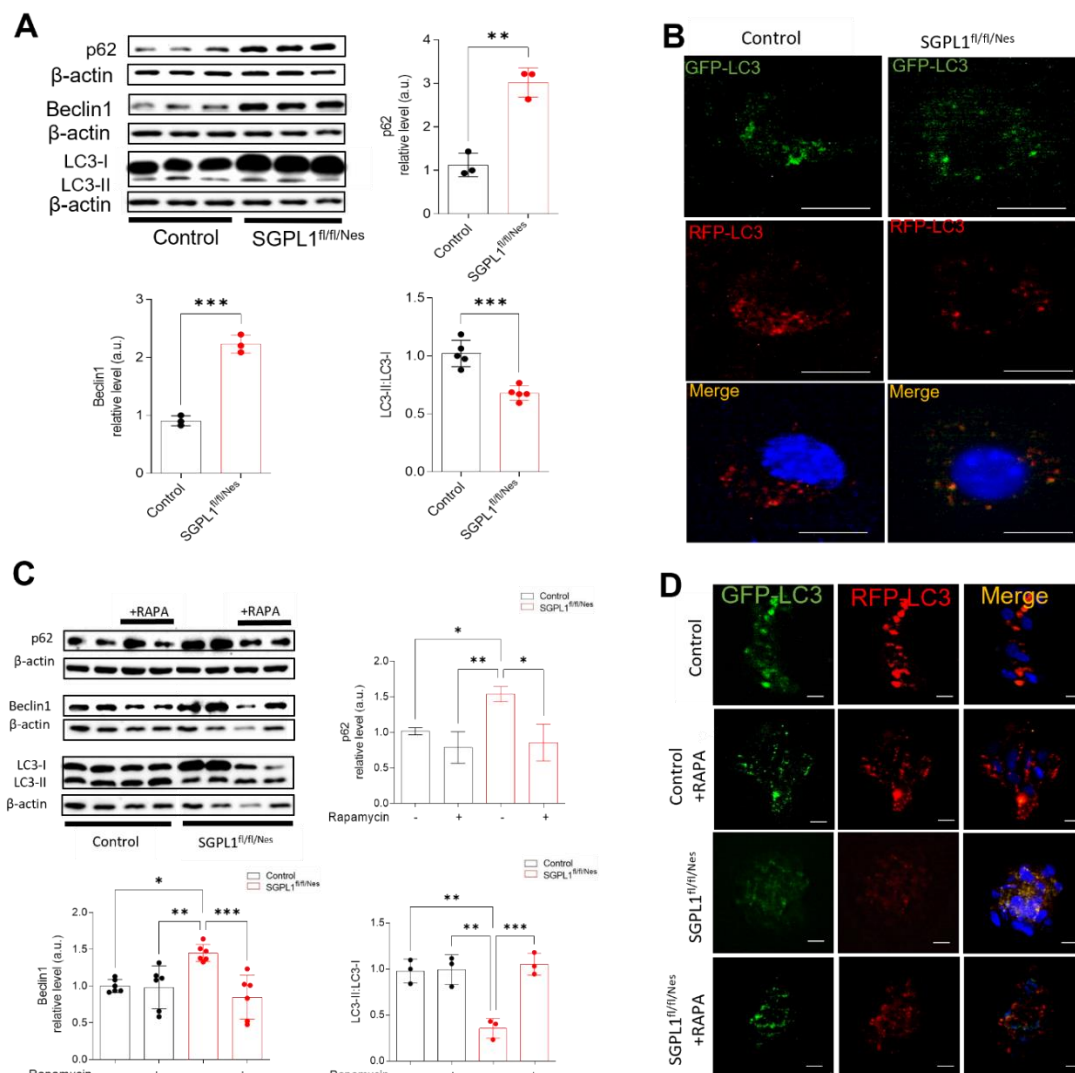
**Figure 12. Inhibition of mTOR rescued impaired autophagy in SGPL1-deficient astrocytes. (A)** Protein expression and quantification of autophagy marker proteins p62, beclin1, and LC3-II: LC3-I ratio were assessed by western immunoblotting. **(B)** Representative images showing the fluorescence of the RFP–GFP tandem fluorescent-tagged LC3 (RFP–GFP–LC3) construct, expressed in cultured astrocytes from SGPL1-deficient and control mice. Red puncta represent autolysosomes because the acidity of lysosomes quenches GFP. Yellow puncta represent autophagosomal structures as both GFP and RFP fluoresce at cytoplasmic pH. Merged confocal images demonstrated that most puncta were red in control astrocytes, showing that GFP had been quenched in lysosomes. In contrast, most puncta were yellow in SGPL1-deficient astrocytes implying autophagy flux blockage. Scale bar: 50 µm. **(C)** Protein expression and quantification of the autophagic marker proteins, p62 and beclin1 expression and the ratio LC3-II: LC3-I with and without rapamycin treatment in control and SGPL1-deficient astrocytes. **(D)** Images showing the fluorescence of the RFP–GFP tandem fluorescent-tagged LC3 (RFP–GFP–LC3) construct expressed with and without rapamycin treatment in control and SGPL1-deficient astrocytes. Scale bar: 200 µm. (Bars represent means ± SEM (n ≥ 3; student unpaired t-test; one way Bonferroni's multiple comparison test, *p < 0.05; **p < 0.005, ***p < 0.0005).

## 2.6 S1PR2/4 MEDIATES GLYCOLYSIS IN SGPL1-DEFICIENT ASTROCYTES

To determine the mechanism by which S1P contributes to the increased expression of glycolysis enzymes and PDH, it was assumed that the role of S1P might be receptor-mediated as S1PR2/4 were significantly increased in SGPL1-deficient astrocytes (Fig.9). Thereafter, astrocytes were treated with JTE-013 and CYM-55380 to inhibit S1PR2 and S1PR4, respectively. As shown in Fig.13, JTE-013 and CYM-55380 treatment (10 µM each, 3 h) reversed the expression of glycolytic enzymes and PDH (Fig13A). Since increased glycolytic flux was found to be S1PR2/4-mediated in SGPL1-deficient astrocytes, hence it was postulated that inhibiting S1PR2/4 could decrease ADP/ATP in culture medium and ultimately decrease P2Y1R expression. Therefore, ADP/ATP ratio and P2Y1R expression were determined in cells treated with and without JTE-013 and Cym-55380 treatment (10 µM, 3 h). Remarkably, S1PR2/4 inhibition increased ADP/ATP ratio in cells, vice-versa in medium (Fig.13B) and reversed P2Y1R expression (Fig.13C-D) in SGPL1-deficient astrocytes.
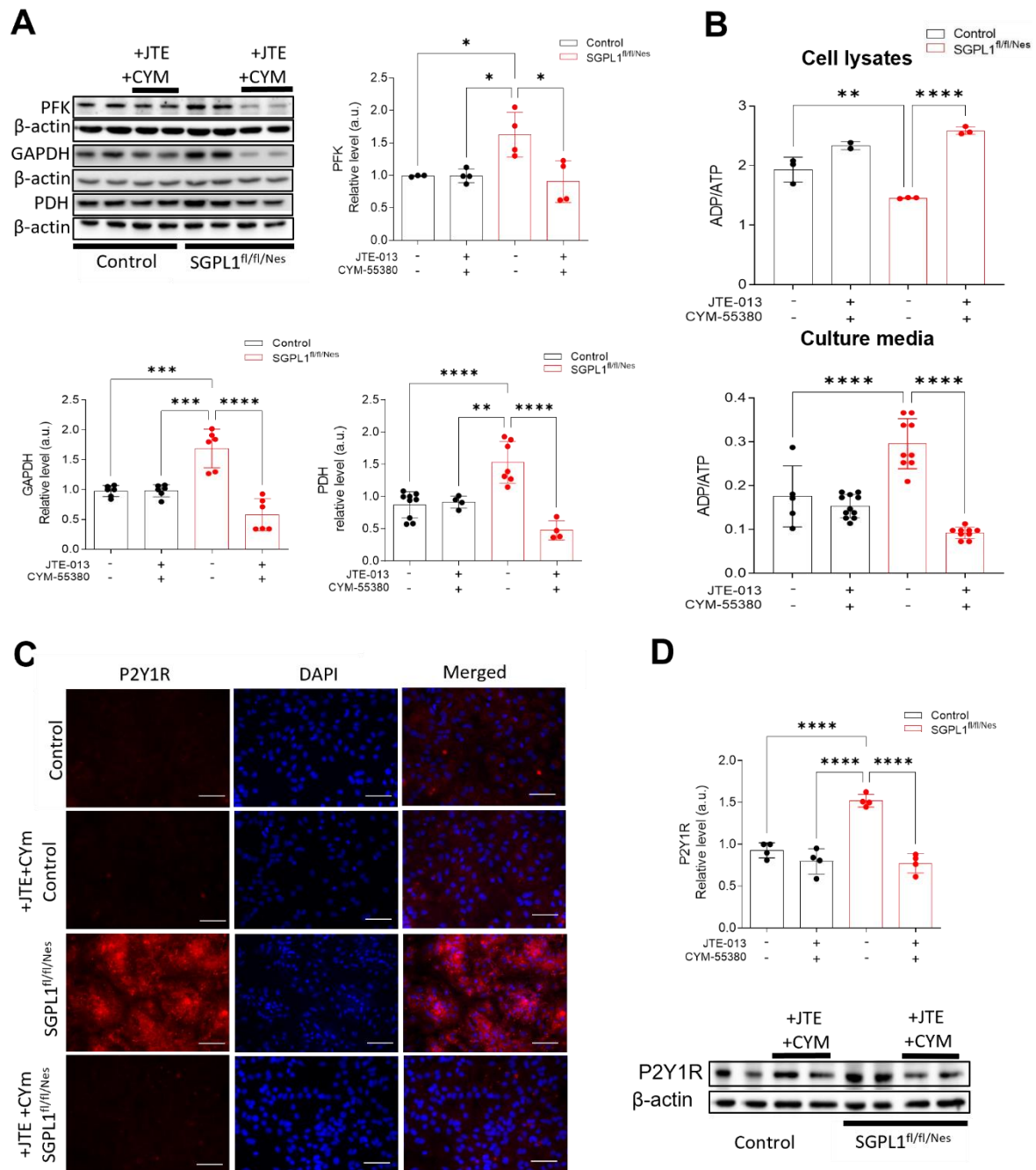
**Figure 13. S1PR2/4 inhibition rescued glycolysis and P2Y1R expression in SGPL1-deficient astrocytes. (A)** Protein expressions and quantification of PFK, GAPDH, and PDH were assessed by western immunoblotting. **(B)** S1PR2/4 inhibition increases ADP/ATP ratio in the cell and vice-versa in culture media in SGPL1-deficient astrocytes. **(C)** Representative images of astrocytes expressing P2Y1R with and without JTE-013/Cym-55380 and DAPI from control. **(D)** P2Y1R expression and quantification in SGPL1-deficient astrocytes with and without JTE-013/Cym-55380 treatment. Bar represents mean +/− S.E.M, one way ANOVA with Bonferroni's multiple comparison test (n=2-11, * $p < 0.05$, ** $p < 0.005$, *** $p < 0.0005$). Scale bar: 200 µm.

## 2.7   P2Y1R BLOCKADE NORMALIZED HYPERACTIVITY OF SGPL1-DEFICIENT ASTROCYTES

Several *in vitro* and *in vivo* experiments verified the important role of nucleotides in the reactive response of astrocytes to brain lesions or injury. Also, purinoceptors were found to regulate morphological remodeling, proliferation, and upregulation of GFAP synthesis. (Neary, Baker et al. 1994, Neary, Whittemore et al. 1994, Brambilla and Abbracchio 2001, Franke, Verkhratsky et al. 2012). Similarly, in cultured astrocytes, it was repeatedly shown that extracellular ATP and its structural analogs increase GFAP via purinoreceptors (Neary and Norenberg 1992, Neary, Whittemore et al. 1994). Moreover, P2Y1 receptors is known to mediate astrocytic hyperactivity in the APPPS1 mouse model (Delekate, Fuchtemeier et al. 2014). Since P2Y1R expression was also enhanced in the SGPL1-deficient murine brain, it was anticipated that inhibition of P2Y1R with a specific inhibitor, MRS2179 might reduce GFAP expression in SGPL1-deficient astrocytes. Application of MRS2179 (100 µM, 24 h) revealed that the GFAP expression were reduced is SGPL1-deficient astrocytes (Fig14C-D). Furthermore, P2Y1R is also known to stimulate calcium mobilization (Gustafsson, Muraro et al. 2011) and inflammation facilitation (Fujita, Tozaki-Saitoh et al. 2009).  Therefore, in MRS2179 treated astrocytes expression of calbindin and secretion of inflammatory cytokines were observed. Inhibition of P2Y1R reversed the expression of calbindin and IL-6 secretion, but not TNFα in SGPL1-deficient astrocytes (Fig.14 A-B, E-F)). These data indicate that P2Y1 receptor blockade normalizes astrocytic hyperactivity in SGPL1-deficient astrocytes.
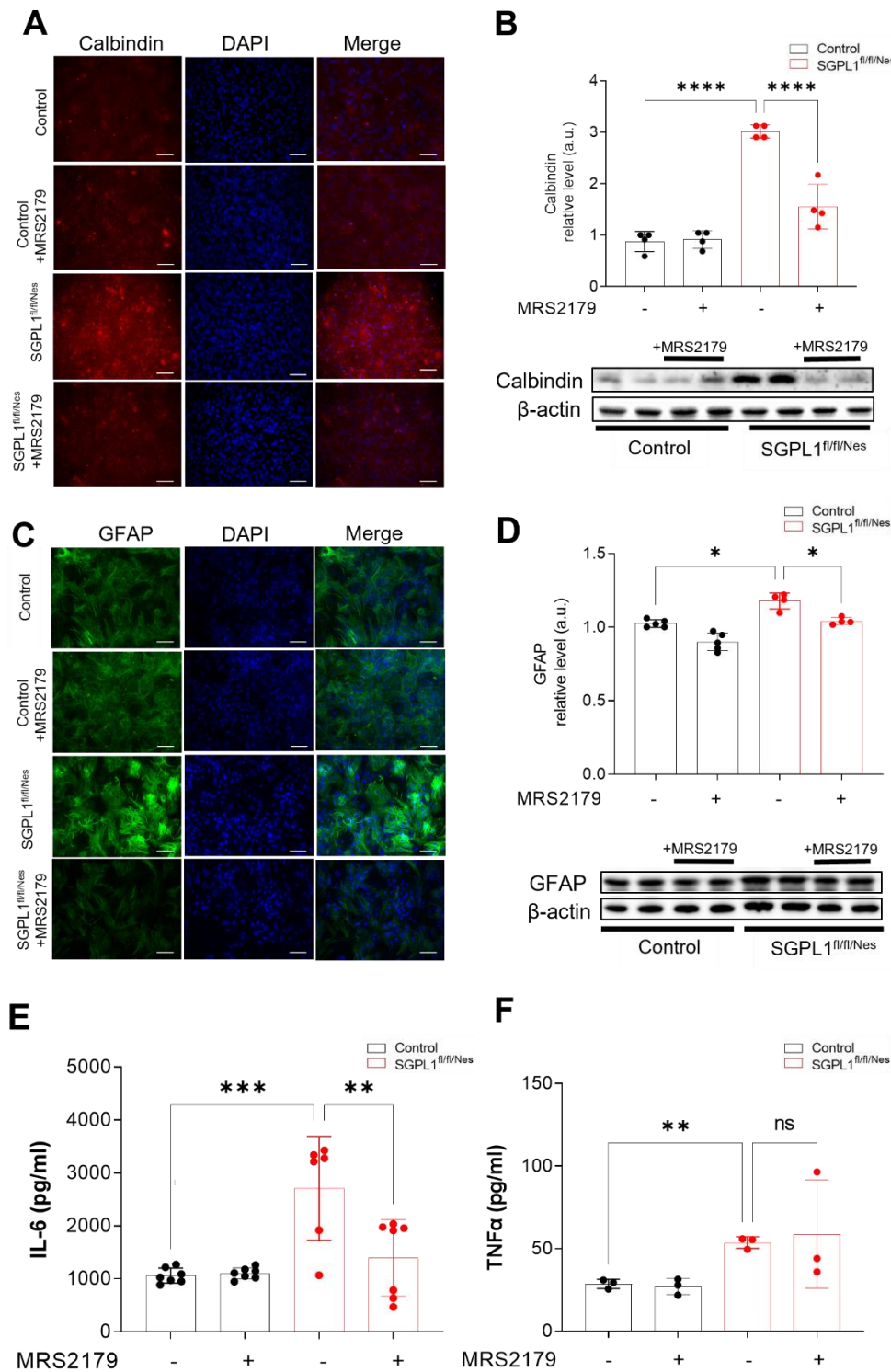
**Figure 14. P2Y1R mediates hyperactivity of SGPL1-deficient astrocytes.** Representative images and protein expression and quantification of calbindin (**A-B**) and GFAP (**C-D**) expression in SGPL1-deficient astrocytes with and without MRS2179 treatment. (**E-F**) Expression of IL-6 and TNFα in control and SGPL1-deficient astrocytes with and without MRS2179 treatment. Bars mean +/− S.E.M, one way ANOVA with Bonferroni's multiple comparison test (n=3–9, *p < 0.05, **p < 0.005, ***p < 0.0005), ns= not significant. Scale bar: 200 μm.

## 2.8 ACCUMULATED S1P ACTIVATES MICROGLIA OF SGPL1$^{FL/FL/NES}$ MICE

In mixed glial culture, microglia grow on top of the astrocyte cell layer. Therefore, it was interesting to investigate lipid profiles in microglia too. As expected, the microglia expression of SGPL1 and lipid profile was unaltered since microglia's origin is not a neural one (Fig.15A-B). However, secreted S1P from astrocytes has a receptor-mediated effect on microglia (Karunakaran, Alam et al. 2019).

Based on the increased secretion of S1P from astrocytes and the notable role of S1P in inflammation (Karunakaran and van Echten-Deckert 2017), increased activation of microglia was speculated in SGPL1-deficient mice. The expression of Iba1 (a microglial marker protein) was analyzed by western immunoblotting and immunohistochemistry in the cortex of control and SGPL1-deficient mice. The expression of Iba1 was significantly increased in the cortex of SGPL1-deficient mice compared to controls, suggesting an increased microglial activation state in the brain of the SGPL1-deficient mice (Fig.15C-D).
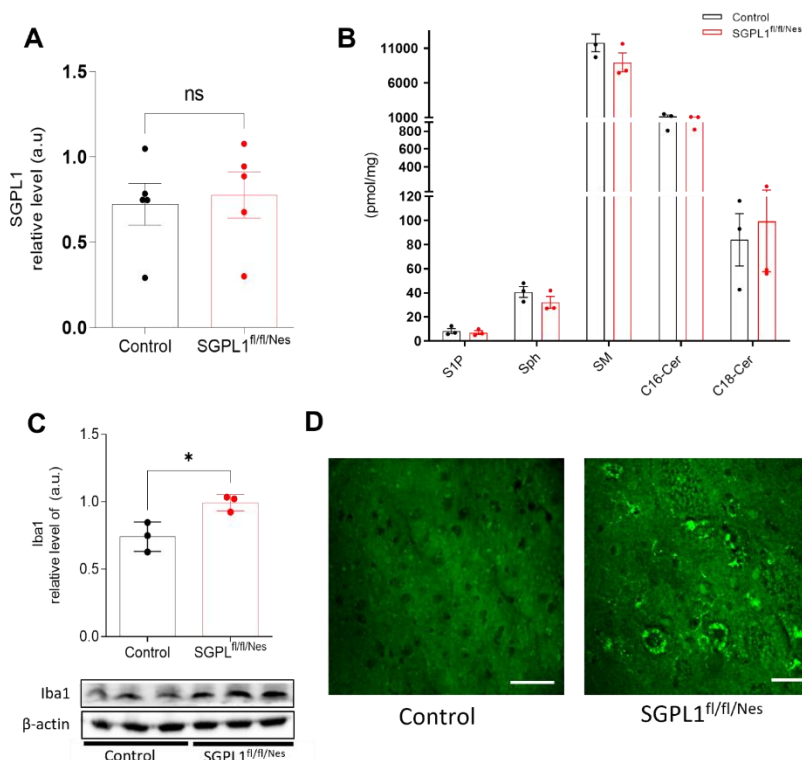


**Figure 15. Lipid profile of primary cultured microglia and increased expression of Iba1 in the cortex of SGPL1-deficient mice.** (**A**) The expression of the SGPL1 was assessed by western immunoblotting. (**B**) The amount of different sphingolipids were determined by LC/MS/MS in primary microglia of control and SGPL1-deficient mice. (**C**) Expression of Iba1 was evaluated in cortex of control and SGPL1-deficient mice by western

immunoblotting. **(D)** Microglia were stained with an anti-Iba1 antibody in the cortex of control and SGPL1-deficient mice. Bars represent means ± SEM (n ≥ 3; unpaired Students t-test, $*p < 0.05$). Cer16, C16-ceramide; Cer18, C18-ceramide; SM, sphingomyelin; Sph, sphingosine; LC/MS/MS, liquid chromatography coupled to triple quadrupole mass spectrometry. Scale bar = 200 μm. (See also (Karunakaran, Alam et al. 2019))

## 2.9 S1P-S1PR2 MEDIATES DEFECTIVE AUTOPHAGY IN MICROGLIA

Autophagy, one of the major mechanisms in the brain that keeps inflammation in check, was later assessed in microglia derived from SGPL1-deficient mice. The expression of beclin1 was significantly decreased in microglia, while expression of p62 was increased (Fig.16A). Further, the ratio of LC3-II:LC3-I was found to be reduced. Upon inhibition of S1PR2 with 1 μM JTE-013, increased p62 level was reversed, and the conversion of LC3-I to LC3-II was rescued, suggesting S1PR2 to be the main receptor that mediates defective autophagy in microglia derived from SGPL1-deficient murine brain (Fig.16B-D).
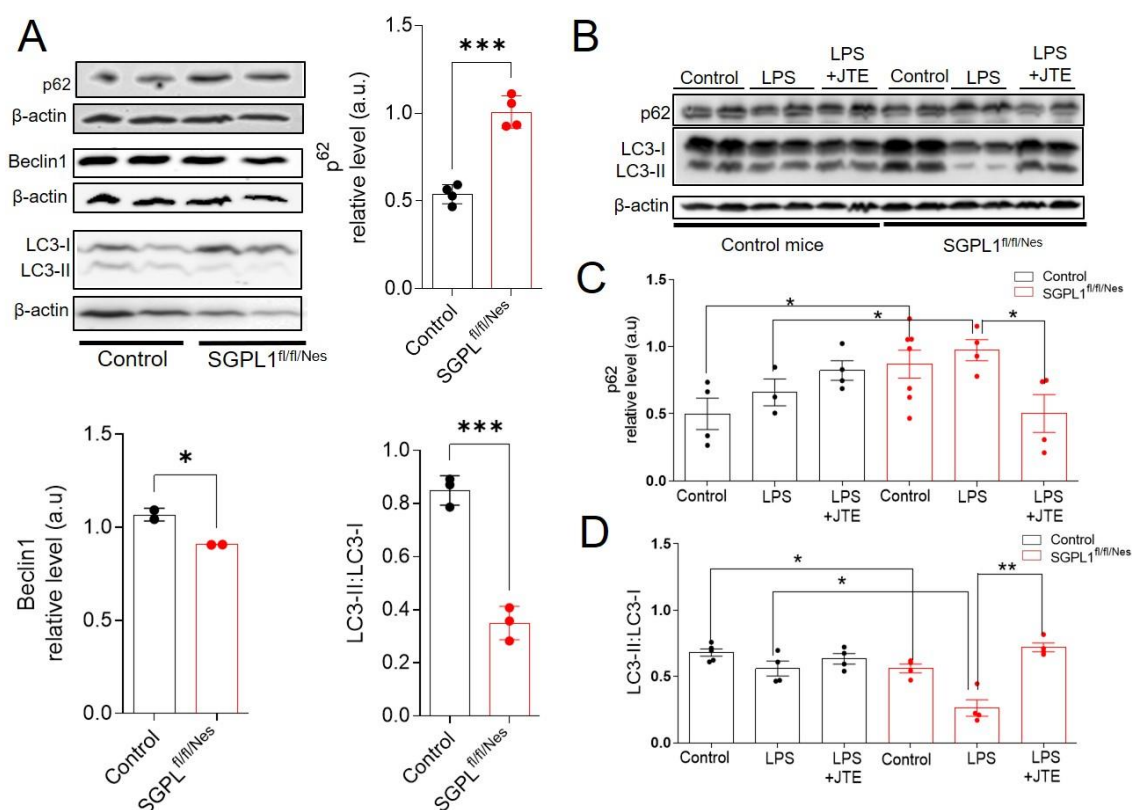


**Figure 16. S1PR2-mediated defective autophagy in microglia of SGPL1-deficient mice**. **(A)** The expression of autophagy marker proteins p62, beclin1, and LC3-II:LC3-I ratio were assessed by western immunoblotting in freshly harvested microglia. **(B-D)** Primary microglial cells were pretreated with 1 μM JTE-013 for 6 h. After

that, LPS (100 ng/mL) was added to primary microglia for 24 h. In primary microglia lysates, the expression of p62 and the ratio LC3-II:LC3-I were assessed by western immunoblotting. Bars represent means ± SEM (n=2-5; student t-test and one way ANOVA; *p < 0.05; **p < 0.001). LPS; Lipopolysaccharide. (See also (Karunakaran, Alam et al. 2019))

## 2.10  S1P ACCUMULATION CAUSES CALCIUM-DEPENDENT TAU PATHOLOGY AND ABNORMAL HISTONE ACETYLATION IN SGPL1-DEFICIENT MURINE BRAIN

In the SGPL1-deficient murine brains, several factors involved in neurodegenerative processes have already been confirmed, such as compromised autophagy and accumulation of APP (Mitroi, Karunakaran et al. 2017), presynaptic dysfunction, cognitive deficits (Mitroi, Deutschmann et al. 2016), and inflammation in the brain (Karunakaran, Alam et al. 2019). Next, two other factors, hyperphosphorylation of tau and excessive histone acetylation involved in neurodegenerative processes, were investigated. See also (Alam, Piazzesi et al. 2020).

### 2.10.1  Tau hyperphosphorylation is cell type-specific in SGPL1-deficient brains

Tau hyperphosphorylation is another attribute of many neurodegenerative diseases, including Alzheimer's disease (Lee, Goedert et al. 2001). Consistent with the previous finding in systemic SGPL1 knockout mice (Hagen, Hans et al. 2011), tau phosphorylation at pathologically relevant phosphorylation sites (phospho-tau$^{S396/404}$, phospho-tau$^{S262/356}$) was found to be increased in hippocampal and cortical slices from SGPL1-deficient mice (Fig. 17A and B). However, total tau (pan tau) was not changed in SGPL1-deficient murine brains (Fig. 17A and B). Furthermore, tau hyperphosphorylation was analyzed separately in neuron and astrocytes cultured from SGPL1-deficient murine brains. Interestingly, tau hyperphosphorylation was found only in neurons but not in astrocytes (Fig.17C). This indicates that tau hyperphosphorylation in the hippocampus and cortex is due to hyperphosphorylation of tau in neurons.
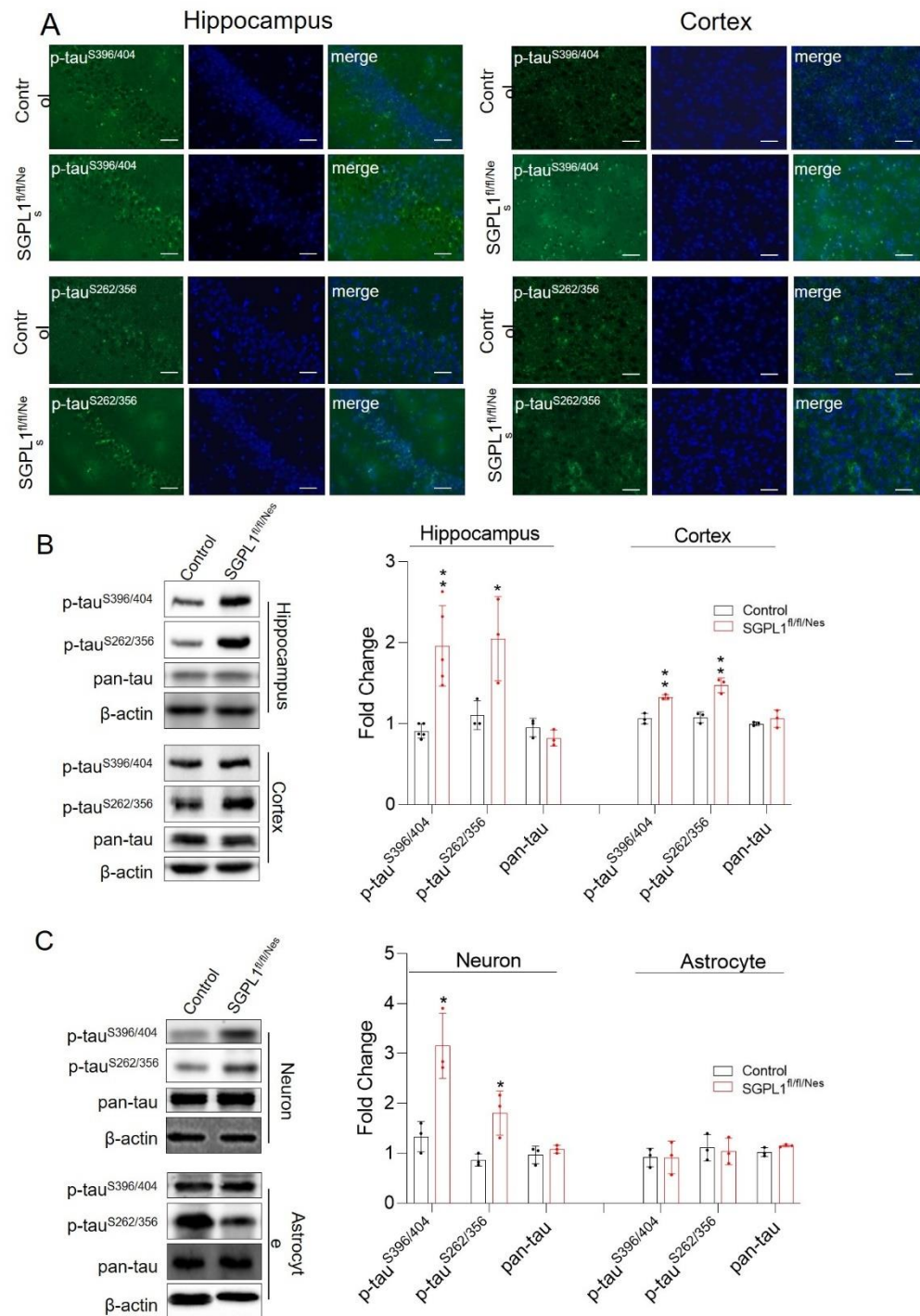
**Figure 17. SGPL1 ablation results in increased tau phosphorylation in the brain. (A)** Representative images of hippocampal and cortical slices stained for phospho-tau$^{S396/404}$, phospho-tau$^{S262/356}$, and DAPI from control and SGPL1-deficient mice. Scale bar: 200 µm. **(B-C)** Western immunoblot analysis of tau phosphorylation using the phospho-tau$^{S396/404}$, phospho-tau$^{S262/356}$, and total tau (pan tau) antibody and quantitative analysis in the hippocampus, cortex, neurons, and astrocytes in control and SGPL1-deficient mice. Black bar as control and red bar as SGPL1-deficient. Bars mean +/- S.E.M, student's t-test with false discovery rate (FDR) correction, n=3-5, *q <0.05, **q <0.01 (see also Alam, Piazzesi et al. 2020).

## 2.10.2 Histone acetylation levels vary in different cell types derived from SGPL1-deficient murine brains

Frost et al. (2014) have found that tau stimulates neurodegeneration through chromatin relaxation in drosophila (Frost, Hemberg et al. 2014). About a decade ago, Hait et al. (2009) found that accumulated S1P elevates histone acetylation in tumorigenic cells (Hait, Allegood et al. 2009). Therefore, acetylation of histones was investigated in hippocampal and cortical slices from SGPL1-deficient mice. Intriguingly, histone3 (H3) acetylation was found to be increased in both hippocampal and cortical slices by about 36% and 32%, respectively (Fig. 18A). Further, it was found that acetylation at H3K9 (histone3 lysine9) position was increased by about 45% in the hippocampus and to a lesser extent (about 35%) in the cortex of SGPL1-deficient murine brains (Fig.18A). Next, histone3 (H3) acetylation were also analyzed separately in neuron and astrocytes cultured from SGPL1-deficient murine brains. Presently, it was found that acetylation of H3 was increased only in astrocytes (Fig.18B), not in neurons (Fig. 18C). However, the total H3 (pan H3) level was only slightly increased in SGPL1-deficient astrocytes (Fig. 18B). Moreover, acetylation of histone4 (H4) at lysine5 (K5) and acetylation of histone2B (H2B) at lysine12 (K12) position was significantly increased in astrocytes of SGPL1-deficient mice (Fig. 18B). Histone acetyltransferases (HATs) and histone deacetylases (HDACs) maintain the delicate, dynamic equilibrium in acetylation levels of nucleosomal histones (Hait, Allegood et al. 2009). Hait et al. (2009) also found that accumulated S1P acted as an inhibitor of histone deacetylases (Hait, Allegood et al. 2009). Next, the expression of HDACs was investigated in SGPL1-deficient mice. In contrast to Hait. et al. (2009) finding, it was found that both mRNA and protein levels of HDAC1, 2, 3 and 6 remained unaffected in SGPL1-deficient mice, compared to controls (Fig. 18D-F). These results show that S1P accumulation in the brain has a cell type-specific effect on protein posttranslational modifications without affecting the expression levels of the responsible deacetylases.
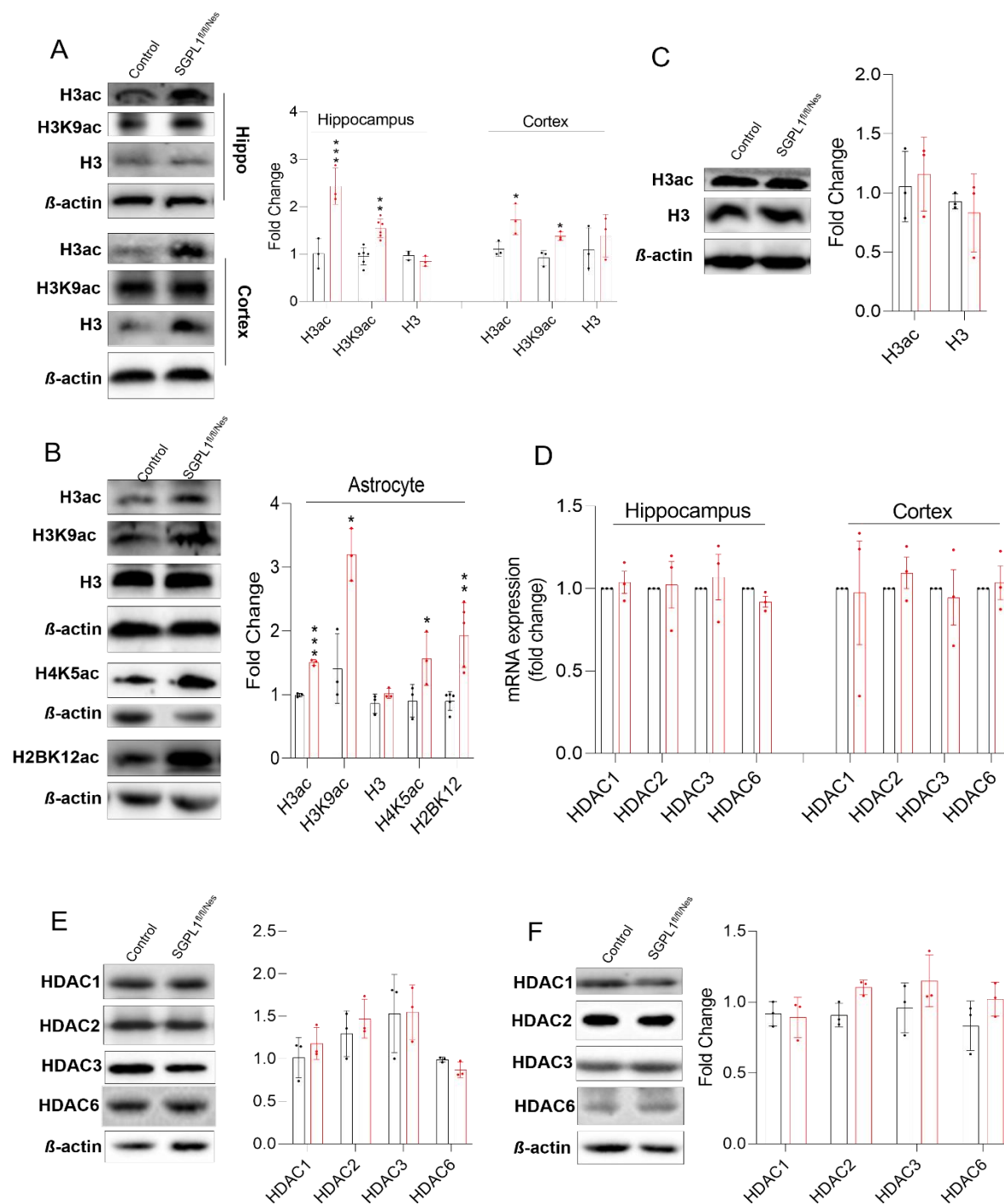
**Figure 18. Altered H3 acetylation without affecting HDAC expression in the SGPL1-deficient murine brain. (A)** Western immunoblot analysis of H3 acetylation using H3 pan-acetylation (H3ac), H3K9 acetylation (H3K9ac), and total H3 and quantitative analysis in the hippocampus and cortex of control and SGPL1-deficient mice. **(B)** Western immunoblot analysis of H3 acetylation in SGPL1-deficient astrocytes using of H3 pan-acetylation (H3ac), H3K9 acetylation (H3K9ac), total H3, H4K5 acetylation (H4K5ac) and H2BK12 acetylation (H2BK12ac) and quantification. **(C)** Western immunoblot analysis of H3 pan-acetylation (H3ac) and total H3 in primary neuronal culture from control and SGPL1-deficient mice. **(D)** mRNA expression (qRT-PCR) of

HDAC1, 2, 3 and 6 in the hippocampus and cortex of control and SGPL1-deficient mice. **(E-F)** Western immunoblot analysis of HDAC1, 2, 3 and 6 and quantitative analysis in the hippocampus **(E)** and cortex **(F)** of control and SGPL1-deficient mice. For all: Black bar as control and red bar as SGPL1-deficient. Bars represents mean +/- S.E.M, Student's t-test with false discovery rate (FDR) correction, n=3-7, *q<0.05, **q<0.01, ***q<0.001, ns=not significant. (See also Alam, Piazzesi et al. 2020)

### 2.10.3 Calcium chelation reverses both tau phosphorylation and histone acetylation in the brain of SGPL1-deficient mice

Previous findings suggest that increased calcium concentrations might have a neurotoxic effect of accumulated S1P in SGPL1-deficient neurons (cultured from systemic SGPL1 knockout mice) (Hagen, Hans et al. 2011). Moreover, in the neural-specific SGPL1-deleted mouse model, a persistent elevation of basal calcium concentration in pyramidal neurons of the CA1 region in the hippocampus, was found to be increased by about 2.5-fold (Raucamp 2019). Hippocampal and cortical slices were treated with BAPTA-AM to determine whether elevated basal calcium concentration is linked to tau phosphorylation. Remarkably, treatment with BAPTA-AM (150 µM, 2 h) reversed tau phosphorylation in SGPL1-deficient hippocampal and cortical slices to control values. However, only the pathological phospho epitope at serine residue $S^{396/404}$ could be rescued (Fig.19A) while phosphorylation of serine residues $S^{262/356}$ was not affected (Fig.19D). Furthermore, it was found that histone acetylation in the same samples also returned to control levels following BAPTA-AM treatment (Fig.19B). As discussed above, tau hyperphosphorylation was found only in neurons, whereas the unusual increase of histone acetylation was restricted to astrocytes. Thus, both neurons and astrocytes cultured from SGPL1-deficient mice were treated with BAPTA-AM (5 h, 500 nM). After treatment of primary cultured neurons and astrocytes with BAPTA-AM, the effect on tau phosphorylation and histone acetylation were reversed (Fig.19C).
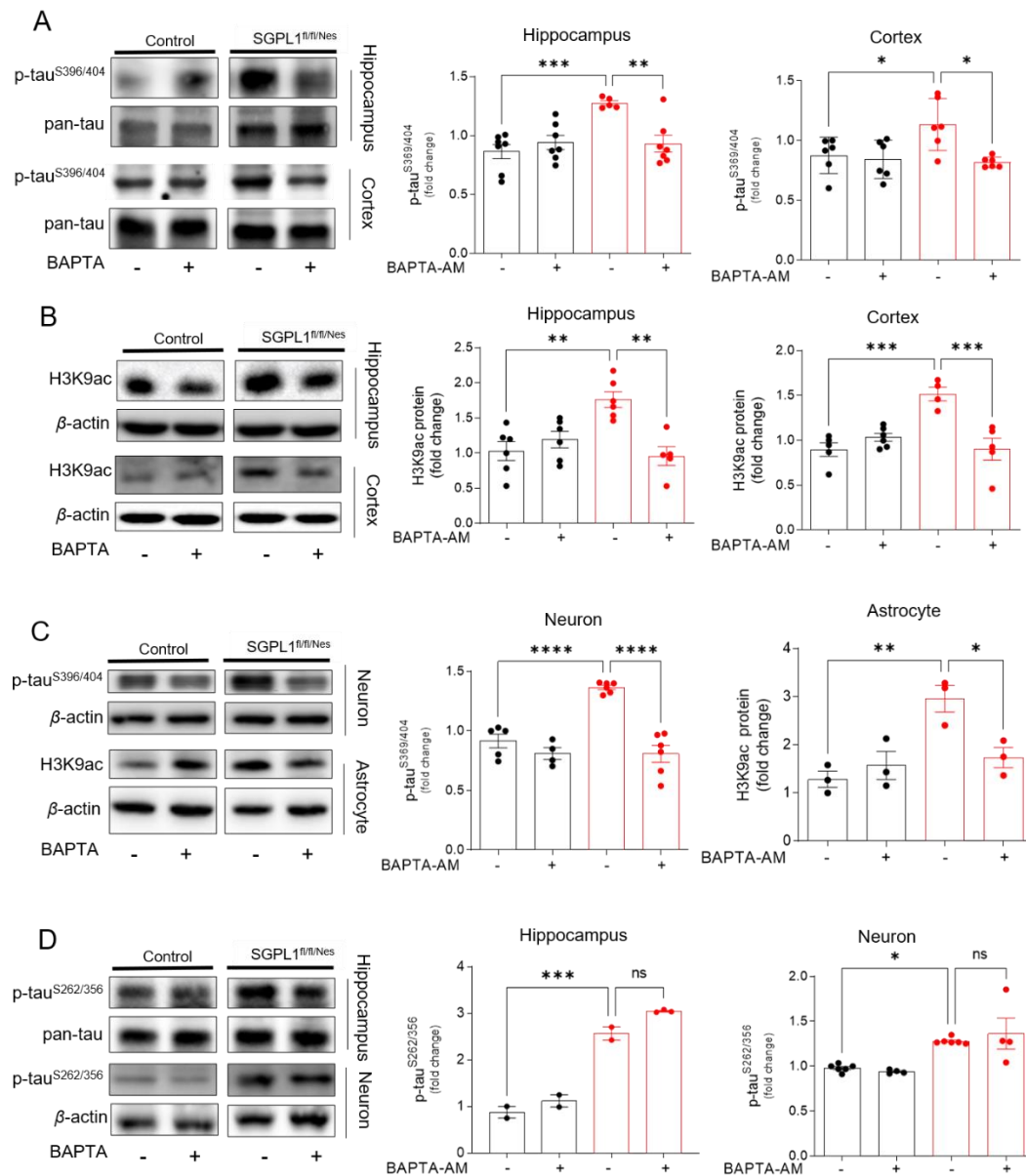
**Figure 19. BAPTA-AM restores tau$^{S396/404}$ hyperphosphorylation and H3K9 acetylation of SGPL1-deficient brains.** **(A)** Western immunoblot analysis of phospho-tau$^{S396/404}$ and total tau and quantitative analysis in the hippocampus and cortex of control and SGPL1-deficient mice with and without BAPTA-AM treatment. **(B)** Western immunoblot analysis of H3K9 acetylation (H3K9ac) and total H3 and quantification in the hippocampus and cortex of control and SGPL1-deficient mice with and without BAPTA-AM treatment. **(C)** Western immunoblot analysis of phospho-tau$^{S396/404}$ and H3K9 acetylation (H3K9ac) and quantification in neurons and astrocytes in control and SGPL1-deficient mice with and without BAPTA-AM treatment. For all: Black bar as control and red bar as SGPL1-deficient. Bars mean +/- S.E.M, One-Way ANOVA with Tukey's post-hoc correction, n=3-7, *p<0.05, **p<0.01, ***p<0.001, ****p<0.0001, ns= not significant. (See also Alam, Piazzesi et al. 2020).

# 3 DISCUSSION

The role of S1P in neurological pathologies is contradictory (van Echten-Deckert, Hagen-Euteneuer et al. 2014, Karunakaran and van Echten-Deckert 2017) albeit, the importance of S1P in brain development is undeniable (Mizugishi, Yamashita et al. 2005). In the case of Alzheimer's disease (AD), reports found a reduced level of S1P in postmortem AD patient's brain, suggesting a protective role of S1P in the brain (Ceccom, Loukh et al. 2014, Couttas, Kain et al. 2014). On the contrary, some studies, including those of the van Echten-Deckert group, suggest that accumulation of S1P under certain conditions become neurotoxic and disease-causative agent (Hagen, Hans et al. 2011, van Echten-Deckert, Hagen-Euteneuer et al. 2014, Karunakaran, Alam et al. 2019, Alam, Piazzesi et al. 2020). SGPL1 enzyme is an essential regulator of S1P level, which irreversibly cleaves S1P in the final step of sphingolipid catabolism, generating ethanolamine phosphate and a long-chain aldehyde (Fig.1). SGPL1 deficiency in the brain has been shown to affect neuronal health and cause neuroinflammation accompanied by cognitive and motor skills impairment in mice (Mitroi, Deutschmann et al. 2016, Mitroi, Karunakaran et al. 2017, Karunakaran, Alam et al. 2019). Of interest, in 2017, different research groups reported that patients and their relatives harboring autosomal recessive mutations in *SGPL1* gene exhibited a variety of pathologies, including congenital steroid-resistant nephrotic syndrome, primary adrenal insufficiency, and central and peripheral neurological defects (Choi and Saba 2019).

In brain, microglia, astrocytes, and neurons perpetually communicate and co-operate with each other and dysregulations in one of these cell types can trigger aberrant responses in others and disrupt the homeostasis of the CNS microenvironment (Jurgens and Johnson 2012, Limatola and Ransohoff 2014). Therefore, the present study is aimed to unravel further S1P signaling in neuronal cells, including microglia, astrocytes, and neurons cultured from the SGPL1-deficient murine brain. Here, results show that neural SGPL1 ablation accumulates S1P in astrocytes, causing astrogliosis. Astrogliosis was observed as increased expression of GFAP and P2Y1R proteins and increased secretion of inflammatory cytokines. Also, S1PR2/4 mediated increase in glycolysis was observed in SGPL1-deficient astrocytes. Moreover, in microglia, via paracrine signaling and/or astrocyte-microglia communication, the S1P-S1PR2 axis modulated microglial autophagic processes. Furthermore, calcium-

dependent tau phosphorylation and histone acetylation was increased in SGPL1-deficient neurons and astrocytes, respectively.

## 3.1 EXPRESSION OF SGPL1 IN MURINE BRAINS AND S1P SIGNALING IN ASTROCYTES

The SGPL1 expression was reduced by about 75-80% in brain tissues and primary cultured astrocytes derived from SGPL1-deficient mice compared to the respective controls. The remaining 20-25% of SGPL1 expression was due to the presence of cells of non-neural origin (e.g., fibroblasts and microglia). In neuron culture, AraC was added, which killed all dividing cells present in the culture. Therefore, SGPL1 expression was reduced by about 95-98% in SGPL1-deficient neurons compared to controls. The remaining 2-5% may be due to the dead non-neural cells present in the culture since the preparation. However, the expression of SGPL1 was similar in microglia generated from control and SGPL1-deficient mice as its origin is not a neural one (Fig.8).

Mitroi et al. (2016) have already shown that neural-targeted ablation of SGPL1 causes accumulation of S1P and to a lesser extent sphingosine in these mice brains (Mitroi, Deutschmann et al. 2016). Similar to mice brains, the level of S1P and sphingosine was found to be increased in the astrocytes while no changes were observed in lipid content (fig.8C), suggesting that S1P is secreted outside of the cell. Interestingly, S1P was found to be increased in the culture media of astrocytes (Fig.8D). However, the level of S1P and sphingosine were unaltered in microglia (Fig.15B) (Karunakaran, Alam et al. 2019). Nevertheless, contrary to the mice brains and neurons (Mitroi, Karunakaran et al. 2017), the level of PE was not changed in primary cultured astrocytes (Fig.8C).

S1P is well-known to act as a second messenger or as a ligand for a family of 5 G-protein coupled receptors, S1PR1-5, which are located on the plasma membrane (Tsai and Han 2016) (Spiegel, Maczis et al. 2019). These receptors are expressed ubiquitously; however, they are expressed at varying degrees in neurons, astrocytes, oligodendrocytes, and microglia (O'Sullivan and Dev 2017). Groves et al. (2013) have shown that S1PR3 and S1PR1 are expressed at the highest levels, with low expression levels of S1PR2 in astrocytes (Groves, Kihara et al. 2013). Moreover, S1P-S1PR signaling are found to regulate many physiological

processes, including inflammation (Karunakaran, Alam et al. 2019) and enhanced glycolysis (Shen, Zhao et al. 2019). S1PR1 and S1PR3 play a role in astrocyte migration, possibly in astrocyte proliferation and astrogliosis (Choi and Chun 2013). Counting them all, increased mRNA levels of S1PR2 and S1PR4 in SGPL1-deficient astrocytes (Fig.10C) argue with specific S1PR upregulation/activation in astrocytes

To interact with S1PRs, S1P must be exported out from the cells (Spiegel, Maczis et al. 2019). There are various transporters which are recognized to transport S1P, such as ABC transporters (Abca1, Abcb1, Abcb1a, Abcb1b, and Abcc1) and S1P specific transporter SPNS2 (Ihlefeld, Vienken et al., 2015). Overexpression of SK1 has shown the upregulation of mRNA expression of Abcb1 and Abcb1b, but not Abcb1a in a cerebral endothelial cell line (Barakat, Demeule et al. 2007). Moreover, several reports suggested that overexpression of SPNS2 increased the secretion of S1P in mammalian cells (Kawahara, Nishi et al. 2009, Hisano, Kobayashi et al. 2011, Nagahashi, Kim et al. 2013). On the contrary, some reports have shown that down-regulation of SPNS2 decreased the release of S1P (Nagahashi, Kim et al. 2013). Additionally, SPNS2 was also found to transport S1P analogs such as FTY720 phosphate (Hisano, Kobayashi et al. 2011, Nagahashi, Kim et al. 2013). These reports confirmed the functional effectiveness of SPNS2 in S1P transport. Taken together, increased mRNA levels of ABC transporters and SPNS2 (Fig.9A-B) in the SGPL1-deficient astrocytes agree with previous findings.

## 3.2 NEURAL ABLATION OF SGPL1 CAUSES ASTROGLIOSIS AND EPIGENETIC MODIFICATION

Neuropathological processes are often accompanied by astrogliosis, a term coined for morphological and functional changes in astrocytes. Astrogliosis is a multi-staged process characterized by molecular and morphological changes (Sofroniew 2009, Neal and Richardson 2018). Increased GFAP is one of the most prevalent protein found in astrogliosis(Sofroniew 2015). In this study, expression of GFAP was also found significantly increased (10-15%) in SGPL1-deficient astrocytes (Fig.9A-C). However, in cortex, it was increased by about 200% - 300% (Mitroi 2016). The possible reason could be due to the abnormalities occurred in neurons owing to SGPL1 deficient in murine brains. Since astrogliosis is a diverse process (Sofroniew 2009, Sofroniew 2015), other potential

contributors in astrogliosis were also considered, such as a recently reported purinoreceptor P2Y1R (Delekate, Fuchtemeier et al. 2014, Rodrigues, Tome et al. 2015), calbindin, which regulates free calcium distribution in the cytoplasm (Toyoshima, Yamagami et al. 1996, Hong and Jeung 2013) and inflammatory cytokines (Sofroniew 2009, Sofroniew 2015) (Fig.9A-D). All these, potential contributors of astrogliosis were found to be increased in SGPL1-deficient astrocytes. Together, these results suggest astrogliosis occurrence in SGPL1-deficient murine brain.

The pathological role of P2Y1R has been predominantly associated with reactive astrocytes (Abbracchio, Brambilla et al. 1999). Most importantly, it entrains the propagation of calcium waves throughout the astrocyte network and promotes astrocytic hyperactivity upon diverse stress conditions (Delekate, Fuchtemeier et al. 2014, Rodrigues, Tome et al. 2015). Nucleotide (ATP or ADP) can bind to these purinergic receptors, acting either as a find-me signal or danger signal (Fujita, Tozaki-Saitoh et al. 2009, Stachon, Geis et al. 2016). As astrocytes are known to release ATP (Coco, Calegari et al. 2003, Pangrsic, Potokar et al. 2007, Falchi, Sogos et al. 2013), it was hypothesized that ATP released from cells goes into the extracellular space and degrades to ADP, AMP, and adenosine, which in turn activates P2Y receptors. Interestingly, the result of the ADP/ATP ratio in cell lysates and culture media of SGPL1-deficient astrocytes supports the hypothesis. The ADP/ATP ratio decreased in cell lysates and increased in culture media, suggesting that released ATP converted into ADP by ectonucleotidases in culture media and acted as a ligand for P2Y1R (Fig.11A). Moreover, some groups found that treatment of cultured astrocytes with ATP initiated a series of events, inducing $[Ca^{2+}]$ transients caused by P2Y receptor activation. It was followed by the production of inositol 3,4,5 trisphosphate ($IP_3$) and subsequent $Ca^{2+}$ release from the endoplasmic reticulum (Fischer, Appelt et al. 2009, Verkhratsky, Krishtal et al. 2009, Franke and Illes 2014). Therefore, it was hypothesized that as a result of P2Y1R activation, there might be presence of $[Ca^{2+}]$ transients or elevated calcium level in cytoplasm. Increased calbindin expression, a calcium binding protein (act as buffer in cytoplasm), in primary cultured astrocyte and cortex of SGPL1-deficient mice (Fig.10E, F), further confirmed the hypothesis and was in agreement with the previous findings.

Astrocytes are mostly glycolytic (Magistretti and Allaman 2015); thus, due to ATP increase in cell, glycolytic enzymes were investigated at the outset. Interestingly, rate-limiting glycolytic enzymes PFK and GAPDH were found to be increased in SGPL1-deficient astrocytes

(Fig.11C, D). However, the PDH enzyme, which converts pyruvate (a glycolysis product) into acetyl-CoA, was found to be increased in SGPL1-deficient astrocytes (Fig.11C, D). Acetyl-CoA is used in the tricarboxylic acid cycle (TCA). Therefore, moving to the next, TCA cycle was investigated. To investigate TCA cycle, IDH2 enzyme expression were investigated. However, no changes in IDH2 enzyme expression were observed in SGPL1-deficient astrocytes (Fig.11E). The reason why IDH enzyme expression did not change in astrocytes could be explained by the so-called astrocyte-neuronal lactate shuttle (ANLS). Through ANLS, astrocytes store energy in the form of lactate which is later utilized by neurons (Halim, McFate et al. 2010, Dienel 2019). These results suggest that only anaerobic glucose metabolism was increased in SGPL1-deficent astrocytes.

Sun, K. et al. (2016) showed that increased S1P level promotes glycolysis in erythrocyte in the hypoxic condition (Sun, Zhang et al. 2016). Also enhanced glycolysis was found to be S1PR dependent in osteosarcoma cells. (Shen, Zhao et al. 2019). Therefore, it was anticipated that regulation of glycolytic enzymes might be S1PR dependent in SGPL1-deficient astrocytes as the level of S1P and expression of S1PR2/4 was increased (Fig.8C, 9C). Upon inhibition of S1PR2/4, the expression of PFK, GAPDH, and PDH enzyme were reduced (Fig.12A). However, either of the inhibitors could not rescue alone. Increased glycolytic enzymes expression was S1PR2/4-mediated; hence inhibiting the receptor was expected to decrease ADP/ATP ratio in culture media and ultimately P2Y1R expression. Indeed, S1PR2/4 inhibition decreased ADP/ATP ratio and reversed P2Y1R expression in SGPL1-deficient astrocytes (Fig.12B-D). To the best of my knowledge, this is the first report showing the role of S1PR2/4 in glucose metabolism and increased P2Y1R expression in SGPL1-deficient astrocytes. S1PR2/4 might increase glycolysis by increasing GLUTs activity, which can lead more glucose inside the cells or can directly act on glycolysis enzymes. Increased GLUT2 mRNA expression (Fig.11B) suggests that S1P-S1PR2/4 axis might directly affect GLUT2 activity which allows more glucose entry inside the SGPL1-deficient astrocytes leading to more glycolysis and ATP production.

Several reports found that treatment of astrocyte cultures with ATP itself or its structural analogs imitated the changes that occur during astrogliosis (Neary 1996, Abbracchio, Brambilla et al. 1999, Franke, Krugel et al. 1999). For example, Microinfusing 2-MeSATP into NAc (Nucleus Accumbens) of rats stimulated the astrogliosis resultant CNS injury, increased GFAP expression and proliferation (Franke, Krugel et al. 1999). It was further

reported that inhibition of P2Y1Rs receptor with antagonist PPADS reversed the same effect. Similarly, treatment of SGPL1-deficient astrocytes with MRS2179 inhibiting P2Y1R reversed the GFAP expression (Fig.13C, D). Moreover, P2Y1R is also known to modulate/induce inflammatory responses upon activation (Fujita, Tozaki-Saitoh et al. 2009, Stachon, Geis et al. 2016). Fig.14 E and F shows that astrocytes treated with P2Y1R inhibitor MRS2179 rescued IL-6 but not TNFα expression. Taken together with these results, it is evident that P2Y1R plays an important role in astrocyte hyperactivity in the SGPL1-deficient murine brain.

As glycolysis was increased in SGPL1-deficient astrocytes, it was interesting to investigate autophagy. Autophagy is an essential process to maintain cellular homeostasis and functions in the cells. As expected, impaired autophagy was observed in SGPL1-deficient astrocytes (Fig.12A, B). Moreover, mTOR has also been found to exert a crucial role in regulating energy metabolism and controls autophagy (Sabatini 2017, Fan, Wu et al. 2021). Although mTOR independent autophagy has also been found (Mitroi, Karunakaran et al. 2017). However, this is far from being black and white. For instance, it has been reported that increased levels of autophagy during development can be harmful but become advantageous in the aging cells or organism, leading to enhanced health span and even longevity (Schmeisser and Parker 2019). Upon inhibition of mTOR with rapamycin, autophagy was rescued, suggesting mTOR dependent impaired autophagy in SGPL1-deficient astrocytes.

Another interesting aspect of accumulated S1P was observed in epigenetic modification in the nucleus of breast cancer cells by directly targeting HDACs and increasing histone acetylation of H3 at K9, of H4 at K5, and rather weakly that of H2B at K12 (Hait, Allegood et al. 2009). Importantly, in aging and age-related neurodegenerative disorders, such as AD, PD and HD, epigenetic dysregulation currently attracts much attention as a pivotal player. In these neurodegenerative disorders, epigenetic dysregulation may mediate interactions between genetic and environmental risk factors, or directly interact with disease-specific pathological factors (Lardenoije, Iatrou et al. 2015, Narayan, Lill et al. 2015). Interestingly, in SGPL1-deficient astrocytes, histone acetylation was increased at H3K9 and H2BK12 (Fig.18) however, overall expression levels of HDAC1, 2, 3 or 6 were unaffected. Calcium chelation by BAPTA-AM restored histone acetylation (Fig.19B, C), suggesting that calcium mediates the effect of S1P on histone acetylation independent of HDAC expression. These results suggest that S1P manipulate histone acetylation via calcium and therefore, may control the

transcription of target genes, linking them to epigenetic regulation in response to environmental signals (Fig.20).
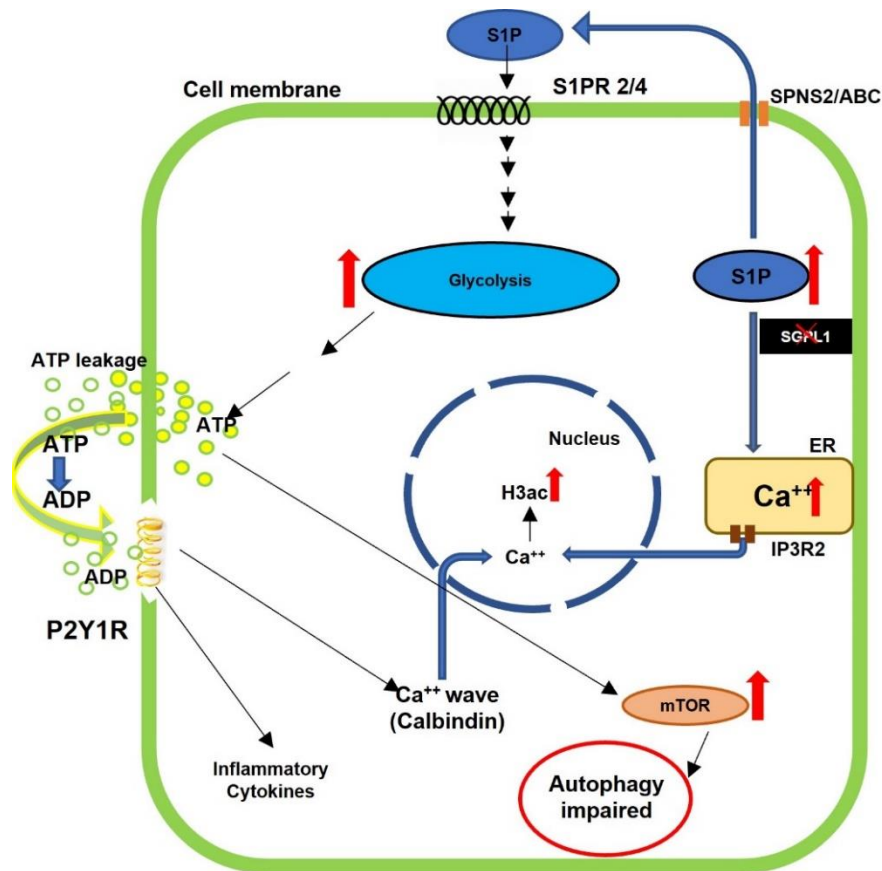


**Figure. 20. Summary of the effect of SGPL1 ablation in astrocytes.** Neural ablation of SGPL1 lead to accumulation of S1P in astrocytes. Subsequently, S1P was released via ABC transporters and/or SPNS2 into culture media. Released S1P enacted either in an autocrine and/or paracrine manner on its receptors S1PR2/4, resulted in elevated glycolysis process and ultimately increased ATP production. Increased ATP was released outside the cell and converted into ADP which in turn acted on P2Y1R. Activated P2Y1R started calcium wave and induced inflammatory cytokines production. mTOR might have sensed the increased energy in the cell and therefore, decreased autophagy. Moreover, accumulated S1P caused ER stress, and lead to Ca$^{++}$ release in cytosol which went in nucleus and altered histone acetylation in SGPL1-deficient astrocytes.

Microglia, astrocytes, and neurons constantly communicate and co-operate with each other (Jurgens and Johnson 2012, Limatola and Ransohoff 2014) and dysregulation in one of these cell types can trigger aberrant responses in others and disrupt the homeostasis of the CNS microenvironment. Therefore, considering the increased S1P accumulation in SGPL1-deficient-astrocytes and a recent report showing the involvement of S1P transporter proteins in the proinflammatory activation of microglia (Zhong, Jiang et al. 2019), it was assumed that S1P accumulation in astrocytes might modulate microglial functions in SGPL1-deficient mice. Moreover, astrocyte secreted cytokines are known to induce transformation from ameboid to ramified morphology in microglia (Schilling, Nitsch et al. 2001).

Certainly, an increase in microglial activation was evidenced in the SGPL1-deficient murine brains as shown by increased expression of microglial activation marker protein, Iba1 (Fig.16) as well as an activated and deramified morphology (Karunakaran, Alam et al. 2019). One important fact to notice is that S1P level was not changed in microglia (Fig.15A). Thus, released S1P form other neural cells such as astrocytes, neurons and oligodendrocytes have acted on microglia in SGPL1-deficient murine brain. However, in cultured microglia, S1P comes from only astrocytes as others are absent in culture (Fig.21).

Additionally, mTOR dependent impaired autophagy was identified in microglia (Fig.16) (Karunakaran, Alam et al. 2019). Furthermore, it was also demonstrated that via paracrine signaling and/or astrocyte-microglia communication, the S1P-S1PR2 axis modulates autophagic processes (Fig.21). In summary, there results show a novel role of the S1P-S1PR2 axis in the microglia of neural-targeted SGPL1-deficient mice (Fig.21). See also Karunakaran, Alam et al. 2019.
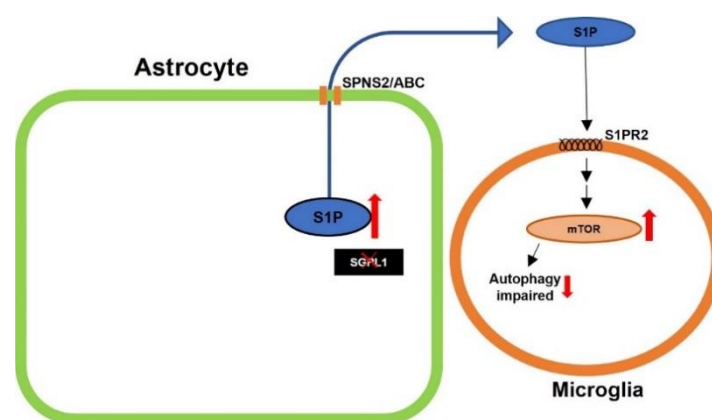


**Figure 21. S1P-S1PR2 axis modulates autophagic processes in microglia.** Released S1P from astrocyte acted via S1PR2 which lead to impaired autophagy via mTOR in primary cultured microglia**.**

## 3.3 SGPL1 DEFICIENCY AFFECT TAU PHOSPHORYLATION IN MURINE BRAINS

Accumulation of S1P in the endoplasmic reticulum membrane activates release of stored calcium (Ghosh, Bian et al. 1994). Mobilization of intracellular calcium stores is well-established as a universal signaling mechanism (Lee and Zhao 2019). Based on Mattson et al. (1991) report that altered calcium homeostasis may be a key event leading to altered tau disposition and neuronal degeneration (Mattson, Engle et al. 1991). Therefore, it was assumed that tau hyperphosphorylation might be linked to calcium homeostasis in SGPL1-deficient neurons. Later it was confirmed that phosphorylation site, phospho-tau$^{S396/404}$ could be reversed by BAPTA-AM treatment, indicating that the effect of SPGL1 deficiency on tau phosphorylation is calcium-dependent (Fig.22). (See also Alam, Piazzesi et al. 2020).
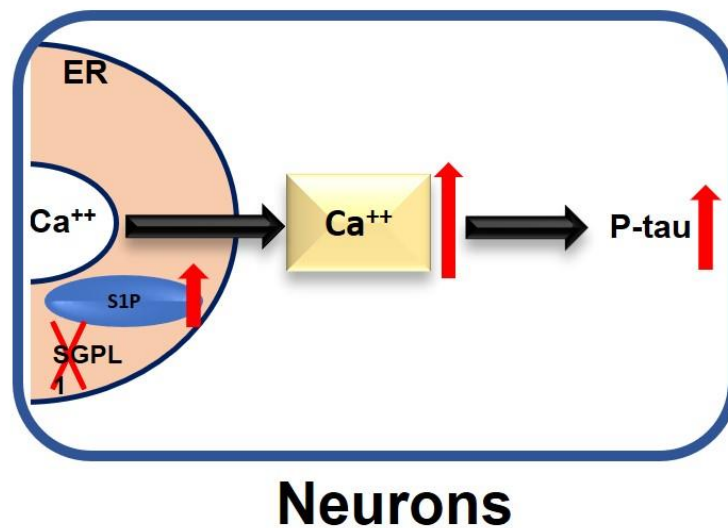


**Figure 22. SGPL1 deficiency results in tau hyperphosphorylation in neurons of SGPL1$^{fl/fl/Nes}$ mice.** SGPL1 ablation lead to ER stress and calcium release which in turn caused tau hyperphosphorylation in neurons cultured from SGPL1-deficient murine brains (modified image from Alam, Piazzesi et al. 2020).

# 4 CONCLUSION AND OUTLOOK

These results here indicate that SGPL1-deficiency causes a prominent neuropathological feature, astrogliosis or reactive astrocytes. In the case of astrocytes reactivity in different neurodegenerative diseases, recently published research articles maintain a high level of conflict and controversy (Li, Li et al. 2019). For example, in most researched neurodegenerative diseases such as AD, PD, ALS and MS, reactive astrocytes can be involved in both neuroprotective and neurodegenerative functions (Li, Li et al. 2019). Furthermore, despite the considerable amount of knowledge since the discovery of reactive astrocytes a century ago, there are no therapies purposely designed against astrocyte-specific targets in clinical practices (Escartin, Galea et al. 2021). The current study will bring additional knowledge to further understanding and astrocyte-specific treatment of neurodegenerative diseases.

SGPL1-deciciency in astrocytes changed epigenetic regulation by modifying histone acetylation in the murine brains. Interestingly, epigenetic dysregulation currently attracts much attention as a pivotal player, in aging and age-related neurodegenerative disorders, such as AD, PD and HD (Lardenoije, Iatrou et al. 2015). The role of S1P in histone acetylation might help to explain the potential molecular mechanisms underlying the diverse neurodegeneration in context of epigenetic regulation.

Sphingosine-1-phosphate lyase insufficiency syndrome (SPLIS) is a rare metabolic disorder caused by a deficiency in SGPL1. However, neuronal defects, including microcephaly, seizures, cranial nerve defects, developmental anomalies of the brain, have also been seen in SPLIS patients (Saba, Keller et al. 2021). The results obtained in this study, highlighting the effects due to SGPL1-deficiency in murine brain may bring in further important understandings to explain the potential molecular mechanisms of the pathogenesis of SPLIS.

Finally, the question of whether S1P-S1PR2 axis directly affects inflammation which in turn leads to autophagy defects or if it modulates autophagy which causes a pro-inflammatory cytokine secretion profile in our mouse model remains to be answered. Also, it could be of great interest to the field of tauopathies to further dissect the molecular mechanism by which SGPL1 deficiency and/or S1P accumulation in the brain affect tau hyperphosphorylation.

# 5 MATERIAL AND METHODS

**Apparatus**

| Apparatus | Company | Place |
| --- | --- | --- |
| Agarose gel apparatus | Bio-RAD | California, USA |
| Agarose gel imager | Alpha Innotech | Kasendorf |
| Blot Imager | Bio-RAD VersaDoc Imaging system | California, USA |
| Blotting Apparatus | Bio-RAD Mini PREOTEAN® 3 cell | California, USA |
| Fluorescence Microscope | Nikon-U2000 | California, USA |
| pH-Meter | PH 537; WTW | Weilheim |
| Pipette | Eppendorf Research | Hamburg |
| qRT-PCR | Bio-RAD CFX96 Real-Time System | California, USA |
| SDS-PAGE apparatus | Bio-RAD Mini PREOTEAN Tetra cell | California, USA |
| Spectrophotometer | Bio-RAD SmartSpec Plus | California, USA |
| Thermocycler | PTC-200; MJ Research/Biozym | Oldendorf |

**Chemical**

| Chemical | Company | Place |
|---|---|---|
| Acrylamidmix 37,5:1, 30% | Roth | Karlsruhe |
| Agarose, Seakem LE | MJ Research/Biozym | Oldendorf |
| BAPTA-AM | Invitrogen | Karlsruhe |
| Cytosin-b-D-Arabino-Furanosid-Hydrochlorid (AraC) | Sigma | Taufirchen |
| DMSO | Applicem | Darmstadt |
| Ethidiumbromid | Applicem | Darmstadt |
| Poly-L-Lysin | Sigma | Taufirchen |
| Tween-20 | Sigma | Taufirchen |

**Media**

| Media | Company | Place |
|---|---|---|
| DMEM | Fischer Scientific | Schwerte |
| FBS | PAN Biotech | Aidenbach |
| HS | PAN Biotech | Aidenbach |

**Primers**

| Target | Primer sequence (forward and reverse) |
|---|---|
| Abca1 | 5'-CGTGTCTTGTCTGAAAAAGGAGG-3'<br>5'-CGTGTCACTTTCATGGTCGC-3' |
| Abcb1a | 5'-GTAGAGACACGTGAGGTCGT-3'<br>5'-AGCGCCACTCCATGGATAAT-3' |
| Abcb1b | 5'-TCTGGGAACTCTCGCTGCTA-3'<br>5'-AGTACTGTTGGGTCCACTTTGA-3' |
| Abcc1 | 5'-ATGTGACTCTCAAGGGCTCC-3'<br>5'-AGGGCACAGGCTTCCATAAC-3' |

61

Abcg2
5'-TTGCATCAGCAGGTTACCAC-3'
5'-CCCTTGGAAGGCTCTTCAGT-3'

Baclin1
5´-ATGTGGAAAAGAACCGCAAG-3´
3´-CGCTGGTACTGAGCTTCCTC-5´

GAPDH
5'-CCCTTAAGAGGGATGCTGCC-3'
5'-TACGGCCAAATCCGTTCACA-3'

GFAP
5'-GAGAACAACCTGGCTGCGTA-3'
5'-CGGAGTTCTCGAACTTCCTCC-3'

Glut 1
5'-CACTGTGGTGTCGCTGTTTG-3'
5'-AAAGATGGCCACGATGCTCA-3'

Glut 2
5'-GGGACTTGTGCTGCTGGATA-3'
5'-GAACACGTAAGGCCCAAGGA-3'

Glut 3
5'-TTGGTGGCATGATTGGCTCT-3'
5'-AGCATAGAGTTGCGTCTGCC-3'

Glut 4
5'-CAATGTCTTGGCCGTGTTGG-3'
5'-GCCCTGATGTTAGCCCTGAG-3'

HDAC1
5'-GATGAGGAGGGAGAAGGTGG-3'
5'-AACTTGGGGAGAAGATGGGG-3'

HDAC2
5'-GTTTTGTCAGCTCTCCACGG-3'
5'-AATTCGAGGATGGCAAGCAC-3'

HDAC3
5'-TGCCCCAGATTTCACACTCC-3'
5'-TGGTCCAGATACTGGCGTGA-3'

HDAC6
5'- GGCGCAGATTAGAGAGCCTT-3'
5'-GAAGGGGTGACTGGGGATTG -3'

IL-11
5'-ATGAACTGTGTTTGTCGCCTG-3'
5'-CAGCTAGTTGCCGTGTGTCT-3'

IL-15
5'-CTCTGCGCCCAAAAGACTTG-3'
5'-GGTGGATTCTTTCCTGACCTC-3'

IL-18
5'-GTTTACAAGCATCCAGGCACAG-3'
5'-GAAGGTTTGAGGCGGCTTTC-3'

IL-6
5'-CTCTGCAAGAGACTTCCATCCA-3'
5'-GACAGGTCTGTTGGGAGTGG-3'

LC3
5'-AGCGCTACAAGGGTGAGAAG-3'
5'-CCGGATGATGATCTTGACCAACT-3'

P62
5´-CCCATGCTATGGAAGAAGTCA-3´
3´-GGGTTCAGGTACTCCGTTCA-5´

PFK
5'-GGTTTGGAAGCCTCTCCTCC-3'
5'-GGGTCATGATCCACTCTTGTAGT-3'

| | |
|---|---|
| SGPL1 | 5'-ATGTGGATGCTTGTCTGGGG-3'<br>5'-ACCTTTAGGAGCATAGCCATACTTA-3' |
| SPNS2 | 5'-ACTCAACGTGCTGACCCATT-3'<br>5'-GTGGGGATGACCACATACATGA-3' |
| S1PR1 | 5´-CTACACAACGGGAGCAACAG-3´<br>3´-CCCCAGGATGAGGGAGAGAT-5´ |
| S1PR2 | 5´-CAGGATCTACTCCTTGGTCAGG-3´<br>3´-GAGATGTTCTTGCGGAAGGT-5´ |
| S1PR3 | 5´-CCCAACTCCGGGACATAGA-3´<br>3´-ACAGCCAGTGGTTGGTTTTG-5´ |
| S1PR4 | 5´-TTCCATATGATGGACACTCC-3´<br>3´-TGGACAAATGAACGCAGGT-5´ |
| S1PR5 | 5´-GCTTTCTGTGTACAGTTGACAAATACT-3´<br>3´-CCAACTGTTCCAACTGTATGCT-5´ |
| TNFα | 5'-TAGCCCACGTCGTAGCAAAC-3'<br>5'-GCAGCCTTGTCCCTTGAAGA-3' |
| β-actin | 5'-CTTTGCAGCTCCTTCGTTGC-3'<br>5'-CCTTCTGACCCATTCCCACC-3' |

## Antibodies

| Name | Company | Place |
|---|---|---|
| anti-mouse Antibody | Cell Signaling | MA, USA |
| anti-rabbit Antibody | Cell Signaling | MA, USA |
| Beclin-1 | Cell Signaling | MA, USA |
| Calbindin | Cell Signaling | MA, USA |
| GAPDH | Cell Signaling | MA, USA |
| GFAP | Cell Signaling | MA, USA |
| H2BK12 | Cell Signaling, 5410 | MA, USA |
| H4K5 | Cell Signaling, 8647 | MA, USA |
| HDACs antibody sampler kit | Cell Signaling, 9928 | MA, USA |

| | | |
|---|---|---|
| Iba 1 | Wako Pure Chemical Industries, | Osaka, Japan |
| LC3 | Cell Signaling | MA, USA |
| P2Y1R | Abcam | Cambridge, UK |
| p62 | Cell Signaling | MA, USA |
| PDH | Cell Signaling | MA, USA |
| PFK | Cell Signaling | MA, USA |
| PHF1, 12E8 and K9JA | DZNE, University of Bonn, Germany | Gift from Prof. Dr. Eckhard Mandelkow and Prof. Dr. Eva-Maria Mandelkow |
| SGPL1 | Abcam | Cambridge, UK |
| β-Actin | Cell Signaling | MA, USA |

**Inhibitors**

| Name | Company | Place |
|---|---|---|
| 5,5′-Dimethyl-BAPTA-AM | Sigma Aldrich | Darmstadt |
| CYM 50380 | Sigma Aldrich | Darmstadt |
| JTE-013 | Sigma Aldrich | Darmstadt |
| MRS2179 tetrasodium salt | Tocris | Bristol, UK |
| Rapamycin | Cayman chemical company | MI, USA |

**Kits**

| Name | Company | Place |
|------|---------|-------|
| ADP/ATP ratio assay kit | Sigma Aldrich, MAK135 | Darmstadt |
| cDNA | Prime Script RT Master Mix (RR036Q) | Shiga, Japan |
| IDH activity kit | Sigma Aldrich, MAK062 | Darmstadt |
| IL-6 ELISA | Invitrogen, 15511037 | Schwerte |
| TNFα ELISA | Invitrogen, 88-7324-86 | Schwerte |
| qPCR | TB Green Premix Ex Taq (Tli RNase H Plus) | CA, USA |
| RNA Isolation | EXTRAzol (Blirt, M30-200) | Gdansk Poland |
| Western Blot Reagent | Takara Bio, T7101A | CA, USA |

## 5.1 MOUSE MODEL

SGPL1 floxed (SGPL1$^{fl/fl}$, control) and neural-specific SGPL1-knockout mice (SGPL1$^{fl/fl/Nes}$, neural-specific SGPL1-deleted mice) were used to study the S1P signaling pathway. Floxed mice were kindly provided by Prof. Dr. Julie Saba (University of California, USA), while Prof. Dr. Martin Theiß (Ħ, previously Uniklinikum Bonn, Germany) contributed to the nestin-Cre transgenic mice. Floxed and nestin-Cre transgenic mice crossbreeding were performed by Dr. Nadine Hagen (in the van-Echten Deckert group, 2013).

The SGPL1$^{fl/fl/Nes}$ mice were generated using Cre-lox recombinase technology. This technique depends on two components: a Cre recombinase and its recognition site, loxP. Both the loxP sequence and Cre-recombinase were obtained from bacteriophage P1. The loxP sequence is 34 bp long and consists of two 13 bp inverted repeats separated by a nonpalindromic sequence of 8 bp. Lox P sites are always used adjoining the gene of interest. The orientation of the loxP determines the excision or inversion of the floxed DNA sequence (Fig.23)

| 13 bp recognition region- | ATAACTTCGTATA |
| 8 bp spacer- | ATGTATGC |
| 13 bp recognition region- | TATACGAAGTTAT |
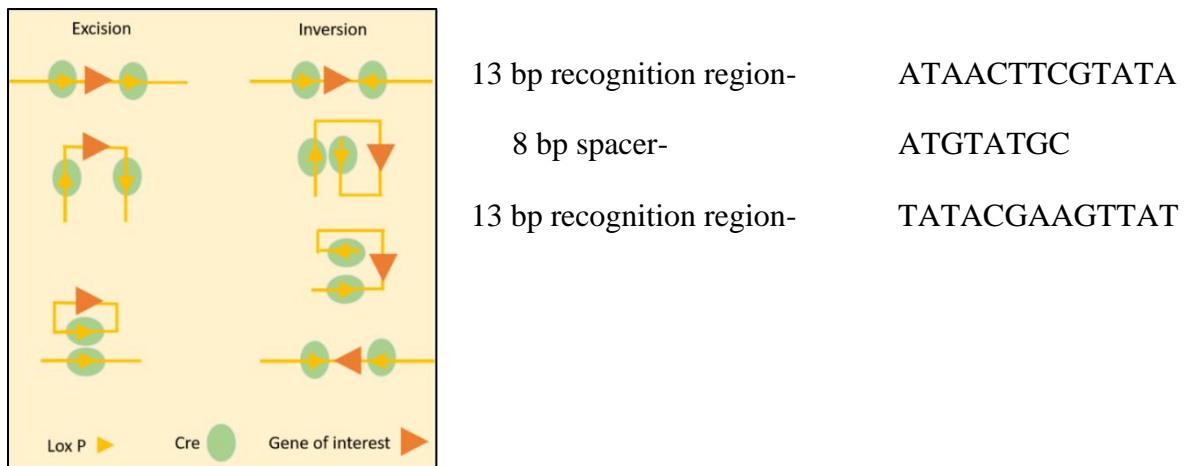
**Figure 23. Schematic representation of Cre/loxP recombination system.** The enzyme Cre recombinase recognizes the loxP-site (34 bp) and cleaves a consensus sequence. Crossbreeding of mice harboring the loxP-framed expressing the Cre recombinase causes a site-specific knockout: The loxP site's orientation decides the excision or inversion. The loxP site's orientation in the same direction cause excision, and the opposite direction causes inversion (left). The loxP sequence consists of two 13 bp inverted repeats separated by a nonpalindromic sequence of 8 bp (right).

In SGPL1$^{flox/flox}$ mice, exons 9/10 and 12/13 encoding for the binding site of the SGPL1 cofactor pyridoxal phosphate (PLP) were flanked by loxP sites (Fig.24). Lox-flanked regions of DNA are called "floxed." A nestin-Cre transgenic mice line Nes-Cre was crossbred with the control mice (SGPL1$^{flox/flox}$) to generate neural cell-specific knockout mice (SGPL1$^{fl/fl/Nes}$). In Nes-Cre mice, Cre recombinase is expressed under the control of the neural intermediate filament nestin promoter, explicitly expressed in neural progenitor cells. Therefore, S1P-lyase was only inactive in neural cells (neurons, astrocytes, and oligodendrocytes).



**Figure 24. Diagram representing neural-specific SGPL1 knockout.** Knockout was mediated by the Cre/loxP recombination system. Crossbreeding of mice harboring the loxP-framed exons 9/10 and 12/13 encoding for the

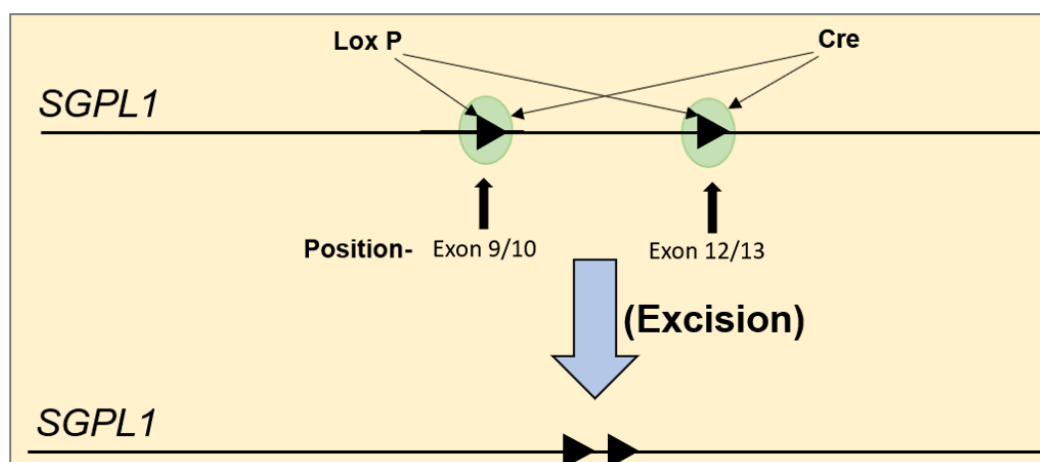binding site of the sphingosine-1-phosphate lyase (SGPL1) cofactor pyridoxal phosphate (PLP) with mice expressing the Cre recombinase causes a site-specific knockout: Since the loxP sites are oriented into the same direction, the Cre recombinase induces excision of the sequence, consequently ablating the expression of SGPL1.

## 5.2 ETHICAL STATEMENT

All animal experiments were conducted in accordance with the guidelines of the Animal Care Committee of the University of Bonn. The experimental protocols were approved by Landesamt für Natur, Umwelt und Verbraucherschutz Nordrhein-Westfalen (LANUV) (LANUV NRW, Az. 87–51.04. 2011. A049).

## 5.3 MOUSE GENOTYPING

In the current study, floxed mice (SGPL1$^{fl/fl}$) served as controls and neural-specific SGPL1-deleted mice (SGPL1$^{fl/fl/Nes}$) as a knockout (KO). SGPL1$^{fl/fl/Nes}$ mice had no noticeable phenotype. Their lifespan was comparable to that of their wild-type littermates. Thus, it represented a promising model to investigate the S1P induced signaling pathway in the brain and neuronal cells.

Mice/pup's genotype was confirmed using standard PCR. Two primer pairs were used: one primer pair for the *Cre* gene and another primer pair for the *flox* gene. *flox* gene amplification was used as a positive PCR control. In control mice/pups, only the *flox gene* was amplified, confirming the absence of the *Cre gene*. Both Cre and flox genes were amplified in SGPL1$^{fl/fl/Nes}$ mice (Fig.25).
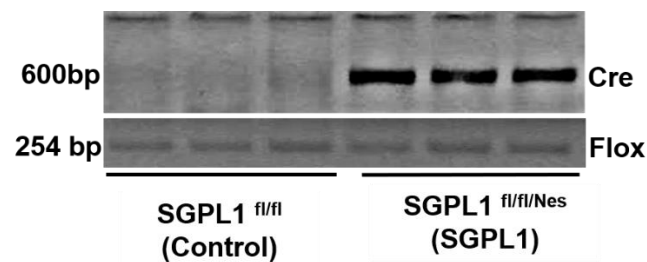


**Figure 25. Representative image of genotyping of control and SGPL1$^{fl/fl/Nes}$ mice.** In SGPL1$^{fl/fl/Nes}$ mice, the *Cre* gene amplification was noticed but not in control mice. *flox* gene was amplified in both control and SGPL1$^{fl/fl/Nes}$ mice. *Cre* gene amplification band was observed at 600bp, and *flox* gene amplification band was observed at 254bp.

Genomic DNA isolated from tails tip (1-3 days old) or ears tag (adult mouse) was used as template DNA for PCR to confirm the mice's genotype (Fig.26). A fragment of the *Cre* and *flox* gene was amplified to identify the control and SGPL1$^{fl/fl/Nes}$ mice. In SGPL1$^{fl/fl/Nes}$ mice, a DNA band of 600bp was expected on agarose gel due to the presence of the Cre recombinase gene. In contrast, no DNA band was expected on the agarose gel in control mice as Cre recombinase was absent (see result section 3.1).
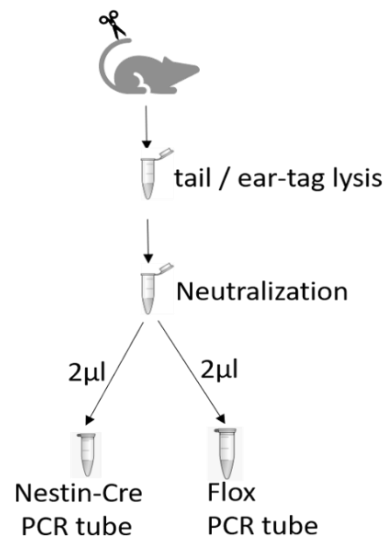


**Figure 26. Schematic representation of the collection of genomic DNA for PCR.**

### 5.3.1 Tissue lysis and genotyping

**Lysis buffer:**

| | |
|---|---|
| NaOH | 25 mM |
| EDTA | 0,2 mM |
| pH | 12 |

**Neutralization Buffer:**

| | |
|---|---|
| MOPS (3-[N-Morpholino] propansulfon acid) | 50 mM |

About 10-20 mm tail tips of the pups or ear-tag of adult mice were taken into a 1.5ml tube. 70 µl of lysis buffer were added in the tube and kept on 95° C and 300 rpm in the thermomixer for 1 h. Every 15 mins, tubes were vortexed for about 20 sec at maximum speed. After one h, 70 µl MOPS were added to neutralize the lysis buffer, and later the samples were centrifuged for 10 min at 10,000 rpm at 4°C. 2µl of supernatant were taken directly from the tube for the PCR (fig.9).

### 5.3.2   PCR

Two PCR tubes were prepared from each sample: one for the Nestin-Cre gene and another for the flox sequence. Flox gene was used as a PCR positive control as it was present in both control (SGPL1$^{fl/fl}$) mice and neural-specific knockout mice (SGPL1$^{fl/fl/Nes}$). PCR components were mixed and centrifuged shortly before starting the PCR program.

**Primers:**

Primer stock solution (100 µM) was prepared according to the manufacturer's instructions. For the working solution, 10 µM aliquots were prepared (1:10 dilution).

| | |
|---|---|
| Nestin-Cre | For- 5' TCC CTT CTC TAG TGC TCC ACG TCC<br>Rev- 5' TCC ATG AGT GAA CGA ACC TGG TCG |
| Flox | For- 5' GTG GTT CTG GAT GGA GTTTA<br>Rev- 5' GAA ATT GAG CAT ATC CGTTC |

Genotyping PCR components

| Components | Volume (µl) |
|---|---|
| 5x Taq polymerase Master-mix | 4.4 |
| primer (For+ Rev) | 1 |
| water | 13.6 |
| Template DNA (supernatant from tail tips or ear-tags) | 2 |
| Total | 20 |

**PCR program:**

To amplify the fragment of the *Cre* and *flox* gene, following PCR program was chosen.

<table>
<tr><td colspan="3" align="center"><b>Nestin-Cre</b></td><td colspan="3" align="center"><b>Flox</b></td></tr>
<tr><td>Steps</td><td>Time</td><td>Temp (°C)</td><td>Steps</td><td>Time</td><td>Temp (°C)</td></tr>
<tr><td>1</td><td>2 min</td><td>94</td><td>1</td><td>2 min</td><td>94</td></tr>
<tr><td>2</td><td>30sec</td><td>94</td><td>2</td><td>30sec</td><td>94</td></tr>
<tr><td>3</td><td>30 sec</td><td>60</td><td>3</td><td>30 sec</td><td>55</td></tr>
<tr><td>4</td><td>1 min</td><td>72</td><td>4</td><td>1 min</td><td>72</td></tr>
<tr><td colspan="3" align="center">35 cycles (4-2)</td><td colspan="3" align="center">35 cycles (4-2)</td></tr>
<tr><td>5</td><td>7 min</td><td>72</td><td>5</td><td>7 min</td><td>72</td></tr>
</table>

### 5.3.3 Agarose gel preparation and PCR product visualization

**TAE buffer:**

50X stock TAE buffer was diluted to 1X working solution.

**Loading dye:**

The following components (table) were added in distilled water, and the total volume was made up to 50ml. Later, the solution was heated at 65°C for 5 min and aliquoted 10 ml each. 25-50 mg of bromophenol blue was added to each aliquot.

**Table 1. Component of 50ml loading dye**

| | |
|---|---|
| Ficoll-400 | (12%, 12.5g) |
| Tris-Cl, pH 7.4 | 1 M (5ml) |
| EDTA | 0.5 M (10ml) |

A 3% agarose gel (4.5g agarose in 150ml 1XTAE buffer) containing 3µl ethidium bromide was prepared to visualize the PCR product. 2µl loading dye was added to 18µl of amplified PCR product and loaded into the gel pocket. The voltage was set to 70V until the samples had

run out of the well. Subsequently, it was increased to 120V for 30 mins. Images were acquired with the AlphaDigiDoc® RT Gel Documentation System.

## 5.4 TISSUE HARVESTING

Old mice (10-15 months) were killed by cervical dislocation. Whole-brain was isolated using a scissor and scalpel and afterward, instructions were followed, as shown in European Journal for Neuroscience's protocol video (EJNeuroscience 2014). The samples were separated and stored in cryovials and kept at -80°C until further use.

## 5.5 CELL CULTURE

### 5.5.1 Isolation and culture of mixed glial cells

#### 5.5.1.1 Microglia culture

The mixed glial culture was performed using P1 to P4 mouse pups. Four pup cortices were pooled together to achieve appropriate astrocyte density per T75 culture flask. The pups' neck was decapitated with a surgical scissor; both skull and skin were removed following the midline with an iris scissor. Skull was removed with curved forceps, and the brain was transferred with the help of a micro scoop into a separate petri dish with ice-cold HBSS buffer. Following this, the cerebellum and meninges were removed using forceps with straight tips. Similarly, another pup's brain hemisphere was prepared and transferred with the micro scoop into a 15 mL tube containing 1-2 ml $Ca^{2+}$- and $Mg^{2+}$-free HBSS and kept on ice until all control and SGPL1 deficient mice brain were dissected. After dissecting both control and SGPL1 deficient mice brain, HBSS was carefully aspirated, and 1-2 mL of 0.05 % Trypsin-EDTA in each tube was added. The tubes were incubated in a water bath at 37 °C for 10 min with constant shaking. 1-2 ml of prewarmed cell culture medium was added to neutralize Trypsin-EDTA. The tubes were centrifuged for a short time, following adding 1-2 ml prewarmed cell culture medium after carefully removing Trypsin-EDTA. Cortices were mechanically dissociated by pipetting up and down with a sterile 10 mL pipette. The cell suspension was loaded on poly L lysin-coated T75 cell culture flasks containing 10 mL prewarmed cell culture medium (3–4 hemispheres/flask) and incubate in a cell culture incubator at 37 °C overnight. The next day, the cell culture medium was removed, and cells were washed with prewarmed sterile PBS to remove cell debris and 10 mL of cell culture medium was added afterward. Cells were incubated for 2–3 days in a cell culture incubator at

37 °C until the astrocyte cell layer was confluent. The cell layer is mainly formed by astrocytes, while microglia and oligodendrocytes grow in a second layer above the astrocytes (Fig.28). The medium was changed and 25% (v/v) of L929 conditioned medium was added to induce microglial proliferation. After 2–3 days, the microglial population is found loosely attached on the top of the astrocytic cell layer. To harvest microglia, flasks were shaken horizontally (by hand), medium was collected in a 50 ml tube, and cell suspension was centrifuged at 900×g for 10 min. In phase-contrast microscopy, microglia appear round with a bright, shiny rim (Fig.27)

### 5.5.1.2  *Astrocytes culture*

To harvest astrocytes, the medium was renewed every two days and no extra L929 medium was added. After about 21 days, flasks were shaken horizontally, and the medium containing detached microglia and oligodendrocyte precursor cells (OPC) was removed (Fig.27). Later, astrocytes were collected and seeded onto 6-well cell culture dishes (35 mm diameter) and used for experiments after 24 h or as needed.
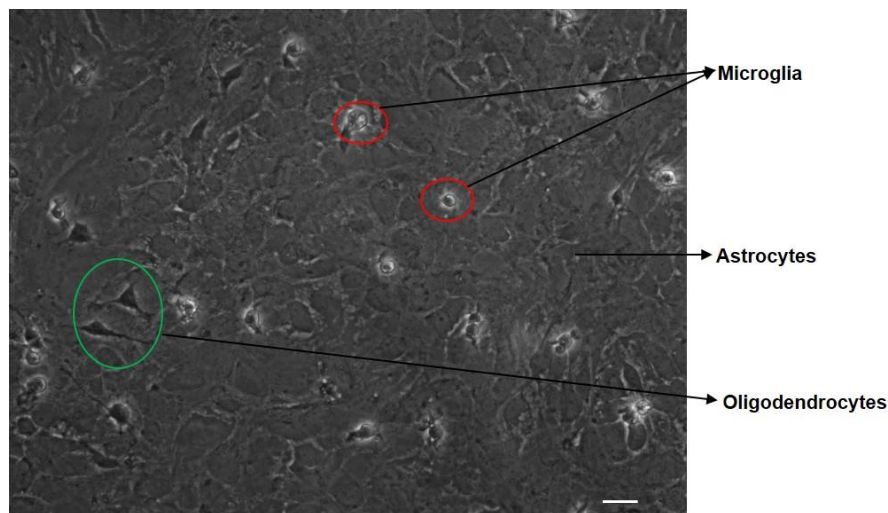


**Figure 27. An overview of mixed glial cell culture.** About a week after culturing the mixed glial cells, astrocyte (black arrows) forms a complete flask layer. Microglia (bright, shiny rim in red circle) and oligodendrocytes (green circle) are grown on top of the astrocyte layer, and neurons are absent. Astrocyte reached their maturity after three weeks in culture. Scale bar =100 μM.

### 5.5.2 Primary Neuron culture

Granular cell culture was performed using P6 or P7 mouse pup's cerebella. Pup's neck was decapitated with a surgical scissor, and both skull and skin were removed following the midline with an iris scissor. Skull was removed with curved forceps, and the brain was transferred with a micro scoop into a separate petri dish with ice-cold HBSS buffer. Then the cerebellum was separated, and meninges were removed using forceps with straight tips. Control and SGPL-lyase deficient cerebella were separately kept in a 15 ml tube with HBSS on ice. Cerebella were washed three times with HBSS, and 1ml Trypsin/DNase (0.05%) was added for 14 min at 37°C. After 14 minutes, Trypsin/DNase was removed, and the cerebella were washed three times with complete media. After a short centrifuge, Trypsin/DNase was aspirated, and 1 ml of DNase solution (0.1%) was added, and cells were dissociated by passing them repeatedly through a constricted Pasteur pipette which was constricted using a flame. The single-cell solution was centrifuged for 5 minutes at 1000 rpm. The cells were then suspended in Dulbecco's modified Eagle's medium supplemented with 10% heat-inactivated horse serum and 100 units/ml penicillin and streptomycin and the suspension was plated onto precoated poly-L-lysine (0.02mg/ml) 6-well plates (35mm in diameter). Twenty-four hours after plating, 1% of cytosine ß-D-arabinofuranoside hydrochloride was added to the medium to arrest the division of non-neuronal cells. After seven days in culture, cells were used for experiments as indicated (Fig.28).
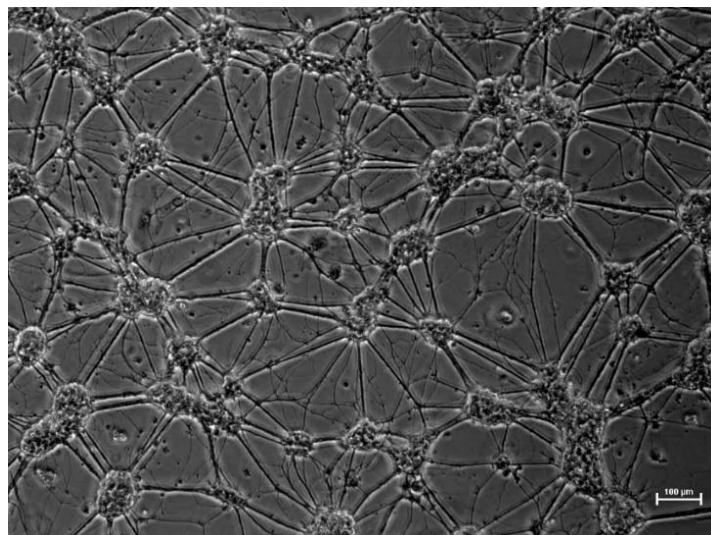


**Figure 28. Bright-field image of 10 days old granular neurons culture.** Granular neurons have a very small soma and several short dendrites. Scale bar =100 µM.

### 5.5.3   Cell harvesting

From a confluent T75 flask, cells were trypsinized for 15 mins for astrocytes and the same amount of complete media was added to neutralize the trypsin. Then, cells were centrifuged at 1000 rpm for 10 min and stored at -80°C until further use.

## 5.6   TISSUE AND CELL LYSATES PREPARATION

Freshly prepared RIPA lysis buffer and Laemilli buffer were used. 50X stock RIPA lysis buffer was diluted to 1X working solution, to which one tablet of protease inhibitor cocktail was added. Stock Laemmli buffer (4x) was ordered from Bio-RAD. To the stock Laemmli buffer (900 µl), β-Mercaptoethanol (100 µl) was added (1:10 ratio) to make a working buffer. Freshly prepared working Laemilli buffer was used for lysate preparation.

Brain tissue samples (hippocampus, cortex, and cerebellum) were weighed, and freshly prepared RIPA lysis buffer was added (three times larger volume than the tissue weight) and the samples were incubated on ice for 15 minutes. Following tissue softens, the tissues were homogenized using a syringe and incubated for further 45 min. Then, the samples were centrifuged for 45 min at 13,000 rpm. The clear supernatant (lysates) was transferred into a fresh tube.

Cell pellets were thawed on ice for 5 min, and then 150 µl of RIPA lysis buffer was added and mixed vigorously using the pipette and kept on ice for 1h. After every 15 mins, samples were vortexed for 10-20 sec at maximum speed. Similarly, tissue samples, cell samples were prepared and centrifuged for 45 min at 13,000 rpm, and clear supernatant (lysates) was transferred into a fresh tube.

Afterward, total protein concentration was measured using Bradford assay (see below). Total protein and Laemilli buffer were added in a 1:4 ratio, and samples were heated for 5 mins at 95°C before loading on SDS–PAGE gel.

## 5.7   DETERMINATION OF PROTEIN CONCENTRATION BY BRADFORD ASSAY

Protein concentration of the tissue and cell samples was determined using Bradford assay. Bradford assay is based on the complex formation of the Coomassie Brilliant Blue G-250 dye and aromatic and basic side chains of amino acids, thereby shifting the absorbance maximum

of the dye from 465 to 595nm. Sample protein concentration was determined using the standard curve as concentrations of the standards (BSA) were known. Tissue samples lysates were diluted in the ratio of 1:100 in distilled water (dilution factor 100) since protein concentration was too high (beyond highest standard concentration) and 5µl were taken for measurement. Cell samples were used as such without dilution since their concentration was within the range of standard curve. Samples were incubated for 10 min at room temperature and then reading was taken using a microplate reader (Table 1). The relative concentrations were calculated using a microplate reader.

**Coomassie solution:**

| | |
|---:|---|
| Coomassie Brilliant Blue G-250 | 250 mg |
| Ethanol | 125 ml |
| 85% phosphoric acid | 250 ml |
| Water | Up to 500 ml |

Protein standard (BSA, 250µg/ml) was prepared from stock solution (2mg/ml), and Coomassie blue solution was diluted in distilled water (1:5) before the experiment.

**Table 1: Determination of unknown protein sample's concentration.** The standard stock concentration was 250 µg/ml. Each standard and samples were pipetted as a doublet. 5 µl from each sample were pipetted. 200 µl Coomassie solution were added in each standard and sample wells. Samples were incubated for 10 min at room temperature, and then absorption was recorded at 620 nM.

| | 1 | 2 | 3 | 4 | 5 | 6 | 7 | 8 |
|---|---|---|---|---|---|---|---|---|
| **A** | 20µl H$_2$O | 20µl H$_2$O | 5µl H$_2$O +15µl BSA | 5µl H$_2$O +15µl BSA | | | | |
| **B** | 19µlH$_2$O +1µl BSA | 19µlH$_2$O +1µl BSA | 3µl H$_2$O +17µl BSA | 3µl H$_2$O +17µl BSA | | | | |
| **C** | 17µl H$_2$O +3µl BSA | 17µl H$_2$O +3µl BSA | 20µl BSA | 20µl BSA | | | | |
| **D** | 15µl H$_2$O +5µl BSA | 15µl H$_2$O +5µl BSA | 15µl H$_2$O +5µl **sample A** | 15µl H$_2$O +5µl **sample A** | | | | |
| **E** | 13µl H$_2$O +7µl BSA | 13µl H$_2$O +7µl BSA | 15µl H$_2$O +5µl **sample B** | 15µl H$_2$O +5µl **sample B** | | | | |
| **F** | 11µl H$_2$O +9µl BSA | 11µl H$_2$O +9µl BSA | 15µl H$_2$O +5µl **sample C** | 15µl H$_2$O +5µl **sample C** | | | | |
| **G** | 9µl H$_2$O +11µl BSA | 9µl H$_2$O +11µl BSA | 15µl H$_2$O +5µl **sample D** | 15µl H$_2$O +5µl **sample D** | | | | |
| **H** | 7µl H$_2$O +13µl BSA | 7µl H$_2$O +13µl BSA | | | | | | |

## 5.8  SDS-PAGE

SDS-PAGE method is used to separate protein or charged molecules according to their molecular weight (Nowakowski, Wobig et al. 2014). SDS (Sodium dodecyl sulfate) is a detergent that denatures the proteins by disturbing the non-covalent forces and linearizing the polypeptide chains. SDS is negatively charged and covers up the amino acid side chains with micelle formation's intrinsic charges. Micelle bonded proteins travel from the cathode to the anode at equal mass-to-charge ratio and separate according to their size. Ammonium persulfate (APS) and the reducing agent tetramethyl ethylene diamine (TEMED) work as an inducer to initiate the bisacrylamide-dependent polymerization. The amount of bisacrylamide decides the gel percentage to separate different molecular weight proteins (Table.2).

**Table 2. SDS-PAGE gel percentage and component**

| Gel percentage | Molecular weight range |
|:---:|:---:|
| 6% | 50 kDa -500 kDa |
| 10% | 20 kDa -300 kDa |
| 12% | 10 kDa -200 kDa |

**For 5 ml stacking gel preparation:**

| | |
|:---:|:---:|
| Water | 2.975 ml |
| Acrylamide/Bis-acrylamide (30%/0.8% w/v | 0.67 ml |
| 0.5 M Tris-HCl, pH 6.8 | 1.25 ml |
| 10% (w/v) SDS | 0.05 ml |
| 10%(w/v) ammonium persulfate (APS) | 0.05 ml |
| TEMED | 0.005 ml |

**For 10 ml separating gel preparation**

| Gel percentage | 6% | 8% | 10% | 12% |
| --- | --- | --- | --- | --- |
| Water | 5.2 ml | 4.6 ml | 3.2 ml | 2.2 ml |
| Acrylamide/Bis-acrylamide (30%/0.8% w/v) | 2 ml | 2.6ml | 3.4 ml | 5 ml |
| 1.5 M Tris-HCl, pH 8.8 | 2.6 ml | 2.6 ml | 2.6 ml | 2.6 ml |
| 10% (w/v) SDS | 0.1 ml | 0.1 ml | 0.1 ml | 0.1 ml |
| 10%(w/v) ammonium persulfate (APS) | 100µl | 100µl | 100µl | 100µl |
| TEMED | 10µl | 10µl | 10µl | 10µl |

10 x SDS running buffer: Tris base (30.23 g)

Glycine (144 g)

SDS (10 g)

ddH2O (900 ml)

Diluted to 1x with ddH2O

During SDS-PAGE, the final protein concentration of 2 µg/µl (5-15 µl) of the sample was used for loading. The samples were heated at 95 °C for 5 min. The gel was made to run for 30 min at 50 V and later, the voltage was increased to 150 V for 90 min.

## 5.9  WESTERN IMMUNOBLOTTING

10x Transfer buffer (1 L stock):  Tris base 25 mM (30.23 g)

Glycine 190 mM (142.63 g)

ddH2O (up to 1 L)

1x Transfer buffer (1 L):        10x Transfer buffer (100 ml)

ddH2O (700 ml)

Methanol (200 ml) (fresh)

10x TBST buffer (1 L stock):     NaCl 150 mM (87.66 g)

Tris 20 mM pH 7.5 (24.3 g)

0.1% tween 20 (10 ml)

1x TBST buffer (1 L ):     10x TBST (100 ml)

ddH2O (900 ml)

Blocking buffer (50 ml):     5% BSA or Milk (2.5 g in 50 ml 1XTBST buffer)

25 µl Tween-20 (add fresh in 50 ml)

Western blot is used to detect a particular protein from the cell or tissue lysates and is mainly used to determine the size of a particular protein and measure protein expression. Protein separated on SDS-PAGE was transferred onto PVDF membrane. The protein transfer was performed at 4°C with 400 mA for 2h in transfer buffer. PVDF membrane was blocked with 5% milk powder or 5% BSA (for phosphorylated proteins) in TBST buffer for 1h, washed 2 times (5 min each), and incubated at 4°C overnight with the primary antibody. After that, membranes were rewashed with TBST buffer (3X10 mins each) and incubated for 1h at room temperature on a rotator with an HRP-conjugated secondary antibody. Again, the membrane was washed (3X times, 10min each) to remove the excess secondary antibody. The PVDF membrane was exposed to Western BLoT chemiluminescence HRP Substrate, and the image was detected with the VersaDoc 5000 imaging system. Quantification was performed using ImageJ and Prism GraphPad program.

## 5.10 RNA ISOLATION

Total RNA was isolated using EXTRAzol from Blirt. The tissue samples (7-30 mg) were homogenized in 1ml EXTRAzol using a micro-pestle, and cells were homogenized in 800µl EXTRAzol. Samples were incubated for 5 min at room temperature in EXTRAzol. For phase separation, 200 µl chloroform were added per 1ml EXTRAzol and vigorously shaken by hand for 15 seconds and kept at room temperature for 3 mins. Afterward, samples were centrifuged for 15 mins at 10000 rpm at 4°C, separating samples into a pale-yellow phase, interphase, and a colorless upper aqueous phase. The upper phase containing RNA was transferred very carefully to another tube.  500 µl of ice-cold isopropyl alcohol was mixed per 1ml EXTRAzol and incubated for 10 mins to precipitate the RNA. After incubation, samples were centrifuged for 10 mins at 12000 rpm at 4°C. A small white pellet was seen at the bottom of the tubes,

which was unpurified RNA. 1ml of 75% ethanol was added, vortexed, and centrifuged for 5 min at 7500 rpm at 4°C to purify the RNA. Ethanol was removed, and samples were air-dried and dissolved in 25 µl of PCR or RNase-free water and kept on ice for short-term and at -80°C for long-term storage.

## 5.11 MEASUREMENT OF RNA CONCENTRATION AND QUALITY

The total RNA sample concentration was measured using SmartSpec™Plus spectrophotometer from Bio-Rad. Samples were diluted in the ratio of 1:70 with RNase-free water (dilution factor 70), and RNA concentration was measured in µg/ml. The spectrophotometer measures the light passing through the cuvette. Nucleic acids absorb light at a wavelength of 260 nm, which decreases upon increasing nucleic acid concentrations. $A_{260/280}$ ratio was taken to check the purity of isolated RNA. For pure RNA, $A_{260/280}$ ratio was expected at a value of 2. A lower $A_{260/280}$ ratio indicates DNA and protein contaminations.

## 5.12 CDNA SYNTHESIS

Complementary DNA or cDNA are synthesized from an RNA template *via* reverse transcription, serving as a qPCR template. Isolated total RNA was used for reverse transcription with the TAKARA kit (Prime Script RT Master Mix). Up to 1 µg RNA was used (max 8 µl), and 2 µl of the 5X master mix was mixed (total volume 10 µl) and incubated at 37°C for 15 mins. The resulting total cDNA was then utilized in real-time PCR.

## 5.13 PRIMER DESIGN FOR REAL-TIME QPCR

NCBI-Nucleotide database was used to search the FASTA sequence of the gene. NCBI Primer-BLAST tool and Primer3web were used to design the primers for real-time PCR obtained from Invitrogen. The primers were designed to have an optimum Tm of 60°C ± 3°C. The product size was a maximum of 250bp. Moreover, most importantly, primers often bind at the exon-exon junction, restricting the primers from binding on genomic DNA. Therefore, primers binding at the exon-exon junction were avoided.

## 5.14 REAL-TIME PCR

Real-time PCR (RT-PCR), also known as quantitative polymerase chain reaction (qPCR), determines the amount of PCR product in real-time. In qPCR, the fluorescent dye SYBR green binds to the amplified dsDNA molecule, and during each cycle, fluorescence is measured. As the cycle progresses, the fluorescent signal increases with a proportional increase in the DNA amount, allowing quantifying the DNA in real-time.

At the beginning of the PCR program, there are undetectable cycles. Eventually, enough amplified PCR product accumulates to yield a detectable fluorescent signal. The cycle at which the detectable signal start is called the threshold cycle (Ct value) or quantification cycle (Cq value). The Cq determines the amount of template DNA present at the start of the amplification reaction. The low Cq value represents the high amount of template DNA present as less cycles are needed to accumulate enough product to detect the fluorescent signal. In contrast, a high Cq value represents a low amount of template DNA; more cycles are needed to accumulate enough product to detect the fluorescent signal (Fig.29).
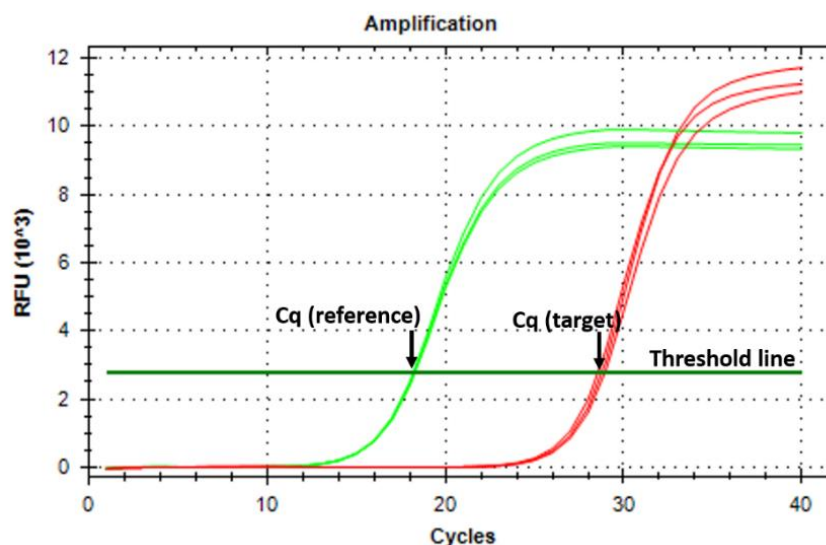


**Figure 29. Representative graph of qPCR amplification on a linear scale.** The green amplification plot represents the reference gene, and the red amplification plot represents the target gene. The threshold was set manually above the baseline in the region of exponential amplification across all plots. Obtained Cq values were used in relative quantification (see section 5.15).

Fluorescent dye SYBR green can bind to all dsDNA present in the reaction mixture. Primers can bind unpacifically to themselves or another place of cDNA. Melt-curve (or dissociation curve) analysis is done to check unspecific binding. A melt-curve presents a graph between

temperature and fluorescence change. As temperature increases, double-stranded DNA incorporated with dye molecules dissociates or "melts" into single-stranded DNA (ssDNA) (Fig.30).
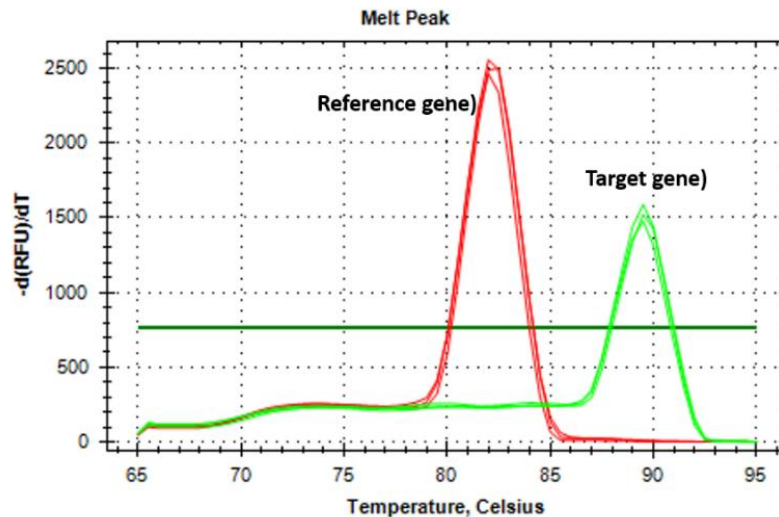


**Figure 30. Image representing a melting peak.** After the qPCR reaction, the temperature was gradually increased. The increased temperature started dissociating the double-stranded cDNA and the incorporated SYBR Green dye resulting in a sudden decrease in fluorescence. The peak represents the melting temperature of a particular DNA fragment present.

The reactions were performed at 95 °C for 30 s, 95 °C for 5 s, and 60 °C for 1 min. Relative normalized mRNA expression was obtained from real-time qPCR (Fig.31).
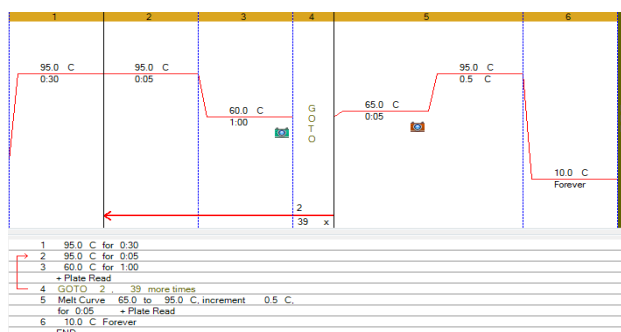


| Time | Temp | Process |
| --- | --- | --- |
| 30 Sec | 95°C | Activation and Denaturation |
| 5 Sec | 95°C | Denaturation |
| 1 min | 60°C | Annealing and extension |

**Figure 31. qPCR program used for amplification.** (qPCR program image (left) and tabular form (right).

## 5.15 REAL-TIME QPCR DATA ANALYSIS

The real-time qPCR data analysis was performed using the $2^{-\Delta\Delta C_T}$ (Livak) method. In this method, the amplification efficiency of the target and reference gene is considered nearly 100%. This method determines the relative difference in the expression level of the target and reference gene (in this case β-actin). The following formula was used to calculate fold change in the sample.

$$\Delta C_{T\,(Control)} = \Delta C_{T\,(Control,\,target)} - \Delta C_{T\,(Control,\,reference)}$$

$$\Delta C_{T\,(KO)} = \Delta C_{T\,(KO,\,target)} - \Delta C_{T\,(KO,\,reference)}$$

$$\Delta\Delta C_T = \Delta C_{T\,(KO)} - \Delta C_{T\,(Control)}$$

Normalized expression ratio $= 2^{-\Delta\Delta C_T}$

The obtained normalized expression ratio is a fold change of the target gene compared to the reference gene. Statistical significance of the relative normalized mRNA expression was determined by t-test in Prism GraphPad9 program.

**Example:**

| Sample | Ct (IL-6) | Ct (β-actin) |
|--------|-----------|--------------|
| Control | 18.0 | 20.8 |
| KO | 15.0 | 19.0 |

$$\Delta C_{T\,(Control)} = \Delta C_{T\,(Control,\,IL6)} - \Delta C_{T\,(Control,\,\beta\text{-actin})}$$

$$\Delta C_{T\,(Control)} = 18.0-20.8$$

$$= -2.8$$

$$\Delta C_{T\,(KO)} = \Delta C_{T\,(KO,\,IL6)} - \Delta C_{T\,(KO,\,\beta\text{-actin})}$$

$$\Delta C_{T\,(KO)} = 15.0-19-0$$

$$= -4.0$$

$$\Delta\Delta C_T = \Delta C_{T\,(KO)} - \Delta C_{T\,(Control)}$$

$$\Delta\Delta C_T = -4-(-2.81)$$

$$= -1.2$$

Normalized expression ratio $= 2^{-\Delta\Delta C_T} = 2^{-(-1.2)} = 2.297$

In this example, IL-6 was 2.297-fold increase in KO sample.

## 5.16 IMMUNOCYTOCHEMISTRY

After about 21 days of growth in T75 flasks, cells were transferred on coverslips and grown for further 2 days. Afterward, coverslips with astrocytes were rinsed 3 times with PBS at room temperature (RT) and then fixed in methanol (-20°C, 5 min). Between each incubation step, cells were always rinsed 3 times with PBS. Subsequently, cells were blocked in 20% (v/v) normal goat serum in PBS for 30 min. and incubated overnight at 4 °C with primary antibody diluted in the ratio of 1:200 with PBS. Following this, cells were incubated with anti-rabbit/mouse Alexa Fluor 488 (1:300)-conjugated secondary antibodies for 50 min at RT. Finally, cells were embedded in Fluoromount G medium with DAPI for microscopic analyses.

## 5.17 IMMUNOHISTOCHEMISTRY

Brains were removed and quick-frozen in liquid nitrogen. Cryo-sectioning was used to produce 10 µm sagittal sections, which were placed on Superfrost Plus positively charged microscope slides. Brain sections were fixed for 5 min in ice-cold 4 % (v/v) paraformaldehyde in PBS. Sections were then permeabilized with 0.1 % (v/v) Triton X-100 in PBS for 30 min at room temperature (RT). Tissue sections were blocked in 20 % (v/v) normal goat serum in PBS for 30 min and incubated overnight at 4 °C with primary antibody. The primary antibodies were diluted 1:200 in PBS containing 0.5% lambda-carrageenan (Sigma) and 0.02% sodium azide and applied overnight to the sections at 4°C. Following a washing step, brain sections were incubated with Cy3-conjugated anti-rabbit antibody diluted 1:300 in PBS with the same additions as above for 1 hour at RT. Finally, antibody-labeled brain sections were embedded in Fluoromount G medium with DAPI for microscopic analysis (Zeiss Axioskop 2 epi-fluorescence microscope equipped with a digital Zeiss AxioCamHRc camera, Carl Zeiss Jena, Germany).

## 5.18 ELISA

Concentrations of IL-6 and TNFα in primary cultured astrocytes and their culture medium were measured using ELISA according to manufacturer's guidelines (Invitrogen™ eBioscience™ Mouse IL-6 ELISA Ready-SET-Go! ™ Kit, 15511037), (Invitrogen™ eBioscience™ Mouse TNF-alpha ELISA Ready-SET-Go! ™ Kit, 88-7324-86) and illustrated as picogram/milliliter and picomol/milligram, respectively.

## 5.19 TREATMENT OF CELLS

### 5.19.1 Rapamycin treatment

For the autophagy rescue experiments with rapamycin, control astrocyte and SGPL1deficient astrocytes were incubated with 5 µM rapamycin 5 h. Rapamycin was added from a stock prepared in ethanol that ensured a final ethanol concentration of less than 1% in the medium to avoid toxicity. Exact amounts of ethanol were added to control astrocyte cultures.

### 5.19.2 JTE-013 and CYM-55380 treatment

For the glycolysis rescue experiments, JTE-013 (JTE) and CYM-55380 (CYM) were used, which block S1P receptors 2 and 4, respectively. Control and SGPL1-deficient astrocytes were incubated with 10 µM each of JTE and CYM for 5hs. JTE and CYM were added from a stock prepared in ethanol and DMSO, respectively, that ensured final ethanol and DMSO concentration of less than 1% in the medium to avoid toxicity. Exact amounts of ethanol and DMSO were added to control astrocyte cultures.

### 5.19.3 MRS2179 treatment

For the rescue experiments of astrocytic hyperactivity, astrocytes were treated with 100 µM of MRS2179 for 24 h to block the P2Y1 receptor. MRS2179 stock solution was prepared in water. Exact amounts of water were added to control astrocyte cultures.

### 5.19.4 BAPTA-AM treatment

Hippocampal and cortical slices of 200 µm thickness were prepared in ice-cold high sucrose solution (220 mM sucrose, 26 mM $NaHCO_3$, 10 mM glucose, 6 mM $MgSO_4.7H_2O$, 3 mM KCL solid, 1.25 mM $NaH_2PO4$. $H_2O$, 0.43 mM $CaCl_2$) gassed with carbogen. Then, both hippocampal and cortical slices were incubated in artificial cerebrospinal fluid (119 mM NaCl, 26.2 mM $NaHCO_3$, 2.5 mM KCl, 1 mM $NaH_2PO4$, 1.3 mM $MgCl_2$, 10 mM glucose) with and without 150 µM BAPTA-AM for 2 h and kept at -80°C until use.

For the tau phosphorylation and histone acetylation in neurons and astrocytes, cells were treated with 500 nM BAPTA-AM for 5hrs. BAPTA-AM stock solution was prepared in ethanol in a concentration (less than 1%) to avoid toxicity. The exact amount of ethanol was also added to control neuron and astrocyte cultures.

## 5.20 mRFP-EGFP TANDEM FLUORESCENT-TAGGED LC3 EXPRESSION

Primary cultured astrocytes were transfected with mRFP-GFP tandem fluorescent-tagged LC3 on day 21. After 24 h, astrocytes were treated with 5 μM rapamycin for 5 h. Finally, astrocytes were fixed with 4% PFA for 10 min. Finally, cells were embedded in Fluoromount G medium with DAPI for microscopic analyses.

## 5.21 MASS SPECTROMETRY

Lipid measurements were performed in cooperation with Prof. Dr. Markus Gräler's lab (University Hospital Jena, Germany) using liquid chromatography coupled to triple-quadrupole mass spectrometry (LC/MS/MS) as described in (Karunakaran, Alam et al. 2019).

## 5.22 STATISTICAL ANALYSIS

The GraphPad Prism 9 software was used for statistical analysis. All values are expressed as means ± SEM obtained from at least 3 independent experiments otherwise stated in the figure ligand. The significance of differences between the experimental groups and controls was assessed by either student's t-test with false discovery rate (FDR) correction or One-Way ANOVA, as appropriate. $P < 0.05$ was considered statistically significant (*$p < 0.05$; **$p < 0.01$; ***$p < 0.001$; compared with the respective control group).

# 6 REFERENCES

Abbracchio, M. P., R. Brambilla, S. Ceruti and F. Cattabeni (1999). "Signalling mechanisms involved in P2Y receptor-mediated reactive astrogliosis." Prog Brain Res **120**: 333-342.

Abbracchio, M. P. and G. Burnstock (1994). "Purinoceptors: are there families of P2X and P2Y purinoceptors?" Pharmacol Ther **64**(3): 445-475.

Abbracchio, M. P., G. Burnstock, J. M. Boeynaems, E. A. Barnard, J. L. Boyer, C. Kennedy, G. E. Knight, M. Fumagalli, C. Gachet, K. A. Jacobson and G. A. Weisman (2006). "International Union of Pharmacology LVIII: update on the P2Y G protein-coupled nucleotide receptors: from molecular mechanisms and pathophysiology to therapy." Pharmacol Rev **58**(3): 281-341.

Abbracchio, M. P., G. Burnstock, A. Verkhratsky and H. Zimmermann (2009). "Purinergic signalling in the nervous system: an overview." Trends Neurosci **32**(1): 19-29.

Abbracchio, M. P. and C. Verderio (2006). "Pathophysiological roles of P2 receptors in glial cells." Novartis Found Symp **276**: 91-103; discussion 103-112, 275-181.

Aguilar, A. and J. D. Saba (2012). "Truth and consequences of sphingosine-1-phosphate lyase." Adv Biol Regul **52**(1): 17-30.

Alam, S., A. Piazzesi, M. Abd El Fatah, M. Raucamp and G. van Echten-Deckert (2020). "Neurodegeneration Caused by S1P-Lyase Deficiency Involves Calcium-Dependent Tau Pathology and Abnormal Histone Acetylation." Cells **9**(10).

Alle, H., A. Roth and J. R. Geiger (2009). "Energy-efficient action potentials in hippocampal mossy fibers." Science **325**(5946): 1405-1408.

Aoki, M., H. Aoki, R. Ramanathan, N. C. Hait and K. Takabe (2016). "Corrigendum to "Sphingosine-1-Phosphate Signaling in Immune Cells and Inflammation: Roles and Therapeutic Potential"." Mediators Inflamm **2016**: 2856829.

Araque, A., V. Parpura, R. P. Sanzgiri and P. G. Haydon (1999). "Tripartite synapses: glia, the unacknowledged partner." Trends Neurosci **22**(5): 208-215.

Avila, J. (2008). "Tau kinases and phosphatases." J Cell Mol Med **12**(1): 258-259.

Barakat, S., M. Demeule, A. Pilorget, A. Regina, D. Gingras, L. G. Baggetto and R. Beliveau (2007). "Modulation of p-glycoprotein function by caveolin-1 phosphorylation." J Neurochem **101**(1): 1-8.

Belanger, M., I. Allaman and P. J. Magistretti (2011). "Brain Energy Metabolism: Focus on Astrocyte-Neuron Metabolic Cooperation." Cell Metabolism **14**(6): 724-738.

Blaho, V. A. and T. Hla (2014). "An update on the biology of sphingosine 1-phosphate receptors." J Lipid Res **55**(8): 1596-1608.

Bonnaud, E. M., E. Suberbielle and C. E. Malnou (2016). "Histone acetylation in neuronal (dys)function." Biomol Concepts **7**(2): 103-116.

Bozoyan, L., J. Khlghatyan and A. Saghatelyan (2012). "Astrocytes Control the Development of the Migration-Promoting Vasculature Scaffold in the Postnatal Brain via VEGF Signaling." Journal of Neuroscience **32**(5): 1687-1704.

Brambilla, R. and M. P. Abbracchio (2001). "Modulation of cyclooxygenase-2 and brain reactive astrogliosis by purinergic P2 receptors." Ann N Y Acad Sci **939**: 54-62.

Burnstock, G. (1976). "Purinergic receptors." J Theor Biol **62**(2): 491-503.

Burnstock, G., B. B. Fredholm and A. Verkhratsky (2011). "Adenosine and ATP receptors in the brain." Curr Top Med Chem **11**(8): 973-1011.

Bushong, E. A., M. E. Martone, Y. Z. Jones and M. H. Ellisman (2002). "Protoplasmic astrocytes in CA1 stratum radiatum occupy separate anatomical domains." Journal of Neuroscience **22**(1): 183-192.

Cai, Z., M. D. Hussain and L. J. Yan (2014). "Microglia, neuroinflammation, and beta-amyloid protein in Alzheimer's disease." Int J Neurosci **124**(5): 307-321.

Ceccom, J., N. Loukh, V. Lauwers-Cances, C. Touriol, Y. Nicaise, C. Gentil, E. Uro-Coste, S. Pitson, C. A. Maurage, C. Duyckaerts, O. Cuvillier and M. B. Delisle (2014). "Reduced sphingosine kinase-1 and enhanced sphingosine 1-phosphate lyase expression demonstrate deregulated sphingosine 1-phosphate signaling in Alzheimer's disease." Acta Neuropathol Commun **2**: 12.

Cho, M. H., K. Cho, H. J. Kang, E. Y. Jeon, H. S. Kim, H. J. Kwon, H. M. Kim, D. H. Kim and S. Y. Yoon (2014). "Autophagy in microglia degrades extracellular beta-amyloid fibrils and regulates the NLRP3 inflammasome." Autophagy **10**(10): 1761-1775.

Choi, J. W. and J. Chun (2013). "Lysophospholipids and their receptors in the central nervous system." Biochim Biophys Acta **1831**(1): 20-32.

Choi, Y. J. and J. D. Saba (2019). "Sphingosine phosphate lyase insufficiency syndrome (SPLIS): A novel inborn error of sphingolipid metabolism." Adv Biol Regul **71**: 128-140.

Coco, S., F. Calegari, E. Pravettoni, D. Pozzi, E. Taverna, P. Rosa, M. Matteoli and C. Verderio (2003). "Storage and release of ATP from astrocytes in culture." J Biol Chem **278**(2): 1354-1362.

Couttas, T. A., N. Kain, B. Daniels, X. Y. Lim, C. Shepherd, J. Kril, R. Pickford, H. Li, B. Garner and A. S. Don (2014). "Loss of the neuroprotective factor Sphingosine 1-phosphate early in Alzheimer's disease pathogenesis." Acta Neuropathol Commun 2: 9.

Crawford, M. A. and A. J. Sinclair (1971). "Nutritional influences in the evolution of mammalian brain. In: lipids, malnutrition & the developing brain." Ciba Found Symp: 267-292.

Cui, W., N. D. Allen, M. Skynner, B. Gusterson and A. J. Clark (2001). "Inducible ablation of astrocytes shows that these cells are required for neuronal survival in the adult brain." Glia 34(4): 272-282.

Cuvillier, O., G. Pirianov, B. Kleuser, P. G. Vanek, O. A. Coso, S. Gutkind and S. Spiegel (1996). "Suppression of ceramide-mediated programmed cell death by sphingosine-1-phosphate." Nature 381(6585): 800-803.

De Duve, C. and R. Wattiaux (1966). "Functions of lysosomes." Annu Rev Physiol 28: 435-492.

De Lucia, C., A. Rinchon, A. Olmos-Alonso, K. Riecken, B. Fehse, D. Boche, V. H. Perry and D. Gomez-Nicola (2016). "Microglia regulate hippocampal neurogenesis during chronic neurodegeneration." Brain Behav Immun 55: 179-190.

de Ruijter, A. J., A. H. van Gennip, H. N. Caron, S. Kemp and A. B. van Kuilenburg (2003). "Histone deacetylases (HDACs): characterization of the classical HDAC family." Biochem J 370(Pt 3): 737-749.

Delekate, A., M. Fuchtemeier, T. Schumacher, C. Ulbrich, M. Foddis and G. C. Petzold (2014). "Metabotropic P2Y1 receptor signalling mediates astrocytic hyperactivity in vivo in an Alzheimer's disease mouse model." Nat Commun 5: 5422.

Dienel, G. A. (2019). "Brain Glucose Metabolism: Integration of Energetics with Function." Physiol Rev 99(1): 949-1045.

Divecha, N. and R. F. Irvine (1995). "Phospholipid signaling." Cell 80(2): 269-278.

Dusaban, S. S., J. Chun, H. Rosen, N. H. Purcell and J. H. Brown (2017). "Sphingosine 1-phosphate receptor 3 and RhoA signaling mediate inflammatory gene expression in astrocytes." J Neuroinflammation 14(1): 111.

Eberharter, A. and P. B. Becker (2002). "Histone acetylation: a switch between repressive and permissive chromatin. Second in review series on chromatin dynamics." EMBO Rep 3(3): 224-229.

EJNeuroscience (2014). "Isolation of adult mouse hippocampus." youtube.

Eroglu, C. and B. A. Barres (2010). "Regulation of synaptic connectivity by glia." Nature **468**(7321): 223-231.

Escartin, C., E. Galea, A. Lakatos, J. P. O'Callaghan, G. C. Petzold, A. Serrano-Pozo, C. Steinhauser, A. Volterra, G. Carmignoto, A. Agarwal, N. J. Allen, A. Araque, L. Barbeito, A. Barzilai, D. E. Bergles, G. Bonvento, A. M. Butt, W. T. Chen, M. Cohen-Salmon, C. Cunningham, B. Deneen, B. De Strooper, B. Diaz-Castro, C. Farina, M. Freeman, V. Gallo, J. E. Goldman, S. A. Goldman, M. Gotz, A. Gutierrez, P. G. Haydon, D. H. Heiland, E. M. Hol, M. G. Holt, M. Iino, K. V. Kastanenka, H. Kettenmann, B. S. Khakh, S. Koizumi, C. J. Lee, S. A. Liddelow, B. A. MacVicar, P. Magistretti, A. Messing, A. Mishra, A. V. Molofsky, K. K. Murai, C. M. Norris, S. Okada, S. H. R. Oliet, J. F. Oliveira, A. Panatier, V. Parpura, M. Pekna, M. Pekny, L. Pellerin, G. Perea, B. G. Perez-Nievas, F. W. Pfrieger, K. E. Poskanzer, F. J. Quintana, R. M. Ransohoff, M. Riquelme-Perez, S. Robel, C. R. Rose, J. D. Rothstein, N. Rouach, D. H. Rowitch, A. Semyanov, S. Sirko, H. Sontheimer, R. A. Swanson, J. Vitorica, I. B. Wanner, L. B. Wood, J. Wu, B. Zheng, E. R. Zimmer, R. Zorec, M. V. Sofroniew and A. Verkhratsky (2021). "Reactive astrocyte nomenclature, definitions, and future directions." Nat Neurosci **24**(3): 312-325.

Fahy, E., S. Subramaniam, R. C. Murphy, M. Nishijima, C. R. Raetz, T. Shimizu, F. Spener, G. van Meer, M. J. Wakelam and E. A. Dennis (2009). "Update of the LIPID MAPS comprehensive classification system for lipids." J Lipid Res **50 Suppl**: S9-14.

Falchi, A. M., V. Sogos, F. Saba, M. Piras, T. Congiu and M. Piludu (2013). "Astrocytes shed large membrane vesicles that contain mitochondria, lipid droplets and ATP." Histochem Cell Biol **139**(2): 221-231.

Fan, H., Y. Wu, S. Yu, X. Li, A. Wang, S. Wang, W. Chen and Y. Lu (2021). "Critical role of mTOR in regulating aerobic glycolysis in carcinogenesis (Review)." Int J Oncol **58**(1): 9-19.

Filous, A. R. and J. Silver (2016). ""Targeting astrocytes in CNS injury and disease: A translational research approach"." Progress in Neurobiology **144**: 173-187.

Fischer, I., C. Alliod, N. Martinier, J. Newcombe, C. Brana and S. Pouly (2011). "Sphingosine kinase 1 and sphingosine 1-phosphate receptor 3 are functionally upregulated on astrocytes under pro-inflammatory conditions." PLoS One **6**(8): e23905.

Fischer, W., K. Appelt, M. Grohmann, H. Franke, W. Norenberg and P. Illes (2009). "Increase of intracellular Ca2+ by P2X and P2Y receptor-subtypes in cultured cortical astroglia of the rat." Neuroscience **160**(4): 767-783.

Franke, H. and P. Illes (2014). "Nucleotide signaling in astrogliosis." Neurosci Lett **565**: 14-22.

Franke, H., U. Krugel and P. Illes (1999). "P2 receptor-mediated proliferative effects on astrocytes in vivo." Glia **28**(3): 190-200.

Franke, H., A. Verkhratsky, G. Burnstock and P. Illes (2012). "Pathophysiology of astroglial purinergic signalling." Purinergic Signal **8**(3): 629-657.

Frost, B., M. Hemberg, J. Lewis and M. B. Feany (2014). "Tau promotes neurodegeneration through global chromatin relaxation." Nat Neurosci **17**(3): 357-366.

Fujita, T., H. Tozaki-Saitoh and K. Inoue (2009). "P2Y1 receptor signaling enhances neuroprotection by astrocytes against oxidative stress via IL-6 release in hippocampal cultures." Glia **57**(3): 244-257.

Gallinari, P., S. Di Marco, P. Jones, M. Pallaoro and C. Steinkuhler (2007). "HDACs, histone deacetylation and gene transcription: from molecular biology to cancer therapeutics." Cell Res **17**(3): 195-211.

Ghosh, T. K., J. Bian and D. L. Gill (1994). "Sphingosine 1-phosphate generated in the endoplasmic reticulum membrane activates release of stored calcium." J Biol Chem **269**(36): 22628-22635.

Groves, A., Y. Kihara and J. Chun (2013). "Fingolimod: direct CNS effects of sphingosine 1-phosphate (S1P) receptor modulation and implications in multiple sclerosis therapy." J Neurol Sci **328**(1-2): 9-18.

Grunstein, M. (1997). "Histone acetylation in chromatin structure and transcription." Nature **389**(6649): 349-352.

Gustafsson, A. J., L. Muraro, C. Dahlberg, M. Migaud, O. Chevallier, H. N. Khanh, K. Krishnan, N. Li and M. S. Islam (2011). "ADP ribose is an endogenous ligand for the purinergic P2Y1 receptor." Mol Cell Endocrinol **333**(1): 8-19.

Hagen, N., M. Hans, D. Hartmann, D. Swandulla and G. van Echten-Deckert (2011). "Sphingosine-1-phosphate links glycosphingolipid metabolism to neurodegeneration via a calpain-mediated mechanism." Cell Death Differ **18**(8): 1356-1365.

Hait, N. C., J. Allegood, M. Maceyka, G. M. Strub, K. B. Harikumar, S. K. Singh, C. Luo, R. Marmorstein, T. Kordula, S. Milstien and S. Spiegel (2009). "Regulation of histone acetylation in the nucleus by sphingosine-1-phosphate." Science **325**(5945): 1254-1257.

Halassa, M. M., T. Fellin and P. G. Haydon (2007). "The tripartite synapse: roles for gliotransmission in health and disease." Trends Mol Med **13**(2): 54-63.

Halim, N. D., T. McFate, A. Mohyeldin, P. Okagaki, L. G. Korotchkina, M. S. Patel, N. H. Jeoung, R. A. Harris, M. J. Schell and A. Verma (2010). "Phosphorylation status of pyruvate dehydrogenase distinguishes metabolic phenotypes of cultured rat brain astrocytes and neurons." Glia **58**(10): 1168-1176.

Hanisch, U. K. and H. Kettenmann (2007). "Microglia: active sensor and versatile effector cells in the normal and pathologic brain." Nat Neurosci **10**(11): 1387-1394.

Hannun, Y. A. and L. M. Obeid (2008). "Principles of bioactive lipid signalling: lessons from sphingolipids." Nat Rev Mol Cell Biol **9**(2): 139-150.

He, X., Y. Huang, B. Li, C. X. Gong and E. H. Schuchman (2010). "Deregulation of sphingolipid metabolism in Alzheimer's disease." Neurobiol Aging **31**(3): 398-408.

Hisano, Y., N. Kobayashi, A. Kawahara, A. Yamaguchi and T. Nishi (2011). "The sphingosine 1-phosphate transporter, SPNS2, functions as a transporter of the phosphorylated form of the immunomodulating agent FTY720." J Biol Chem **286**(3): 1758-1766.

Ho, C. L., C. Y. Yang, W. J. Lin and C. H. Lin (2013). "Ecto-nucleoside triphosphate diphosphohydrolase 2 modulates local ATP-induced calcium signaling in human HaCaT keratinocytes." PLoS One **8**(3): e57666.

Hong, E. J. and E. B. Jeung (2013). "Biological significance of calbindin-D9k within duodenal epithelium." Int J Mol Sci **14**(12): 23330-23340.

Ihlefeld, K., H. Vienken, R. F. Claas, K. Blankenbach, A. Rudowski, M. ter Braak, A. Koch, P. P. Van Veldhoven, J. Pfeilschifter and D. Meyer zu Heringdorf (2015). "Upregulation of ABC transporters contributes to chemoresistance of sphingosine 1-phosphate lyase-deficient fibroblasts." J Lipid Res **56**(1): 60-69.

Iqbal, K., F. Liu and C. X. Gong (2016). "Tau and neurodegenerative disease: the story so far." Nat Rev Neurol **12**(1): 15-27.

Itagaki, K. and C. J. Hauser (2003). "Sphingosine 1-phosphate, a diffusible calcium influx factor mediating store-operated calcium entry." J Biol Chem **278**(30): 27540-27547.

Jha, M. K., S. Jeon and K. Suk (2012). "Glia as a Link between Neuroinflammation and Neuropathic Pain." Immune Netw **12**(2): 41-47.

Jurgens, H. A. and R. W. Johnson (2012). "Dysregulated neuronal-microglial cross-talk during aging, stress and inflammation." Exp Neurol **233**(1): 40-48.

Karunakaran, I., S. Alam, S. Jayagopi, S. J. Frohberger, J. N. Hansen, J. Kuehlwein, B. V. Holbling, B. Schumak, M. P. Hubner, M. H. Graler, A. Halle and G. van Echten-Deckert (2019). "Neural sphingosine 1-phosphate accumulation activates microglia and links impaired autophagy and inflammation." Glia **67**(10): 1859-1872.

Karunakaran, I., S. Alam, S. Jayagopi, S. J. Frohberger, J. N. Hansen, J. Kuehlwein, B. V. Holbling, B. Schumak, M. P. Hubner, M. H. Graler, A. Halle and G. van Echten-Deckert (2019). "Neural sphingosine 1-phosphate accumulation activates microglia and links impaired autophagy and inflammation." Glia.

Karunakaran, I. and G. van Echten-Deckert (2017). "Sphingosine 1-phosphate - A double edged sword in the brain." Biochim Biophys Acta Biomembr **1859**(9 Pt B): 1573-1582.

Kawahara, A., T. Nishi, Y. Hisano, H. Fukui, A. Yamaguchi and N. Mochizuki (2009). "The sphingolipid transporter spns2 functions in migration of zebrafish myocardial precursors." Science **323**(5913): 524-527.

Klein, H. U., C. McCabe, E. Gjoneska, S. E. Sullivan, B. J. Kaskow, A. Tang, R. V. Smith, J. Xu, A. R. Pfenning, B. E. Bernstein, A. Meissner, J. A. Schneider, S. Mostafavi, L. H. Tsai, T. L. Young-Pearse, D. A. Bennett and P. L. De Jager (2019). "Epigenome-wide study uncovers large-scale changes in histone acetylation driven by tau pathology in aging and Alzheimer's human brains." Nat Neurosci **22**(1): 37-46.

Klionsky, D. J., J. M. Cregg, W. A. Dunn, Jr., S. D. Emr, Y. Sakai, I. V. Sandoval, A. Sibirny, S. Subramani, M. Thumm, M. Veenhuis and Y. Ohsumi (2003). "A unified nomenclature for yeast autophagy-related genes." Dev Cell **5**(4): 539-545.

Kohama, T., A. Olivera, L. Edsall, M. M. Nagiec, R. Dickson and S. Spiegel (1998). "Molecular cloning and functional characterization of murine sphingosine kinase." J Biol Chem **273**(37): 23722-23728.

Kolarova, M., F. Garcia-Sierra, A. Bartos, J. Ricny and D. Ripova (2012). "Structure and pathology of tau protein in Alzheimer disease." Int J Alzheimers Dis **2012**: 731526.

Kosik, K. S. (1993). "The molecular and cellular biology of tau." Brain Pathol **3**(1): 39-43.

Lardenoije, R., A. Iatrou, G. Kenis, K. Kompotis, H. W. Steinbusch, D. Mastroeni, P. Coleman, C. A. Lemere, P. R. Hof, D. L. van den Hove and B. P. Rutten (2015). "The epigenetics of aging and neurodegeneration." Prog Neurobiol **131**: 21-64.

Lavieu, G., F. Scarlatti, G. Sala, S. Carpentier, T. Levade, R. Ghidoni, J. Botti and P. Codogno (2006). "Regulation of autophagy by sphingosine kinase 1 and its role in cell survival during nutrient starvation." J Biol Chem **281**(13): 8518-8527.

Lee, H. C. and Y. J. Zhao (2019). "Resolving the topological enigma in Ca(2+) signaling by cyclic ADP-ribose and NAADP." J Biol Chem **294**(52): 19831-19843.

Lee, V. M., M. Goedert and J. Q. Trojanowski (2001). "Neurodegenerative tauopathies." Annu Rev Neurosci **24**: 1121-1159.

Lei, M., A. Shafique, K. Shang, T. A. Couttas, H. Zhao, A. S. Don and T. Karl (2017). "Contextual fear conditioning is enhanced in mice lacking functional sphingosine kinase 2." Behav Brain Res **333**: 9-16.

Lepine, S., J. C. Allegood, M. Park, P. Dent, S. Milstien and S. Spiegel (2011). "Sphingosine-1-phosphate phosphohydrolase-1 regulates ER stress-induced autophagy." Cell Death Differ **18**(2): 350-361.

Levine, B. and J. Yuan (2005). "Autophagy in cell death: an innocent convict?" J Clin Invest **115**(10): 2679-2688.

Li, K., J. Li, J. Zheng and S. Qin (2019). "Reactive Astrocytes in Neurodegenerative Diseases." Aging Dis **10**(3): 664-675.

Liddelow, S. A. and B. Barres (2017). "Reactive Astrocytes: Production, Function, and Therapeutic Potential." Immunity **46**(6): 957-967.

Limatola, C. and R. M. Ransohoff (2014). "Modulating neurotoxicity through CX3CL1/CX3CR1 signaling." Front Cell Neurosci **8**: 229.

Lv, M., D. Zhang, D. Dai, W. Zhang and L. Zhang (2016). "Sphingosine kinase 1/sphingosine-1-phosphate regulates the expression of interleukin-17A in activated microglia in cerebral ischemia/reperfusion." Inflamm Res **65**(7): 551-562.

Maceyka, M., K. B. Harikumar, S. Milstien and S. Spiegel (2012). "Sphingosine-1-phosphate signaling and its role in disease." Trends Cell Biol **22**(1): 50-60.

Magistretti, P. J. and I. Allaman (2015). "A cellular perspective on brain energy metabolism and functional imaging." Neuron **86**(4): 883-901.

Mandelkow, E. M., J. Biernat, G. Drewes, N. Gustke, B. Trinczek and E. Mandelkow (1995). "Tau domains, phosphorylation, and interactions with microtubules." Neurobiol Aging **16**(3): 355-362; discussion 362-353.

Mansuroglu, Z., H. Benhelli-Mokrani, V. Marcato, A. Sultan, M. Violet, A. Chauderlier, L. Delattre, A. Loyens, S. Talahari, S. Begard, F. Nesslany, M. Colin, S. Soues, B. Lefebvre, L. Buee, M. C. Galas and E. Bonnefoy (2016). "Loss of Tau protein affects the structure, transcription and repair of neuronal pericentromeric heterochromatin." Sci Rep **6**: 33047.

Mattson, M. P., M. G. Engle and B. Rychlik (1991). "Effects of elevated intracellular calcium levels on the cytoskeleton and tau in cultured human cortical neurons." Mol Chem Neuropathol **15**(2): 117-142.

Menzies, F. M., A. Fleming and D. C. Rubinsztein (2015). "Compromised autophagy and neurodegenerative diseases." Nat Rev Neurosci **16**(6): 345-357.

Min, R. and T. Nevian (2012). "Astrocyte signaling controls spike timing-dependent depression at neocortical synapses." Nature Neuroscience **15**(5): 746-753.

Mitroi, D. N. (2016). The role of sphingosine-1-phosphate lyase (SPL) in the brain Phd thesis.

Mitroi, D. N., A. U. Deutschmann, M. Raucamp, I. Karunakaran, K. Glebov, M. Hans, J. Walter, J. Saba, M. Graler, D. Ehninger, E. Sopova, O. Shupliakov, D. Swandulla and G. van Echten-Deckert (2016). "Sphingosine 1-phosphate lyase ablation disrupts presynaptic architecture and function via an ubiquitin- proteasome mediated mechanism." Sci Rep **6**: 37064.

Mitroi, D. N., I. Karunakaran, M. Graler, J. D. Saba, D. Ehninger, M. D. Ledesma and G. van Echten-Deckert (2017). "SGPL1 (sphingosine phosphate lyase 1) modulates neuronal autophagy via phosphatidylethanolamine production." Autophagy **13**(5): 885-899.

Mizugishi, K., T. Yamashita, A. Olivera, G. F. Miller, S. Spiegel and R. L. Proia (2005). "Essential role for sphingosine kinases in neural and vascular development." Mol Cell Biol **25**(24): 11113-11121.

Mizushima, N. and M. Komatsu (2011). "Autophagy: renovation of cells and tissues." Cell **147**(4): 728-741.

Mizushima, N., B. Levine, A. M. Cuervo and D. J. Klionsky (2008). "Autophagy fights disease through cellular self-digestion." Nature **451**(7182): 1069-1075.

Moruno-Manchon, J. F., N. E. Uzor, C. R. Ambati, V. Shetty, N. Putluri, C. Jagannath, L. D. McCullough and A. S. Tsvetkov (2018). "Sphingosine kinase 1-associated autophagy differs between neurons and astrocytes." Cell Death Dis **9**(5): 521.

Moruno Manchon, J. F., N. E. Uzor, Y. Dabaghian, E. E. Furr-Stimming, S. Finkbeiner and A. S. Tsvetkov (2015). "Cytoplasmic sphingosine-1-phosphate pathway modulates neuronal autophagy." Sci Rep **5**: 15213.

Nagahashi, M., E. Y. Kim, A. Yamada, S. Ramachandran, J. C. Allegood, N. C. Hait, M. Maceyka, S. Milstien, K. Takabe and S. Spiegel (2013). "Spns2, a transporter of phosphorylated sphingoid bases, regulates their blood and lymph levels, and the lymphatic network." FASEB J **27**(3): 1001-1011.

Narayan, P. J., C. Lill, R. Faull, M. A. Curtis and M. Dragunow (2015). "Increased acetyl and total histone levels in post-mortem Alzheimer's disease brain." Neurobiol Dis **74**: 281-294.

Neal, M. and J. R. Richardson (2018). "Epigenetic regulation of astrocyte function in neuroinflammation and neurodegeneration." Biochim Biophys Acta Mol Basis Dis **1864**(2): 432-443.

Neary, J. T. (1996). "Trophic actions of extracellular ATP on astrocytes, synergistic interactions with fibroblast growth factors and underlying signal transduction mechanisms." Ciba Found Symp **198**: 130-139; discussion 139-141.

Neary, J. T., L. Baker, S. L. Jorgensen and M. D. Norenberg (1994). "Extracellular ATP induces stellation and increases glial fibrillary acidic protein content and DNA synthesis in primary astrocyte cultures." Acta Neuropathol **87**(1): 8-13.

Neary, J. T. and M. D. Norenberg (1992). "Signaling by extracellular ATP: physiological and pathological considerations in neuronal-astrocytic interactions." Prog Brain Res **94**: 145-151.

Neary, J. T., S. R. Whittemore, Q. Zhu and M. D. Norenberg (1994). "Destabilization of glial fibrillary acidic protein mRNA in astrocytes by ammonia and protection by extracellular ATP." J Neurochem **63**(6): 2021-2027.

Nedergaard, M., B. Ransom and S. A. Goldman (2003). "New roles for astrocytes: redefining the functional architecture of the brain." Trends Neurosci **26**(10): 523-530.

Nowakowski, A. B., W. J. Wobig and D. H. Petering (2014). "Native SDS-PAGE: high resolution electrophoretic separation of proteins with retention of native properties including bound metal ions." Metallomics **6**(5): 1068-1078.

O'Sullivan, S. and K. K. Dev (2017). "Sphingosine-1-phosphate receptor therapies: Advances in clinical trials for CNS-related diseases." Neuropharmacology **113**(Pt B): 597-607.

Ohsumi, Y. (2014). "Historical landmarks of autophagy research." Cell Res **24**(1): 9-23.

Olivera, A. and S. Spiegel (1993). "Sphingosine-1-phosphate as second messenger in cell proliferation induced by PDGF and FCS mitogens." Nature **365**(6446): 557-560.

Olsen, A. S. B. and N. J. Faergeman (2017). "Sphingolipids: membrane microdomains in brain development, function and neurological diseases." Open Biol **7**(5).

Oyarzabal, A. and I. Marin-Valencia (2019). "Synaptic energy metabolism and neuronal excitability, in sickness and health." J Inherit Metab Dis **42**(2): 220-236.

Pangrsic, T., M. Potokar, M. Stenovec, M. Kreft, E. Fabbretti, A. Nistri, E. Pryazhnikov, L. Khiroug, R. Giniatullin and R. Zorec (2007). "Exocytotic release of ATP from cultured astrocytes." J Biol Chem **282**(39): 28749-28758.

Patel, M. S., N. S. Nemeria, W. Furey and F. Jordan (2014). "The pyruvate dehydrogenase complexes: structure-based function and regulation." J Biol Chem **289**(24): 16615-16623.

Paugh, B. S., L. Bryan, S. W. Paugh, K. M. Wilczynska, S. M. Alvarez, S. K. Singh, D. Kapitonov, H. Rokita, S. Wright, I. Griswold-Prenner, S. Milstien, S. Spiegel and T. Kordula (2009). "Interleukin-1 regulates the expression of sphingosine kinase 1 in glioblastoma cells." J Biol Chem **284**(6): 3408-3417.

Perea, G., M. Navarrete and A. Araque (2009). "Tripartite synapses: astrocytes process and control synaptic information." Trends Neurosci **32**(8): 421-431.

Raucamp, M. (2019). "Impact of sphingosine 1-phosphate lyase on the synaptic transmission in mouse hippocampus" PhD Thesis, University Bonn.

Rodrigues, R. J., A. R. Tome and R. A. Cunha (2015). "ATP as a multi-target danger signal in the brain." Front Neurosci **9**: 148.

Rothhammer, V., J. E. Kenison, E. Tjon, M. C. Takenaka, K. A. de Lima, D. M. Borucki, C. C. Chao, A. Wilz, M. Blain, L. Healy, J. Antel and F. J. Quintana (2017). "Sphingosine 1-phosphate receptor modulation suppresses pathogenic astrocyte activation and chronic progressive CNS inflammation." Proc Natl Acad Sci U S A **114**(8): 2012-2017.

Saba, J. D., N. Keller, J. Y. Wang, F. Tang, A. Slavin and Y. Shen (2021). "Genotype/Phenotype Interactions and First Steps Toward Targeted Therapy for Sphingosine Phosphate Lyase Insufficiency Syndrome." Cell Biochem Biophys.

Sabatini, D. M. (2017). "Twenty-five years of mTOR: Uncovering the link from nutrients to growth." Proc Natl Acad Sci U S A **114**(45): 11818-11825.

Salter, M. W. and B. Stevens (2017). "Microglia emerge as central players in brain disease." Nat Med **23**(9): 1018-1027.

Sasaki, T., N. Matsuki and Y. Ikegaya (2011). "Action-Potential Modulation During Axonal Conduction." Science **331**(6017): 599-601.

Schildge, S., C. Bohrer, K. Beck and C. Schachtrup (2013). "Isolation and culture of mouse cortical astrocytes." J Vis Exp(71).

Schilling, T., R. Nitsch, U. Heinemann, D. Haas and C. Eder (2001). "Astrocyte-released cytokines induce ramification and outward K+ channel expression in microglia via distinct signalling pathways." Eur J Neurosci **14**(3): 463-473.

Schmeisser, K. and J. A. Parker (2019). "Pleiotropic Effects of mTOR and Autophagy During Development and Aging." Front Cell Dev Biol **7**: 192.

Seifert, G., K. Schilling and C. Steinhauser (2006). "Astrocyte dysfunction in neurological disorders: a molecular perspective." Nat Rev Neurosci **7**(3): 194-206.

Shen, Y., S. Zhao, S. Wang, X. Pan, Y. Zhang, J. Xu, Y. Jiang, H. Li, Q. Zhang, J. Gao, Q. Yang, Y. Zhou, S. Jiang, H. Yang, Z. Zhang, R. Zhang, J. Li and D. Zhou (2019). "S1P/S1PR3 axis promotes aerobic glycolysis by YAP/c-MYC/PGAM1 axis in osteosarcoma." EBioMedicine **40**: 210-223.

Sheng, R., T. T. Zhang, V. D. Felice, T. Qin, Z. H. Qin, C. D. Smith, E. Sapp, M. Difiglia and C. Waeber (2014). "Preconditioning stimuli induce autophagy via sphingosine kinase 2 in mouse cortical neurons." J Biol Chem **289**(30): 20845-20857.

Snider, A. J., K. A. Orr Gandy and L. M. Obeid (2010). "Sphingosine kinase: Role in regulation of bioactive sphingolipid mediators in inflammation." <u>Biochimie</u> **92**(6): 707-715.

Sofroniew, M. V. (2009). "Molecular dissection of reactive astrogliosis and glial scar formation." <u>Trends Neurosci</u> **32**(12): 638-647.

Sofroniew, M. V. (2010). "Essential barrier functions of scar-forming reactive astrocytes." <u>Faseb Journal</u> **24**.

Sofroniew, M. V. (2014). "Multiple roles for astrocytes as effectors of cytokines and inflammatory mediators." <u>Neuroscientist</u> **20**(2): 160-172.

Sofroniew, M. V. (2015). "Astrocyte barriers to neurotoxic inflammation." <u>Nature Reviews Neuroscience</u> **16**(5): 249-263.

Sofroniew, M. V. (2015). "Astrocyte barriers to neurotoxic inflammation (vol 16, pg 249, 2015)." <u>Nature Reviews Neuroscience</u> **16**(6).

Sofroniew, M. V. (2015). "Astrogliosis." <u>Cold Spring Harbor Perspectives in Biology</u> **7**(2).

Sofroniew, M. V. (2020). "Astrocyte Reactivity: Subtypes, States, and Functions in CNS Innate Immunity." <u>Trends in Immunology</u> **41**(9): 758-770.

Sofroniew, M. V. and H. V. Vinters (2010). "Astrocytes: biology and pathology." <u>Acta Neuropathologica</u> **119**(1): 7-35.

Sorensen, S. D., O. Nicole, R. D. Peavy, L. M. Montoya, C. J. Lee, T. J. Murphy, S. F. Traynelis and J. R. Hepler (2003). "Common signaling pathways link activation of murine PAR-1, LPA, and S1P receptors to proliferation of astrocytes." <u>Mol Pharmacol</u> **64**(5): 1199-1209.

Spiegel, S., M. A. Maczis, M. Maceyka and S. Milstien (2019). "New insights into functions of the sphingosine-1-phosphate transporter SPNS2." <u>J Lipid Res</u> **60**(3): 484-489.

Spiegel, S. and S. Milstien (2000). "Sphingosine-1-phosphate: signaling inside and out." <u>FEBS Lett</u> **476**(1-2): 55-57.

Spiegel, S. and S. Milstien (2011). "The outs and the ins of sphingosine-1-phosphate in immunity." <u>Nat Rev Immunol</u> **11**(6): 403-415.

Stachon, P., S. Geis, A. Peikert, A. Heidenreich, N. A. Michel, F. Unal, N. Hoppe, B. Dufner, L. Schulte, T. Marchini, S. Cicko, K. Ayata, A. Zech, D. Wolf, I. Hilgendorf, F. Willecke, J. Reinohl, C. von Zur Muhlen, C. Bode, M. Idzko and A. Zirlik (2016). "Extracellular ATP Induces Vascular Inflammation and Atherosclerosis via Purinergic Receptor Y2 in Mice." <u>Arterioscler Thromb Vasc Biol</u> **36**(8): 1577-1586.

Staricha, K., N. Meyers, J. Garvin, Q. Liu, K. Rarick, D. Harder and S. Cohen (2020). "Effect of high glucose condition on glucose metabolism in primary astrocytes." Brain Res **1732**: 146702.

Sun, K., Y. Zhang, A. D'Alessandro, T. Nemkov, A. Song, H. Wu, H. Liu, M. Adebiyi, A. Huang, Y. E. Wen, M. V. Bogdanov, A. Vila, J. O'Brien, R. E. Kellems, W. Dowhan, A. W. Subudhi, S. Jameson-Van Houten, C. G. Julian, A. T. Lovering, M. Safo, K. C. Hansen, R. C. Roach and Y. Xia (2016). "Sphingosine-1-phosphate promotes erythrocyte glycolysis and oxygen release for adaptation to high-altitude hypoxia." Nat Commun **7**: 12086.

Takasugi, N., T. Sasaki, K. Suzuki, S. Osawa, H. Isshiki, Y. Hori, N. Shimada, T. Higo, S. Yokoshima, T. Fukuyama, V. M. Lee, J. Q. Trojanowski, T. Tomita and T. Iwatsubo (2011). "BACE1 activity is modulated by cell-associated sphingosine-1-phosphate." J Neurosci **31**(18): 6850-6857.

Thudichum, J. L. W. (1884). " A treatise on the Chemical Constitution of the Brain. Archon Books." Glasgow Med J. **22(5)**: 363–364.

Thuy, A. V., C. M. Reimann, N. Y. Hemdan and M. H. Graler (2014). "Sphingosine 1-phosphate in blood: function, metabolism, and fate." Cell Physiol Biochem **34**(1): 158-171.

Toyoshima, T., S. Yamagami, B. Y. Ahmed, L. Jin, O. Miyamoto, T. Itano, M. Tokuda, H. Matsui and O. Hatase (1996). "Expression of calbindin-D28K by reactive astrocytes in gerbil hippocampus after ischaemia." Neuroreport **7**(13): 2087-2091.

Tsai, H. C. and M. H. Han (2016). "Sphingosine-1-Phosphate (S1P) and S1P Signaling Pathway: Therapeutic Targets in Autoimmunity and Inflammation." Drugs **76**(11): 1067-1079.

Turner, B. M. (2000). "Histone acetylation and an epigenetic code." Bioessays **22**(9): 836-845.

Ullian, E. M., S. K. Sapperstein, K. S. Christopherson and B. A. Barres (2001). "Control of synapse number by glia." Science **291**(5504): 657-661.

van Echten-Deckert, G. and S. Alam (2018). "Sphingolipid metabolism - an ambiguous regulator of autophagy in the brain." Biol Chem **399**(8): 837-850.

van Echten-Deckert, G., N. Hagen-Euteneuer, I. Karaca and J. Walter (2014). "Sphingosine-1-phosphate: boon and bane for the brain." Cell Physiol Biochem **34**(1): 148-157.

van Echten-Deckert, G. and T. Herget (2006). "Sphingolipid metabolism in neural cells." Biochim Biophys Acta.

Van Veldhoven, P. P. (2000). "Sphingosine-1-phosphate lyase." Methods Enzymol **311**: 244-254.

Verkhratsky, A., O. A. Krishtal and G. Burnstock (2009). "Purinoceptors on neuroglia." Mol Neurobiol **39**(3): 190-208.

Volterra, A. and J. Meldolesi (2005). "Astrocytes, from brain glue to communication elements: the revolution continues." Nat Rev Neurosci **6**(8): 626-640.

Wang, G. and E. Bieberich (2018). "Sphingolipids in neurodegeneration (with focus on ceramide and S1P)." Adv Biol Regul **70**: 51-64.

Wang, Y. and E. Mandelkow (2016). "Tau in physiology and pathology." Nat Rev Neurosci **17**(1): 5-21.

Ward, C., N. Martinez-Lopez, E. G. Otten, B. Carroll, D. Maetzel, R. Singh, S. Sarkar and V. I. Korolchuk (2016). "Autophagy, lipophagy and lysosomal lipid storage disorders." Biochim Biophys Acta **1861**(4): 269-284.

Williams, A., S. Sarkar, P. Cuddon, E. K. Ttofi, S. Saiki, F. H. Siddiqi, L. Jahreiss, A. Fleming, D. Pask, P. Goldsmith, C. J. O'Kane, R. A. Floto and D. C. Rubinsztein (2008). "Novel targets for Huntington's disease in an mTOR-independent autophagy pathway." Nat Chem Biol **4**(5): 295-305.

Wollny, T., M. Watek, B. Durnas, K. Niemirowicz, E. Piktel, M. Zendzian-Piotrowska, S. Gozdz and R. Bucki (2017). "Sphingosine-1-Phosphate Metabolism and Its Role in the Development of Inflammatory Bowel Disease." Int J Mol Sci **18**(4).

Yang, Z. and D. J. Klionsky (2010). "Eaten alive: a history of macroautophagy." Nat Cell Biol **12**(9): 814-822.

Zhong, L., X. Jiang, Z. Zhu, H. Qin, M. B. Dinkins, J. N. Kong, S. Leanhart, R. Wang, A. Elsherbini, E. Bieberich, Y. Zhao and G. Wang (2019). "Lipid transporter Spns2 promotes microglia pro-inflammatory activation in response to amyloid-beta peptide." Glia **67**(3): 498-511.

# 7 ABBREVIATIONS

ABC   ATP-binding cassette

AD   Alzheimer's disease

ADP   Adenosine diphosphate

Akt   serine/threonine kinase

ALS   amyotrophic lateral sclerosis

AMP   adenosine monophosphate

ANLS   astrocyte-neuronal lactate shuttle

APOE   apolipoprotein E

APP   amyloid precursor protein

APS   ammonium peroxydisulfate

AraC   cytosine-b-D-arabinofuranoside-hydrochloride

ASM   acid sphingomyelinase

ATG   autophagy related protein

ATP   adenosine triphosphate

BAPTA-AM   1,2-bis- (o-Amino phenoxy)-ethane-N, N, N', N'-tetra acetic acid,
            tetra acetoxymethyl       ester

BDNF   brain-derived neurotrophic factor

BDNF   brain-derived neurotrophic factor

BSA   bovine serum albumin

cDNA   complementary deoxyribonucleic acid

CDase   ceramidase

CMA   chaperone-mediated autophagy

CNTF   ciliary neurotrophic factor

CerS   ceramide synthase

CNS   central nervous system

CSPGs   chondroitin sulfate proteoglycans

DAMP   damage- or danger-associated molecular pattern

DMEM   dulbecco's modified eagle medium

DMSO   dimethyl sulfoxide

EAP   ethanolamine phosphate

EDTA   ethylenediaminetetraacetate

EGF   epidermal growth factor

ELISA   enzyme-linked immunosorbent assay

ER   endoplasmic reticulum

FBS   fetal bovine serum

FGF   fibroblast growth factor

GABA   gamma-aminobutyric acid

GAPDH   glyceraldehyde 3-phosphate dehydrogenase

GDNF   glial cell-derived neurotrophic factor

GFAP   glial fibrillary acidic protein

GFP   green fluorescent protein

GPCs   glypicans

IFN   interferon

IGF   insulin-like growth factor

HD   huntingtin's disease

HAT   histone acetyltransferase

HDAC   histone deacetylase

HRP   horseradish peroxidase

IHC   immunohistochemistry

IHF   immunohistofluorescence

IL   interleukin

kDa   kilodalton

LC3   microtubule-associated protein 1A/1B-light chain 3

LPS   lipopolysaccharide

MAPK   mitogen-activated protein kinase

mM   millimolar

mRNA    messenger ribonucleic acid

mTOR    mammalian target of rapamycin

nM    nanomolar

NO    Nitric oxide

PAS    phagophore assembly site

PBS    phosphate buffer saline

PCR    polymerase chain reaction

PD    parkinson's disease

PDH    pyruvate dehydrogenase

PE    phosphatidylethanolamine

PFA    paraformaldehyde

PFK    Phosphofructokinase

PGE    prostaglandin E2

PI3K    phosphatidylinositol-4,5-biphosphate 3-kinase

PLP    pyridoxal phosphate

P2Y1R    purinergic receptor 1

ROS    reactive oxygen species

S1P    sphingosine 1-phosphate

S1PR    sphingosine 1-phosphate receptor

SK    sphingosine kinase

SL    sphingolipid

SM    sphingomyelin

SMase    sphingomyelinase
SMS    sphingomyelin-Synthase

SNCA    synuclein alpha

Sph    sphingosine

SGPL1    sphingosine 1-phosphate lyase

SPP    sphingosine 1-phosphate phosphohydrolase

SPT    serine palmitoyl transferase

TCA   tri carboxylic acid

TNF   tumor necrosis factor

μl   microliter

μg   microgramm

μM   micromol

# 8  ACKNOWLEDGMENT

# 9 PUBLICATIONS

Parts of the dissertation have been published:

- **Alam, S.,** Piazzesi, A.; Abd El Fatah, M.; Raucamp, M.; van Echten-Deckert, G. Neurodegeneration Caused by S1P-Lyase Deficiency Involves Calcium-Dependent Tau Pathology and Abnormal Histone Acetylation. **Cells**, 9, 2189 **(2020).** https://doi.org/10.3390/cells9102189

- Karunakaran, I*., **Alam, S.*,** et al. Neural sphingosine 1-phosphate accumulation activates microglia and links impaired autophagy and inflammation**. GLIA**,67:1859-1872 **(2019).** https://doi.org/10.1002/glia.23663

- Van Echten-Deckert, G., **Alam, S**. Sphingolipid metabolism - an ambiguous regulator of autophagy in the brain. **Biol Chem** 399(8): 837 - 850 **(2018)**. https://doi.org/10.1515/hsz-2018-0237

Publication in progress:

- **Alam, S.**, Afsar, S.Y., van Echten-Deckert, G. Metabotropic P2Y1 receptor mediates astrogliosis in SGPL1-deficient murine brain.